AN INVESTIGATION OF THE EFFECT OF OBSTRUCTIVE SLEEP APNEA ON CEREBRAL HEMODYNAMICS IN RELATION WITH SYSTEMIC HEMODYNAMICS

by

RAICHEL MARY ALEX

Presented to the Faculty of the Graduate School of
The University of Texas at Arlington in Partial Fulfillment
of the Requirements
for the Degree of

DOCTOR OF PHILOSOPHY

THE UNIVERSITY OF TEXAS AT ARLINGTON
August 2015

Acknowledgements

This work would have never come to fulfillment without the help, support and love of almighty God, guidance from my committee members and encouragement from my friends and family.

I would like to express my heartfelt gratitude to my mentor Dr. Khosrow Behbehani for all his valuable help, thoughts and motivation amidst his busy schedule. He has been a great mentor, constantly guiding me throughout the success and failures encountered in the completion of this research work.

Without the subject recruitment by Dr. Donald E Watenpaugh from Sleep Consultants Inc., this study would not have materialized. I would like to sincerely thank him for all his advices and helpful suggestions throughout the research period.

I would also like to thank Dr. Hanli Liu for her constant encouraging words and continuous support with my research work.

I am indebted to my committee member Dr. Rong Zhang from Texas Health Presbyterian Hospital Dallas, for giving me new research directions by frequently sending me recent publications and conference proceedings.

I would also like to thank Dr. Sun Mitchell, from Mathematics department, UTA, for her advices regarding the statistical analysis that can be applied to my research.

I express my heartfelt gratitude to Dr. Liping Tang, for his proactive suggestions, constant support and motivation.

My sincere gratitude goes to the staff at Sleep Consultants, Inc.: Melvin Keierleber, Dzu Dao, Ana Trutza, Ronald Peterson and Terry Clontz for their support throughout the overnight data collection at sleep lab.

I express my gratitude to Karthik Machiraju, Nazaneen Mousavi, Suvidha Manchikatla, Essam Altuwaijri, Varun Kanal and Kevin Jepsen, my fellow colleagues at

the Biosignals Processing lab at UTA, for extending their support and help in all possible ways during long nights of data collection.

Special thanks to Ms. Shelly Douglass for all her help and encouragement and faith in me. I would not have been able to complete this work without the motivation and faith shown by my mother, my sister and my friends Sophia Lawrance, Ivy George, Aswini Kanneganti and Varsha Sundaresan. They always stood by me through the good times and bad.

July 29, 2015

Abstract

AN INVESTIGATION OF THE EFFECT OF OBSTRUCTIVE SLEEP APNEA ON CEREBRAL HEMODYNAMICS IN RELATION WITH SYSTEMIC HEMODYNAMICS

Raichel Mary Alex, PhD

The University of Texas at Arlington, 2015

Supervising Professor: Khosrow Behbehani

Obstructive Sleep Apnea (OSA) is a major sleep disorder affecting approximately 18 million adults in the US. Recent studies have observed cognitive impairments and brain structural changes in OSA subjects where these deficits were related to peripheral hypoxia and sleep fragmentation. Nonetheless, underlying cerebral hemodynamics and cerebral oxygenation might play an important role in the development of these impairments. Hence, in this study it is hypothesized that 1) OSA induces significant variations in cerebral hemodynamics, and 2) level of variations in cerebral hemodynamics can be related to the changes in systemic hemodynamics.

To test these hypotheses, 8 hours of nocturnal polysomnography was conducted on 11 OSA subjects (6 Males, 5 Females; Age: 54.27±6.23 years, BMI:34.95±7.06kg/m^2, AHI: 57.39±28.43) who have been positively diagnosed of having OSA. Systemic hemodynamics [arterial blood pressure (BP), arterial oxygen saturation (SaO_2), end tidal CO_2 concentration ($ETCO_2$)] and cerebral hemodynamics [cerebral blood flow velocity (CBFV) and brain tissue oxygenation] were recorded concurrently with polysomnography. OSA elicited an average increase of 41.98±1.88% (Mean±SEM) in mean CBFV compared to its value prior to the start of OSA. The rate of rise in mean CBFV was

observed to be 0.56±0.03 cm/s^2. Additionally, OSA induced an average drop of -2.03±0.14μM/L in brain oxy hemoglobin concentration. All the metrics derived from CBFV and brain oxygenation data (except the rate of rise in diastolic and mean CBFV and level of drop in oxy hemoglobin) were significantly correlated with the OSA duration ($p<0.001$). However, there was no correlation of cerebral hemodynamics with AHI, the OSA severity index.

Further, features derived from cerebral hemodynamics showed a significant correlation with one or more of their systemic counterparts ($p<0.03$). Average time delays of 6.20±0.45s, 3.98±0.27s and 6.05±0.95s were observed between changes in systolic BP *vs* systolic CBFV, diastolic BP *vs* diastolic CBFV and SaO_2 *vs* brain oxy hemoglobin concentration, respectively. Moreover, mathematical modelling of dynamic cerebral autoregulation using autoregressive moving average model indicated that a second order system can be used to predict BP related dynamic changes in CBFV during OSA.

Hence this study suggests that OSA induces significant variations in cerebral hemodynamics which can be related to the changes in systemic hemodynamics. Furthermore, inclusion of OSA duration in addition to AHI might be beneficial while assessing the severity of OSA.

Table of Contents

List of Illustrations

List of Tables

Chapter 1

Introduction

1.1 Sleep Apnea: Definition and Prevalence

Sleep apnea is one of the most common form of sleep disordered breathing characterized by intermittent, cyclical cessations (apnea) or reductions of airflow (hypopnea), with or without obstructions of the upper airway, for at least 10 s during sleep [1]. With reduced or zero air ventilating the lungs, arterial oxygen concentration decreases (hypoxia) and CO_2 accumulates (hypercapnia) thus, signaling the brain to briefly arouse the sleep apnea patients from sleep to resume breathing. Hyperventilation ensues, followed by next episode of apnea. The duration of apnea episodes may last from few seconds to over a minute and may recur hundreds of times during a single night of sleep [2]. These frequent respiratory pauses can lead to intermittent microarousals for breathing resumption, resulting in extreme sleep fragmentation and thereby disrupting normal sleep homeostasis [3].

Based on the cause of breathing pauses, apneas can be classified into obstructive (OSA), central (CSA) and mixed apneas. OSA occurs when mechanical closure of upper airway due to excessive muscle relaxation in the posterior oropharynx takes place during sleep thereby obstructing the air flow to the lungs [1, 4]. Central apnea is characterized by a temporary failure of respiratory control from the brainstem inspiratory neural center to respiratory muscles. As a result there will not be any inspiratory effort, naso-oral airflow and abdominal respiratory movements. This is more common in infants with prematurity or congenital disorders and in adults with cardiac insufficiency or opiate usage [4]. Central sleep apnea may also occur in healthy subjects at high altitudes [5]. In some instances, breathing cessations are driven initially by the absence of neurochemical control of upper airway and/or chest wall respiratory

musculature (CSA) followed by upper airway closure (OSA). These kinds of apnea are known as mixed apneas [4].

Obstructive sleep apnea (OSA) is the most common form of sleep apnea. An estimated 84% of patient population having sleep apnea suffers from OSA [6]. Estimates show that about 5% - 25% of the adults across the Western countries are affected by OSA [7]. In US alone, approximately 15 % of adult population (over 18 million) is being affected with a prevalence of 24% men and 9% women [8, 9]. However, around 2- 4 % of adults in US (1 in every 50 individuals) have an undiagnosed case of sleep apnea adding to the disease complexity [9]. OSA prevalence is expected to rise in future since the prominent OSA risk factors such as obesity and older age are increasing at an astounding rate [7, 10]. Approximately 60% of the adult population in developed countries is classified under overweight category (BMI ≥ 25 kg/m^2) and about 30% under obese group (BMI ≥ 30 kg/m^2) [10]. Obesity can predispose or worsen OSA due to fat depositions in and around upper airway, thorax, chest and abdominal areas. Prevalence of OSA is about 45 % in obese population compared to 25% in general adult population [10]. Second risk factor for OSA is older age. OSA prevalence appears to increase with age. Studies show that, elderly adults within 65-90 years of age have a threefold higher prevalence rate (30%–80%) than middle-aged adults [11, 12].

Sleep apneas are usually detected by using an overnight polysomnography (NPSG) study in a sleep laboratory. NPSG includes measurement of electroencephalogram (EEG), electrocardiogram (ECG), blood oxygen saturation, electro-oculogram (EOG), electromyogram (EMG), oral-nasal air flow and chest-abdominal movement. The number of apneas and hypopneas occurring during entire sleep study is recorded and is divided by number of hours of sleep to calculate apnea-hypopnea index (AHI). AHI of 5-15 events/hour is generally classified as mild apnea and

15-30 events/hour as moderate apnea. If AHI is above 30 it is categorized as severe apnea [1, 9].

The treatment of choice for OSA is to apply pressurized air to patient's airway to prevent obstruction; called continuous positive airway pressure (CPAP). CPAP delivers air through a mask that fits over nose and in some instances mouth and the lowest air pressure which is needed to keep the airway open during sleep is used. However, an estimate of 30 % of OSA subjects has poor compliance in adhering to the persistent usage of CPAP due to discomforts arising from strapping the mask over the nose and mouth during sleep [7]. Other treatment techniques include changing the sleep position, medications, dental interventions and surgical treatments [13]. These are mainly beneficial for mild OSA patients; for moderate to severe OSA subjects, CPAP remains the most effective therapy [7].

1.2 Physiological Impacts of OSA

Over time, OSA can lead to serious health complications such as hypertension, stroke, cardiovascular diseases, neurocognitive disorders, increased risk for automobile accidents, and poor performance in everyday activities due to excessive day time sleepiness [6, 7, 14-17]. In order to understand the physiological consequences of OSA, it is necessary to recognize the underlying OSA induced neurocirculatory modulations.

1.2.1 Pathophysiology of OSA

Normal inspiration-expiration cycle is controlled by the medullary input from brain stem, which depends on carotid and aortic O2 receptors and mechanoreceptors in the respiratory tract and lungs; whereas the airway patency is dependent on the relative balance between the intraluminal pressure (airway suction) and the upper airway dilator muscle tone [18]. Various inputs including the peripheral and central chemoreceptors as well as other factors that increase neural input to either the diaphragm (inspiratory drive)

or upper airway muscles (upper airway drive) will be important in determining upper airway patency.

In OSA, upper airway closure results in the development of a negative intra thoracic pressure. The negative pressure is further potentiated by the normal respiratory effort from the respiratory muscles and contraction of the diaphragm leading to an added constriction of the upper airway [18]. Reduced stimulation of pulmonary stretch receptors arising from this negative pressure will activate the vagus nerve, thereby reducing the heart rate and inhibiting the sympathetic activity during initial stage of sleep apnea. However, due to the airway occlusion, blood oxygen saturation can drop to dangerously low levels resulting in hypoxia and hypercapnia, which are detected by the peripheral and central chemoreceptors [19]. Hypoxia acts primarily on peripheral chemoreceptors in the carotid bodies. Hypercapnia acts primarily on central chemoreceptors, located in the brainstem. Both of these stimuli activate the sympathetic nervous system thereby increasing the heart rate, blood pressure and vasoconstriction [19].

Therefore, the two opposing effects: Negative intra-thoracic pressure, which causes a reduction in both arterial pressure and sympathetic outflow early in the apnea, and the chemoreflex stimulation, which overcomes this initial inhibitory effect and causes sympathetic activation; determines the neurocirculatory response to OSA [18, 19].

1.2.2 Cardiovascular Consequences

OSA induces cardiovascular disorders through chemical, autonomic, mechanical and inflammatory mechanisms [20]. Frequent chemoreflex stimulations by hypoxia-hypercapnia, lead to surges in sympathetic nerve activity which in turn promotes release of the stress hormone adrenaline [21]. Sympathetic nerve activity together with stress hormone causes constriction of peripheral blood vessels thereby raising the blood pressure. Hence heart has to pump blood to constricted peripheral arteries despite the

increased blood pressure, resulting in increased CO_2 concentration and decreased arterial blood oxygen saturation. This in turn places increased stress on the heart throughout night [6, 21, 22]. Further, breathing against a closed pharynx results in negative intra-thoracic pressure leading to an increase in left ventricular transmural pressure, arterial wall tension and venous return to right ventricle. This ultimately leads to right ventricular distension, leftward shifting of inter-ventricular septum. Consequently stroke volume is reduced due to the lowered left ventricular filling [20]. This increased cardiac afterload unique to OSA can trigger hypertension, hypertrophy and dilatation [23]. Further, due to over excitation of sympathetic system, overall vagal tone is diminished in OSA patients resulting in reduced heart rate variability [20]. Another factor to be considered is the recurrent hypoxia followed by reoxygenation leading to formation of reactive oxygen species. This oxidative stress will result in systemic inflammation and endothelial dysfunction [24]. Over the time all these chemical, autonomic, mechanical and inflammatory responses lead to persistent hypertension, arrhythmias, myocardial infarction, cardiac remodeling and accelerated heart failure [20, 25].

1.2.3 Cerebrovascular Consequences

Sleep, a naturally occurring phenomenon in our everyday life, plays a vital role in maintaining longevity, learning, memory consolidation, removal of potentially toxic metabolites from brain and overall central nervous system homeostasis [26, 27]. OSA induced asphyxia is avoided by repeated microarousals for breathing resumption. This sleep fragmentation disrupts the normal sleep homeostasis [3]. Further, due to repetitive hypoxia and hypercapnia during apnea episodes, brain and other vital organs are repeatedly deprived of oxygenated blood which can lead to stroke, irreversible tissue damage and cognitive impairments [28]. Under normal conditions, cerebral blood flow autoregulation mechanism tries to maintain a consistent supply of oxygen and blood flow

to brain tissue despite the fluctuations in arterial blood pressure, CO_2 concentration and arterial oxygen saturation. The adult brain requires about 50 to 54 ml of blood per 100 gm of tissue per minute [29] which is closely regulated by autoregulation. Excessive blood flow can be dangerous, as it can increase intracranial pressure and damage brain tissue by compression. Increased oxidative stress due to hypoxemia-reoxygenation during apnea episodes, together with elevated arterial blood pressure can lead to the disruption of this autoregulation. As a result there will be a rise in both blood pressure and cerebral blood flow velocity during apnea episodes, followed by a rapid decrease in both during post-apneic hyperventilation period, resulting in oscillations of cerebral blood flow during the entire night. These can lead to increased intracranial pressure and can predispose apnea subjects to increased risk of cerebral ischemia and stroke [28, 30]. Moreover, cerebral vasodilator reserve has been found to be diminished in OSA subjects augmenting the inability of cerebral vessels to adapt to brain metabolic needs [30]. Incidence of reduction in brain gray and white matter (especially in frontal cortex, parietal cortex, temporal lobe, anterior cingulate, and hippocampus) associated with impairments in cognitive skills (working memory, short term memory and executive functions including problem solving, reaction time, mental flexibility, ability to plan and predict events, initiating new mental process, and inhibiting automatic mental processes) have been observed in OSA patients [31-35].

1.3 Study Motivations and Objectives

1.3.1 Significance of the Study

Three decades of intensive research on OSA, the most common sleep disorder, has revealed two very significant facts. First, OSA is highly prevalent in the U.S with approximately 15 % of adult population (over 18 million) being affected [8, 9] and in future years, this prevalence is most likely to increase two to three fold due to increase in

obesity and older age [7, 10-12]. Second, OSA mediates severe cardiovascular diseases [6, 15] and is also concomitant with brain structural and cognitive impairments [16, 17, 31]. Recent studies have related OSA induced brain structural/functional changes to peripheral hypoxia and sleep fragmentation [16, 31, 33, 36]. Even though, repetitive hypoxia has been considered as a major contributor for cerebrovascular diseases, a recent study observed that repetitive hypoxia of low frequency and shorter duration, interspersed with periods of normoxia, prevents ischemic damage in rodent brain [37]. In addition, the effect of CPAP in the reversibility of cerebrovascular impairments is still inconclusive. While a few studies observed improvement in brain structure and function following CPAP treatment, almost equal number of studies showed no significant improvement at all [31, 35, 38, 39].

However, none of these studies have examined the combined effects of cerebral hemodynamics, cerebral oxygenation and arterial blood pressure which may play a significant role in the development of these impairments. Moreover, our group and other researchers have observed that cerebral blood flow velocity (CBFV) and blood pressure increases profoundly during an apnea episode [40-42] and drop below the baseline following apnea termination. Further, CO_2 is an important cerebral vasodilator [30]; hence OSA induced hypercapnea together with the above mentioned CBFV increase may lead to increased cerebral blood volume resulting in an increased brain oxygen supply and there by attempting to minimize brain injury [43]. Hence understanding the relations between blood pressure (BP), CBFV and brain oxygenation during apnea episode may provide more insight into the cerebral hemodynamics.

Since it has been shown that OSA elicits significant hemodynamic variations and results in cerebral oxygen desaturation [44], it is important to quantify the cerebrovascular variations induced by OSA and relate them to the systemic responses. From this study,

we will be able to elucidate and quantify the OSA elicited variations in cerebral hemodynamics concomitant with brain tissue oxygenation, as well as systemic variations in BP, CO2 and saturation of O2 in the blood. This can enable us to formulate a descriptive model for the relation between cerebral and systemic responses during obstructive sleep apnea.

1.3.2 Novelty of the Study

There are several innovations this study brings about: 1) for the first time it will provide data on simultaneous changes in cerebral blood flow (CBF), brain tissue oxygenation (BTO) and blood pressure (BP) during apnea episodes; 2) it will identify quantitative measures that can be derived from the recording of these hemodynamic responses to apnea; 3) descriptive models will be explored that will relate cerebrovascular changes to systemic variations mediated by apnea.

Only very limited number of studies have explored the apnea induced variations in cerebral hemodynamics by measuring the cerebral blood flow velocity changes during nocturnal sleep study mainly due to limitations in adhering the ultrasound transducer to the subject's head while sleeping. We have developed techniques to overcome this limitation and have successfully measured CBF from sleep apnea subjects throughout the entire night of polysomnography (nocturnal sleep study). Further, we have made customized forehead probes which can be used to successfully measure cerebral oxygenation from prefrontal cortex while minimizing subject discomfort.

The long term goal of this study is to assist physicians in deciding on the therapy regime for OSA patients based on a better understanding of how OSA affects the brain. The outcome of the proposed research can be used to improve the current CPAP treatment methodology. For instance, one may determine an effective treatment pressure

which will keep the airway open and at the same time eliminate the hemodynamic swings thereby minimizing cerebrovascular consequences.

1.3.3 Hypotheses

In order to explore a quantitative model for the cerebral hemodynamic variations during obstructive sleep apnea, we propose the following hypotheses:

I. Obstructive Sleep Apnea mediates significant variations in nocturnal cerebral blood flow and brain tissue oxygenation

II. Degree of fluctuations in cerebral blood flow velocity and brain tissue oxygenation during obstructive sleep apnea (OSA) is related to the OSA mediated systemic variations in arterial blood pressure, arterial oxygen saturation and carbon dioxide concentration.

To test these hypotheses and to quantity OSA elicited cerebral and systemic variations, we conducted overnight sleep study with 11 subjects suspected of having OSA. Features were extracted from cerebral and systemic hemodynamics and quantitative analysis were performed. The following chapters describe the methods employed to approach the hypotheses, present the results and discuss the findings in context of related literature.

Chapter 2 discusses the principle of operation of all the non-invasive monitors used in the study. This chapter also explains the experimental set up and protocol for sleep study.

Chapter 3 focuses on the development of a signal processing algorithms used and the feature extraction techniques. This chapter also deals with the development of mathematical model for dynamic cerebral autoregulation.

Chapters 4 present the hemodynamic variations during overnight sleep study. The postulations presented in the hypotheses are investigated.

Discussion of these results is presented in Chapter 5. Chapter 5 concludes this work with a summary of the results, laying the ground work for future research direction.

Chapter 2

Multi-Modal Physiological Recording and Experimental Protocols

Quantification of OSA effect on cerebral hemodynamics requires continuous noninvasive monitoring of blood pressure (BP), cerebral blood flow velocity (CBFV), arterial oxygen saturation (SaO2), carbon dioxide concentration (CO2) and brain tissue oxygenation (cerebral oxygenated [HbO] and de-oxygenated [HbR] hemoglobin concentrations). The following section describes in detail the measurement systems used.

2.1 Multi-Modal Physiological Recording

2.1.1 Noninvasive Blood Pressure Monitoring-Finapres

Blood pressure is traditionally measured by arm cuff measurement systems. Since the blood pressure changes during obstructive sleep apnea are extremely rapid, they cannot be completely estimated by intermittent cuff measurement [45]. One alternative to this standard method is noninvasive continuous beat to beat arterial blood pressure monitoring based on vascular unloading: Finapres (acronym for FINger Arterial PRESsure).

2.1.1.1 Principle of Operation

Finapres is based on pulsatile unloading of finger arteries with the Penaz method coupled with photoelectric transmission plethysmography [46-48]. In this method an electro-pneumatic servo controller generates a pulsating external cuff pressure which is equal and opposite to the intra-arterial pressure. This process is known as dynamic or pulsatile unloading of arteries and is used to clamp the artery at steady size irrespective of the pulsatile variations in blood flow. In this technique vascular unloading of radial and ulnar digital arteries are used. The non-pulsating diameter of the artery is obtained by

using the equation of transmural pressure (Pt), defined as the difference between intra-arterial pressure (Pa) and external cuff pressure (Pc) and given as follows;

$$Pt = Pa - Pc$$

As transmural pressure, P_t, increases the arterial wall dilates and as P_t goes to negative the arteries constrict due to viscoelasticity. Dynamic unloading of artery is obtained when the transmural pressure is zero, as follows:

$$P_t=0;$$

$$\text{i.e; } 0= P_a-P_c;$$

$$\text{i.e; } P_a=P_c$$

In this condition the blood volume stays constant and the cuff pressure will become equivalent to the intra-arterial pressure. This unloading process of the artery is enabled by the light absorbed by the photodiode of the plethysmograph and the variable set point of the servo control system. If the diameter of arteries increases due to increase in blood pressure, more light will be absorbed by the blood and less light reaches the photodiode of the plethysmograph, thereby decreasing its output to the servo system. The servo system instantaneously increases cuff pressure such that the transmural pressure remains at zero there by allowing the cuff pressure to be equivalent to arterial blood pressure.

2.1.1.2. Blood Pressure Monitor

Beat-to-beat nocturnal arterial blood pressure (BP) is measured noninvasively using Nexfin HD monitor (BMEYE, Amsterdam, Netherlands) which works on the Finapres principle discussed above. An additional feature of the unit that we used is that, it has an integrated heart-level compensation system that accounts for any hydrostatic pressure difference between the finger to which the sensor is attached and the level of the heart [47]. Validation studies have compared the blood pressure readings from Nexfin

monitor against invasive intra-arterial pressure measurements and with auscultatory measurements such as Riva Rocci / Korotkoff [49-51]. Average differences between Nexfin measurement and intra-arterial pressure measurements obtained from 50 patients were observed to be -1±7, 3±6, 2±6, and -3±4 mmHg respectively for systolic, diastolic, mean arterial pressure and pulse pressure [51]. These studies have shown that Nexfin provides accurate pressure measurements with good within-subject precision.

2.1.2 Cerebral Blood Flow Velocity Using Transcranial Doppler

Cerebral blood flow (CBF) can be measured indirectly by using Transcranial Doppler ultrasonography (TCD). TCD measures the blood flow velocity in major cerebral arteries (CBFV). Middle cerebral artery (MCA) is usually selected for this measurement since it is one of the major arteries supplying blood to the brain. Section 2.1.2.1 discusses the basic principles of operation of TCD and calculation of CBFV.

2.1.2.1 Principle of Operation

TCD works on the principle of ultrasound doppler to detect and measure the velocity of flow of liquids. The basic principle of the ultrasound doppler is that, sound waves are reflected by moving targets resulting in a frequency shift of the reflected waves. This shift in frequency corresponds to the velocity of the moving target. In TCD, piezoelectric crystals are used as transmitters and receivers. When an alternating voltage is applied, the crystal produces pressure waves which can be modulated to ultrasonic frequencies. Ultrasound pulse emitted by the transmitter travels through the tissue until it is reflected by a red blood cell. Continuous flow of red blood cells in the arteries will result in a frequency shift of the reflected wave. For example, if a red blood cell is moving with a velocity V, with the beam to flow angle θ, the Doppler shift can be expressed as:

$$f_d = \frac{2 f_t V Cos(\theta)}{c}$$

where, fd is the doppler shift (Hz); C is speed of sound in tissue (cm/s); ft is the transmitted beam frequency (Hz); V: velocity of blood (cm/s) or CBFV; θ is angle of insonation (degrees).

Furthermore, since the velocity of the ultrasound pulse in tissue is approximately constant, reflected pulse travels with the same velocity but with a shifted frequency. Thus, the round trip time of the pulse can be easily measured. This time is directly related to the distance of the red blood cell that reflected the beam, from the transducer surface.

Ultrasound can be used diagnostically in two modalities: Continuous wave and pulsed wave Doppler. In the continuous wave modality, the separate piezoelectric transducers are used as transmitters and receivers. In pulsed-wave Doppler, a single element transmits and receives ultrasound energy.

2.1.2.2 CBFV Monitor

In this study we have used TCD system TCD system (DWL, Compumedics, Singen, Germany) along with 2MHz pulsed transducer was placed on the temple of the subject to insonate the root of the MCA. The mean blood flow velocity in the MCA under normal conditions (in the supine posture) is approximately 55 cm/s with a standard deviation of about 12 cm/s. CBFV measured by TCD principle is proportional to the rate of blood flow and can be used as an index of CBF provided the diameter of artery remains constant [52]. Studies have shown that diameter of major arteries like MCA does not change significantly under different conditions and hence CBFV measured via TCD can be used as a reasonable measure of blood flow [7, 52].

2.1.3 Monitoring Changes in Brain Tissue Oxygenation

Functional near-infrared spectroscopy (fNIRS), a relatively new, noninvasive and low cost technology with high temporal resolution has been used widely to monitor the brain oxygenation and hemodynamics. Near-infrared (NIR) light typically ranges from

650-950 nm, where the absorption by water, melanin and hemoglobin are typically low thereby allowing the light to penetrate to several centimeters deep within a biological tissue [53-55]. Hence this wavelength range is often referred to as “optical window” [53]. The two dominant and clinically significant chromophores in this NIR region are (oxyhemoglobin (HbO) and deoxyhemoglobin (Hb) present in red blood cells) which absorb the NIR light based on the level of brain activity [53]. Hence measurement of NIR absorption can provide valuable information regarding brain oxygenation.

2.1.3.1 Principle of Operation

The basic principle of fNIRS utilizes the fact that, within the optical window, NIR light can penetrate around 1.5-2 cm through the scalp/skull and reach approximately 5-10 mm of outer cortical layer of the brain [55]. During fNIRS measurement, NIR light generated by laser diodes are guided through optical fibers to the brain surface. Since the human head is a highly scattering medium, photons do not travel in straight line; instead they change their directions after each scattering process. By placing an optical detector usually 3-4 cm away from source position, the photons exiting the head surface can be detected and guided via optical fibers to the fNIRS monitor [55]. The intensity of light returning from brain depends on the optical absorption of underlying tissue which can be quantified via natural logarithm of light attenuation referred to as optical density (OD). OD can be expressed using modified Beer-Lambert Law as given below:

$$OD = \ln\frac{I_e}{I_d} \cong \varepsilon CL(\mathrm{DPF}) + G$$

where, I_e and I_d are the emitted and detected light intensities, ε is the extinction coefficient; C is the chromophore concentration, L represents the mean path length travelled by photons from source to detector, DPF (differential path-length factor) accounts for compensation of various effective path lengths and G represents the

scattering loss [55-57]. Generally, L, G and DPF can be considered as constants during a monochromatic illumination in a turbid media with unchanging geometry [57]. Hence any changes in optical density (ΔOD) arising from increased cerebral blood flow, blood volume or oxygen metabolism, can be related to changes in chromophore concentration (ΔC) as:

$$\Delta OD = \varepsilon \Delta C L(\mathrm{DPF})$$

Since the major chromophores in NIR region are HbO and Hb, the above equation can be modified as:

$$\Delta OD^{\lambda} = (\varepsilon_{HbO}^{\lambda} \Delta[\mathrm{HbO}] + \varepsilon_{Hb}^{\lambda} \Delta[\mathrm{Hb}]) DPF^{\lambda} L$$

where $\Delta[\mathrm{HbO}]$ and $\Delta[\mathrm{Hb}]$ represents the change in HbO and Hb concentration; ε_{HbO} and ε_{Hb} are the molar extinction coefficients of oxygenated and deoxygenated hemoglobin respectively [56, 57]. The changes in optical density are dependent on the wavelength of NIR light used and hence is indexed by λ [55]. Hence by measuring the changes in OD at two or more wavelengths, concentration changes in HbO and Hb can be calculated [56].

fNIRS measurements can be performed by using three different instrumentation systems such as continuous wave, time domain and frequency domain measurement systems [53, 54]. A continuous wave (CW) system uses continuous light with constant amplitude and detects the amplitude decay of emitted light. They are the mostly commonly used fNIRS systems for brain imaging applications due to its low cost and high temporal resolution[55]. In time domain systems, ultrashort pulses of light (picosecond) are emitted to the brain, which will be broadened and attenuated by tissue layers such as scalp, skull, cerebrospinal fluid etc. Based on the shape of the temporal distribution of emerging light intensity, absorption and scattering properties can be determined. In frequency domain systems, light source is amplitude modulated at radio

frequencies and the amplitude decay and phase shift of detected light with respect to the incident light is used to calculate tissue optical properties [53, 54].

2.1.3.2 Brain Oxygenation Monitor

For this study, we have used a CW fNIRS system (NIRS 2, NIRSOptix by TechEn, Milford, Massachusetts) with frequency encoded laser diodes as emitters and Avalanche photo diodes (APD) as detectors. Frequency encoding enables to perform simultaneous measurement by each of the detectors. Optical measurements are obtained at two different wavelengths of 690nm and 830nm and are sampled at 200 Hz. Further, two sources and two detectors are used with a source-detector separation of 3.5cm. fNIRS systems have been widely used in measuring brain functional activities due to their excellent temporal resolution, low cost, portable and does not require any physically constraints thereby having a clear advantage over fMRI [58].

2.1.4 Peripheral Arterial Oxygen Saturation using Pulse Oximetry

Pulse oximetry is a non-invasive method of continuously monitoring arterial oxygen saturation in blood. Section 2.1.4.1 discusses the underlying principles of pulse oximetry.

2.1.4.1 Principle of Operation

Pulse oximetry combines the principles of spectrophotometry and photoplethysmography. The measurement system consists of two light emitting diodes (LED) which emits red (690nm) and infrared (940nm) light through blood perfused tissue such as digits or ear lobes [59]. These wavelengths are selected in such a way that there is a maximum difference between the absorption coefficients of the two major components of the blood which are oxyhemoglobin (HbO) and deoxyhemoglobin (Hb). In the red region absorption by Hb is almost ten times higher than HbO, whereas in near infrared HbO absorbs more light. Furthermore, the amount of blood perfusing the

underlying tissue will vary cyclically during each cardiac cycle. If more blood is present, less light that travels through the tissue bed to reach the photodetector. This pulsatile nature (AC) of the arterial blood flow allows pulse oximeters to isolate the signal attenuation caused by arterial blood flow, since light absorption from other components such as tissue, venous blood, and non-pulsatile arterial blood is generally static or unchanging (DC). Hence by combining the differential absorption of red and infrared light by Hb/HbO and the ratio of pulsatile to non-pulsatile light at the red and infrared wavelengths, arterial oxygen saturation can be calculated. Equation used for calculating percentage arterial oxygen saturation (%SaO_2) is given below:

$$\%SaO_2 = \frac{HbO}{HbO + Hb} * 100$$

Pulse oximetry can be used either in transmission mode or reflectance mode. In transmission mode, the emitter and photodetector are placed on the opposite sides of finger or ear lobes. In reflectance method, the emitter and photodetector are placed side by side with each other to detect the back scattered light [59].

2.1.4.2 Pulse Oximeter Monitor

A Nellcor oximax N-600x monitor (Nellcor Inc., Pleasanton, CA) is used for this study. A finger probe which houses the light emitting diodes (LEDs) and photodetector will be used in conjunction with the above pulse oximeter. Studies have shown that pulse oximeters have an excellent accuracy of ±2 to ±3% over the range of oxygen saturation between 60-100% [59, 60].

2.1.5 Measurement of End Tidal Carbon Dioxide using Capnography

Absence of breathing during OSA can lead accumulation of carbon dioxide in the tissues leading to hypercapnia. Since hypercapnia can adversely affect the pulmonary, central nervous system and cardiopulmonary system, monitoring of CO_2 during OSA is

essential [61]. The noninvasive monitoring of CO_2 is achieved by Capnography and is described in detail in Section 2.1.5.1.

2.1.5.1 Principle of Operation

Most capnographic devices work on the principle of absorption of infrared (IR) light by CO_2 molecules and uses a non-dispersive Infrared (NDIR) sensor [62]. NDIR sensor consists of an infrared source, light tube or sample chamber, interference filter and infrared detector. CO_2 sensor uses a beam splitter to split the generated IR light such that one beam passes through the sample chamber containing CO_2 mixture and another beam through a reference chamber free of CO_2. Since, maximum IR absorption by CO_2 molecules occurs at 4.26 μm, IR light passing through the sample chamber is filtered at this specific wavelength. Meanwhile, a nasal-oral cannula is used to collect the exhaled gas mixture and is transported to the sample chamber. Presence of CO_2 in the gas mixture leads to decline in the intensity of IR light falling on the detector. Higher the amount of CO_2 present in gas mixture, higher the IR absorption and lower the detected light. Hence by comparing the difference in detected intensities between the sample and reference chamber, CO_2 concentration can be calculated using Beer Lambert's Law as given below:

$$I = I_0 \cdot e^{kC}$$

where, I_0 is the intensity measured from reference chamber , I is the intensity of the light after CO_2 absorption, k is a constant, C is concentration of CO_2 in the gas mixture. The CO_2 concentration measured by this method is usually expressed as partial pressure of CO_2 (PCO_2) in mmHg. This can be converted to percentage CO_2 by dividing PCO_2 by the atmospheric pressure [62, 63].

2.1.5.2 CO_2 Monitor

In this study we have used a Capnogard ETCO2 monitor (Model 1265, Philips Respironics, PA, USA). End-tidal carbon dioxide (ETCO2) is the maximum concentration or partial pressure of the CO2 at the end of exhalation. The normal ETCO2 range is 35-45 mmHg. Infrared light is generated on one side of the U-shaped sensor and the detector is placed on the opposite side with an airway adapter in between. The exhaled gas is sampled via vacuum through nasal-oral cannula to the sample chamber of the adapter. Amount of detected light is converted into CO2 levels by a proprietary adaptive digital detection algorithm system. CAPNOGARD measures ETCO2 in the range of 0-100 mmHg. The system is accurate to ±2 mmHg from 0-40 mmHg, and between ±5% ─ ±8% of reading from 41-100mmHg [64].

2.1.6 Computer Based Data Acquisition System

The analog outputs from BP, CBFV, SaO_2 and CO_2 monitors are given to the Data Acquisition Unit (DAQ). This study used DAQ 6024 E which is a 200 kS/s, 12 Bit, 16 Analog Input Multifunction DAQ. It has two 12 bit analog output lines, 8 digital I/O lines, and two 24 bit counters manufactured by the National Instruments (Austin, TX). The analog outputs from monitors are passed on to a printed circuit board that interfaces with the DAQ called CB-68 LP. CB-68 LP is a 64 Pin I/O connector Block which acts as an interface between the monitors and DAQ. The output from CB-68 LP is passed on to the DAQ. DAQ digitizes the signals at a sampling frequency of 1 kHz and the output is acquired using custom program developed in Lab VIEW 9.0 software. The digitized data from the DAQ is stored as .lvm (LABVIEW Measurement) files which can be imported as text file in MATLAB for further analysis. The brain oxygenation data collected by the NIRS2 CW system was synchronized with the digitized data from DAQ.

2.2 Experimental Set Up

In order to quantity the effect of OSA on systemic and cerebral hemodynamics, we conducted 8 hour overnight polysomnography on 11 OSA subjects (6 Males, 5 Females; Age: 54.27±6.23 years, BMI:34.95±7.06kg/m2, AHI: 57.39±28.43) in supine position. Initially 15 subjects were enrolled for the study. However, due to issues with data acquisition, data from 4 subjects were not used in this study. Prior to polysomnography, the subjects were given complete instructions about the experiment and signed an informed consent that was approved by the institutional review board. The following section describes the experimental set up.

2.2.1 Commencing Multimodal Physiological Monitoring

The wrist unit of BP monitor which connects the finger cuff and heart reference system to the Nexfin monitor was wrapped around the wrist of subject as seen in Figure 2-1 (a) and (b). The finger cuff was placed on left hand middle finger between the two knuckles (inter phalangeal joints) of the middle phalanx (Figure 2-1(b)).

(a) (b)

Figure 2-1 Blood Pressure Monitor and Sensor Attachment

Pressure transducer of the heart reference system was fastened to a finger strap and was wrapped around the middle phalanx of left hand index finger; whereas the heart reference box was attached to the subject's clothes at approximately heart level. Calibration of the heart reference system was done to zero the HRS before attaching the

sensor to the subject's arm. An automatic recalibration of the unit, called Physiological was performed approximately every 70 heart beats to preserve the accuracy of the measurement for prolonged measurements [65].

For the CBFV measurement, a 2MHz transducer was placed on the temple of the subject and the ultrasonic beam was adjusted to insonate the root of the MCA. With the volunteer in a comfortable sitting position ultrasonic gel was applied to the transducer and the temporal region of the volunteer's cranium, just above the eye. After the MCA signal was found, in order to stabilize the blood flow velocity sensors against motion artifacts arising from subject movement during sleep, we have customized the way sensor was attached to the forehead. A customized mold was made for each subject based on his/her temporal region just in front of the ear and strapped using velcro band as shown in Figure 2-2 top leftmost panel.

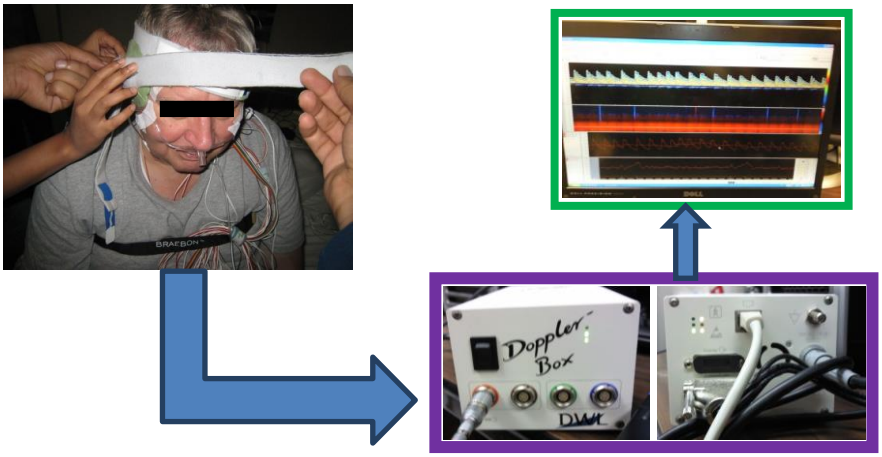

Figure 2-2 Doppler Ultrasonic Monitor and Sensor Attachment

Brain oxygenation data was collected by using a pair of fNIRS sensor and two detectors with a nearest inter-optode distance of 3.5 cm was attached to the subject's left

forehead using medical adhesive band and elastic bandage. Care was taken to avoid the sinuses. Inter-optode distance of 3.5 cm enables to measure hemodynamic changes within the top 2–3 mm of the cortex. Figure 2-3 shows the brain oxygenation monitor. Figure 2-4 (a) and (b) illustrates the configuration of source and detectors as well as the placement of optodes.

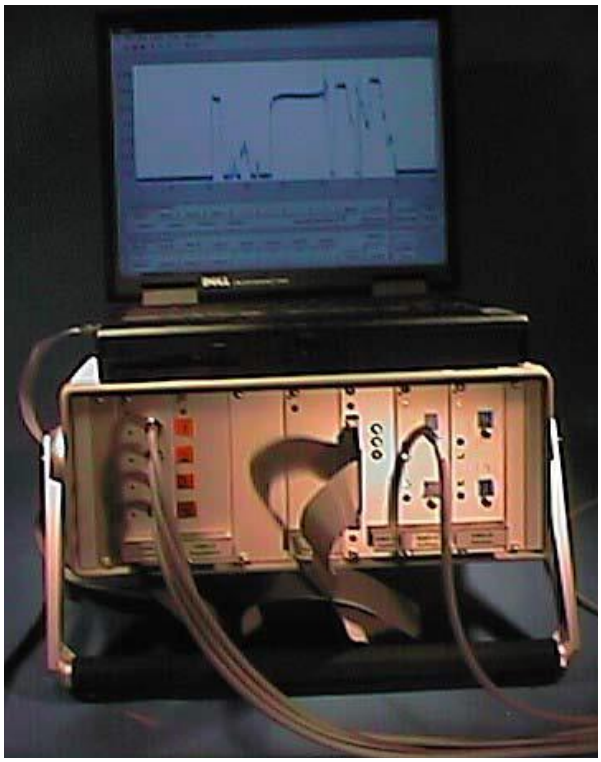

Figure 2-3 Brain Oxygenation Monitor

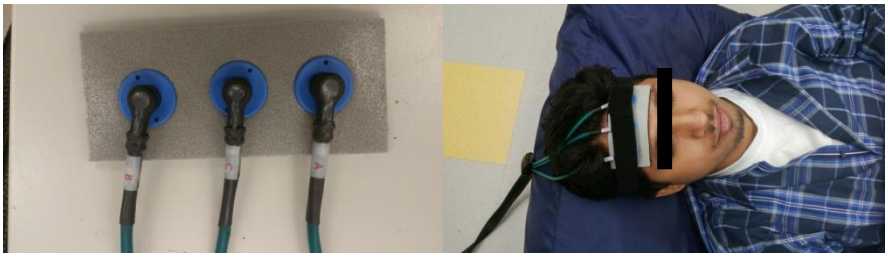

(a) (b)

Figure 2-4 Source-Detector Configuration and Optode placement on Forehead

For accurate measurements of CO_2, calibration of the sensor was done by first zeroing it to room air, and then placing it on a reference cell which consists of a gas of known CO_2 concentration. After the calibration procedure, an oral-nasal sampling cannula was inserted in the nasal cavity and over the mouth of the subject and was secured using a medical adhesive tape as depicted in Figure 2-5 (a) and (b).

(a) (b)

Figure 2-5 Carbon Dioxide Monitor and Sensor Attachment

As shown in Figure 2-6 (a) and (b), SaO_2 finger probe was fastened on the right hand index finger of the subject using medical adhesive tape.

(a) (b)

Figure 2-6 Oxygen Saturation Monitor and Sensor Attachment

2.2.2 Experimental Protocol for Sleep Study

Overnight polysomnography was conducted on 11 subjects who have been previously diagnosed of having OSA. Experimental set up is as shown in Figure 2-7 Experimental Set UpFigure 2-7.

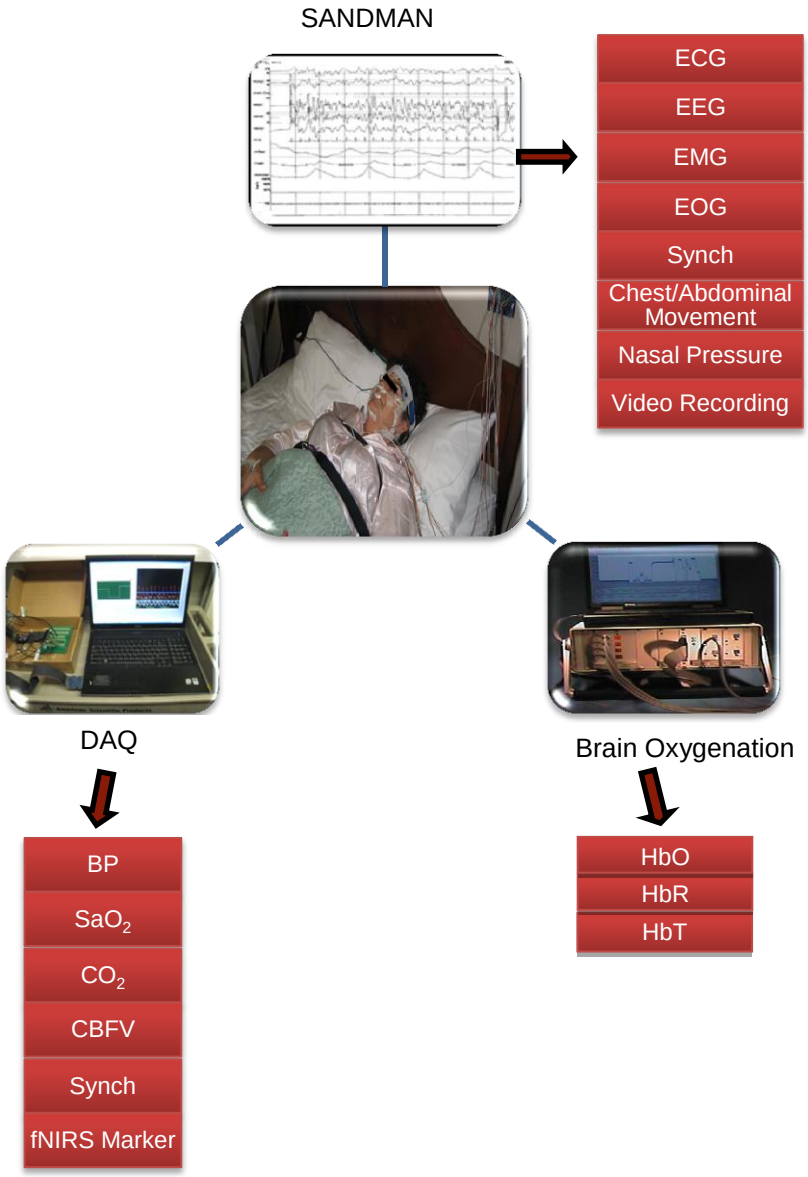

Figure 2-7 Experimental Set Up

BP, CBFV, SaO_2 and CO_2 were recorded concurrently using the DAQ system described in section 2.1.6. Brain oxygenation data was collected using fNIRS monitor (section 2.1.3.2). In addition, full polysomnography including electroencephalogram (EEG), electro-oculogram (EOG), electromyogram (EMG), oral-nasal airflow, chest-abdominal

movement, leg movements, snoring, blood oxygen saturation and a video monitoring of the subject was conducted. Polysomnography data was recorded separately on a sleep diagnostic system (Digital 32+ Amplifier, Embla, Broomfield, CO) integrated with Sandman Elite software (Embla, Broomfield, CO) for offline scoring of the data. Data from Sandman, DAQ board and brain oxygenation monitor were synchronized to ensure that there is no time lag between the data collected on these systems which is described in the following section.

2.2.2.1 Synchronizing DAQ and Sandman Systems

During the sleep study, LabView program was used to generate a synchronizing signal (Synch) simultaneously with the data acquisition (Figure 2-7). This synch signal takes the system time as input and generates three pulses corresponding to hours, minutes and seconds as shown in Figure 2-8 .

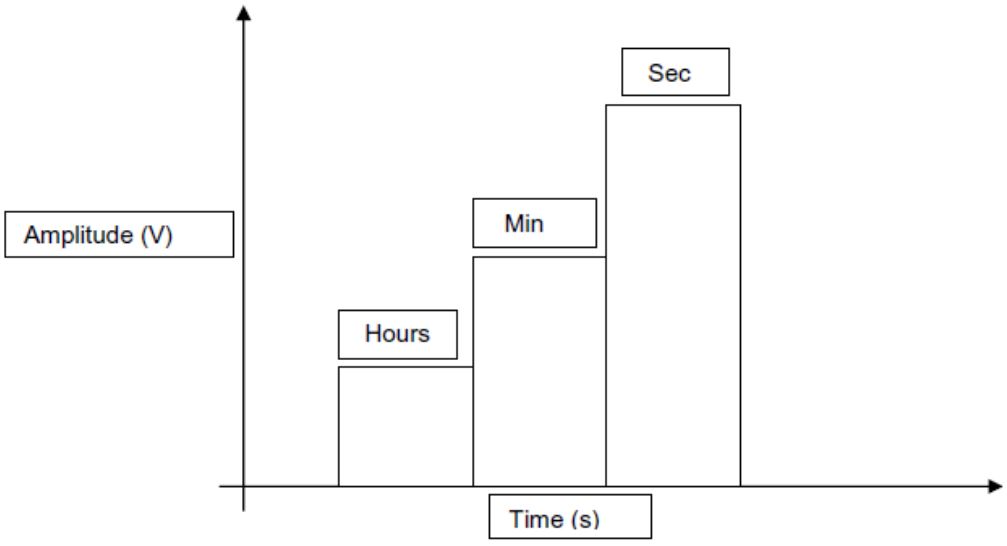

Figure 2-8 Synchronizing Signal

The magnitude of each pulse depends on the value of the hour, minutes and seconds at the time of signal generation. These values were further converted to a

particular voltage within the range of 0-1 V which was compatible with the Sandman system. The corresponding voltages for hours, minutes and seconds represent the amplitudes of each of the square pulses. The synch signal was then fed back into the DAQ and Sandman systems. Acquiring this synch signal via both DAQ and Sandman systems ensures that both systems can be synchronized perfectly with no time lag between them. Further, the DAQ system also received an electrical marker signal (fNIRS Marker, Figure 2-7) which indicates the onset and end time of brain oxygenation data collection.

Chapter 3

Data Processing and Quantitative Modelling of Cerebral Hemodynamics

The raw data collected from the polysomnography underwent a series of preprocessing steps before useful features were extracted from the cerebral and systemic hemodynamic waveforms. These preprocessing steps and the feature extraction steps are described in detail in first section of this chapter. The second section of this chapter presents the quantitative methods used to test hypotheses I and II.

3.1 Data Pre Processing and Feature Extraction

As mentioned in 2.2.2, overnight sleep data from subjects were collected using three different systems: Sandman, DAQ and Brain Oxygenation monitor. The sections below describe the steps used in preprocessing, data segmentation and feature extraction from this data.

3.1.1 Data Preprocessing

3.1.1.1 Sleep Study

The data obtained from Sandman system were used to perform apnea scoring by a certified sleep technician, blind to the objectives of this study. The scoring is based on the sleep stages and the types of apnea events, subjects have experienced during the study [66]. This file also contained the onset time and duration of sleep stages as well as apnea events. This information was used to create an apnea marker signal. This signal comprised of normal breathing, apnea and hypopnea events. To distinguish between different events, normal breathing was assigned an amplitude of 10 arbitrary units (A.U), hypopnea as 4 (A.U), and obstructive sleep apnea as 1 (A.U). An example of this generated apnea marker signals is as shown in Figure 3-1.

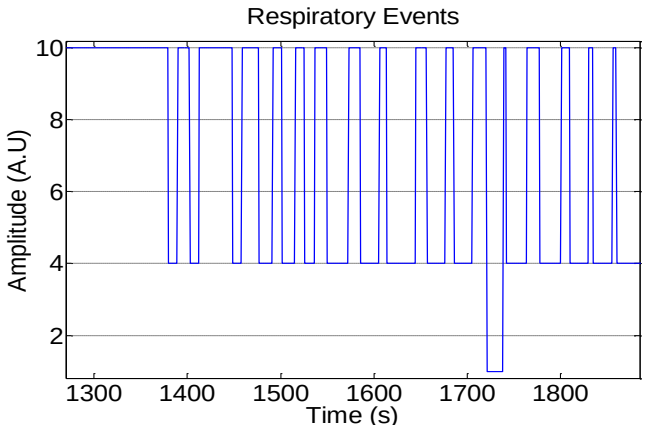

Figure 3-1 Apnea Marker Signal

After the marker signals were generated, the synch signal described in 2.2.2.1 was used to merge apnea marker signal obtained from the Sandman software with the signals collected using the DAQ board to obtain a single synched DAQ-Sandman file.

Meanwhile, raw oxygenation data from brain oxygenation monitor was imported into MATLAB software for further processing. Using the modified Beer-Lambert's law explained in 2.1.3.1, MATLAB algorithms were used to convert the optical light intensity to HbO, HbR and tHB values. Further, the time when brain oxygenation monitor started its data collection was specified by the fNIRS marker signal (Figure 2-7) in the DAQ board. Based on this signal, the HbO, HbR and HbT data derived from raw oxygenation data were merged into the synched DAQ-Sandman data file to form a single final synchronized data file for each subject. MATLAB graphical user interface (GUI) described in the following section was developed and used to segment this final synchronized data file into OSA clips, based on apnea marker signal.

3.1.2 Graphical User Interface for Data Segmentation and Feature Extraction

A multi-purpose GUI was designed in MATLAB environment to visualize the data, followed by clipping it into apnea episodes as well as to extract the features of different waveforms from each clip. The functionality provided in this software is explained below:

3.1.2.1 Data Segmentation

Waveforms of interest can be plotted by entering the specific channel numbers in a custom-designed MATLAB GUI. The GUI can accept .lvm type or .mat type files and allows the user to display up to four different signal channels at a time. It has the capability of visualizing large quantities of data at a time and saving various parts of the data as separate binary files. Figure 3-2 shows a screen shot of the GUI.

For the purpose of data segmentation, the data points of interest can be specified by using data cursor in the tool bar on the top of GUI. Required points can be selected by placing the cursor on top of the point in the waveform followed by double click. Once the starting and ending points are selected, the smallest value among the two is chosen as the start time and the data is clipped according to these positions. For extracting OSA episodes, the points are chosen such that, the data clip contains at least 5 s before the start of an OSA episode until the time when SaO_2 has returned back to its level before the apnea episode commenced (approximately 30-40s after the termination of OSA). Even though only four channels are displayed in the GUI, while clipping, all the channels present in the data file will be segmented based on the points selected. In this present study, there were 37 channels in the raw data file.

Once the data is clipped, it can be saved in a separate file. The user can name the file in which the data has to be stored as desired. The file will not be stored if a path is not entered. A text box is provided for this purpose. Clicking on the ‘Save Clip’ push button will save the clip in the specified file.

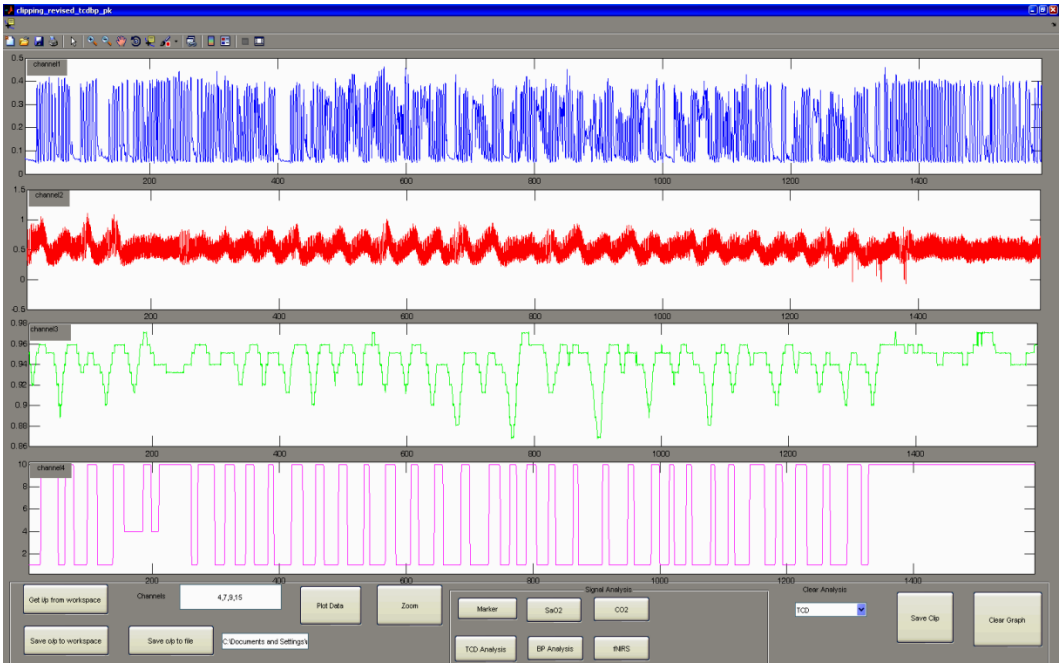

Figure 3-2 Screen Shot of the GUI for Clipping Data

The panels from top to bottom show (1) Channel 1: CO_2 (2) Channel 2: CBFV (3) Channel 3: SaO_2 (4) Channel 4: Apnea Marker

3.1.2.2 Feature Extraction

The clipped data file has 37 channels consisting of all the physiological signals and marker signals. GUI can also be used to extract features from BP, CBFV, SaO_2, CO_2, HbO, HbR and HbT present in this clipped data. The signal analysis section is framed within the red rectangle in Figure 3-3. It has several push buttons with the name of physiological signals associated with it. The functionality is explained below:

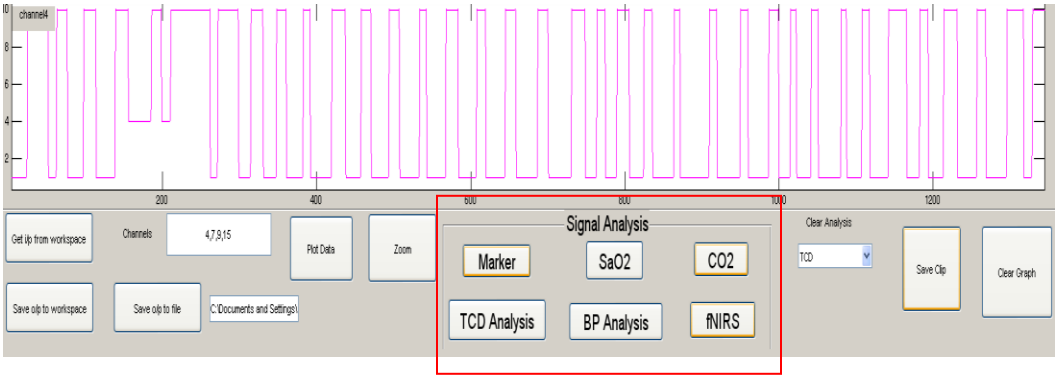

Figure 3-3 Screen Shot of GUI with Signal Analysis Section

Apnea Marker Signal: Once the "Marker" push button is pressed, GUI loads the currently clipped apnea episode. Further, the duration of the apnea episode is calculated and saved into an Excel file.

SaO2 Metrics: Amount of peripheral oxygen desaturation is an important feature in the detection of an apnea episode [67]. In order to extract this percentage drop, SaO_2 signal is loaded and the peaks and valleys are detected using custom designed peak detection algorithm as shown in Figure 3-4. The red straight red line indicates the apnea phase.

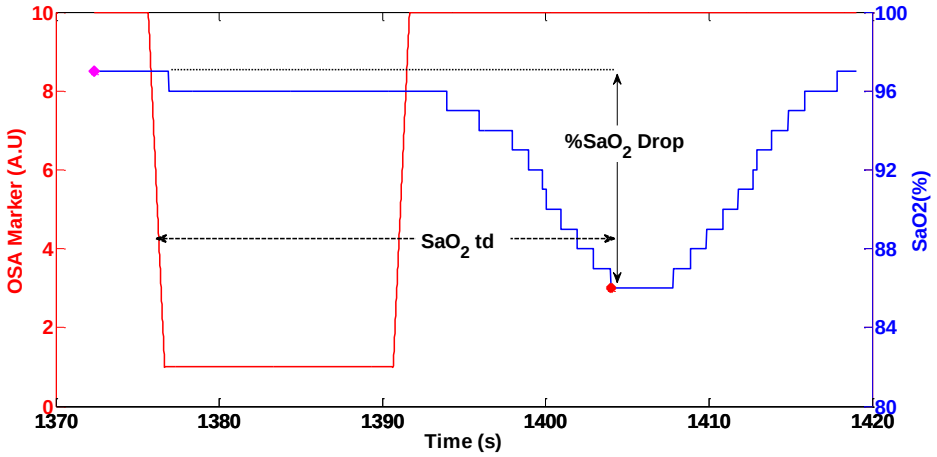

Figure 3-4 SaO_2 Feature Extraction

The maximum value of SaO_2 prior to the start of an apnea as well as its lowest value after the apnea termination is obtained. The drop in the SaO_2 (%SaO_2 Drop) was

calculated as the difference between these two values, as shown in Figure 3-4. Further, the time it took for the SaO_2 to reach its minimum value from the start of an apnea episode is calculated as shown in the figure by the abbreviation of SaO2_td.

CO2: ETCO2 can be used as a surrogate of arterial CO2 concentration and changes in ETCO2 are observed during hypoventilation [67]. In order to capture these changes, the CO2 waveform – recorded from capnograph -- was loaded into the GUI (Figure 3-5). The rising portion of the signal corresponds to the expiration and the falling portion of the signal corresponds to the inspiration. ETCO2 values were detected by finding the highest value of CO2 prior to inspiration (Figure 3-5). These values were detected using peak and valley detection algorithm by comparing the samples in each peak with the preceding and succeeding samples. Change in ETCO2 (ΔETCO2) was obtained by calculating the difference between ETCO2 value prior to the apnea and after apnea termination as shown in Figure 3-5.

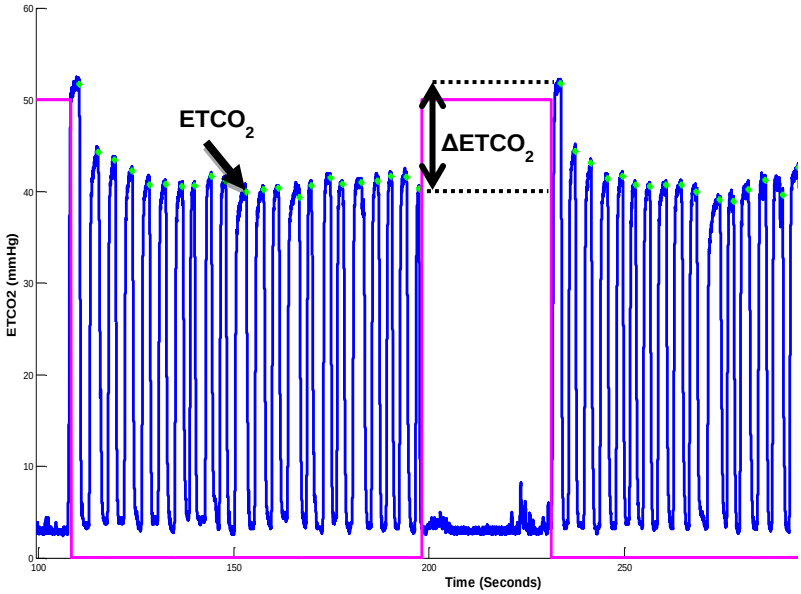

Figure 3-5 Feature Extraction from CO2 Waveform

BP and TCD Metrics: Features extracted from BP and CBFV waveforms were similar in nature. Hence the explanation of BP and CBFV feature extraction is given in one single section. A custom made program was developed to detect the peaks and valley of recorded blood pressure and CBFV waveforms contained in each of the clips. The detection of the proper peaks and troughs were validated by visual inspection and any missed detection or erroneously detected points were corrected. Peaks represents the systolic values, valleys represents the diastolic values in both BP and CBFV waveforms (Figure 3-6). Area under each pulse is calculated by numerically integrating the waveform between two consecutive diastolic troughs as shown in Figure 3-6. The average value of the waveform between two diastolic valleys was used for Mean calculation.

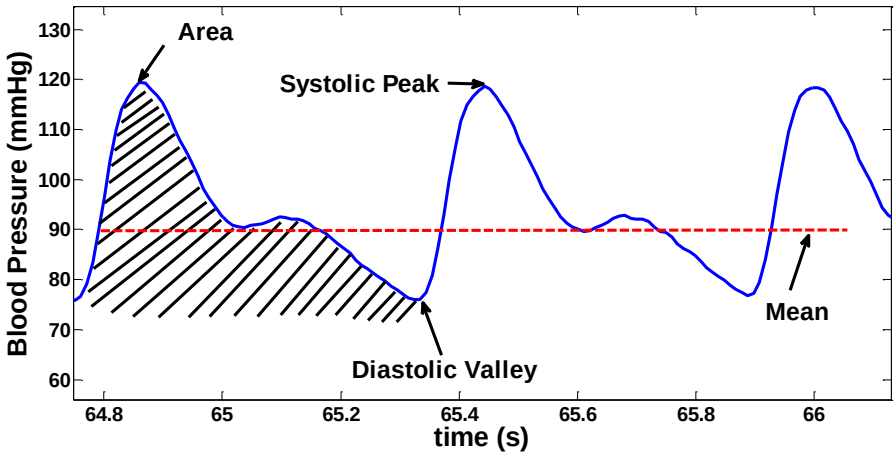

Figure 3-6 Extraction of Features from BP/CBFV Waveform

After the detection of systolic, diastolic, and computation of area and mean values, the following features were extracted for both BP and CBFV: 1) Percentage rise in systolic peak (%sys), 2) percentage rise in diastolic valley (%dia), 3) percentage rise in mean (%mean) 4) percentage rise in area (%area), 5) time to peak (tp), 6) slope of peak trend (sys_slope), 7) slope of valley trend (dia_slope) and 8) slope of mean trend

(mean_slope). For BP, these features were denoted by %sys_bp, %dia_bp, %mean_bp, %area_bp, tp_bp, sys_slope_bp, dia_slope_bp and mean_slope_bp. For CBFV, features were designated as %sys_cbfv, %dia_cbfv, %mean_cbfv, %area_cbfv, tp_cbfv, sys_slope_cbfv, dia_slope_cbfv and mean_slope_cbfv. Figure 3-7 shows a representative recording of the blood pressure waveform from an apnea clip along with peak and valley detection for amplitude and area calculation.

As explained in 3.1.2.1, each OSA episode consists of at least 5 seconds prior to the beginning of apnea marker signal. Hence minimum systolic peak (P2) and the corresponding diastolic valley within this ±5 seconds from the start of apnea marker were obtained. The peak average value, P_min was calculated as

$$P\_min = (P1 + P2 + P3)/3 \qquad (1)$$

where P1 and P3 are the preceding and succeeding peaks respectively. Similarly average value of diastolic valley was calculated. Further, area under each of these three pulses (A1, A2 and A3) was evaluated as the cumulative integration of waveform between two troughs as shown in Figure 3-7(b). Average area (A_{min}) was calculated similar to that of P_{min}. Average value of mean pressure or flow was also calculated under these three pulses. Further, the highest peak P5 occurring at the end or within 10s after the apnea termination, was obtained. Average values of amplitude and area, P_{max} and A_{max} were calculated similar to P_{min} and A_{min}.

For finding P5, a post-apnea window of 10 second was chosen based on visual inspection of CBFV and BP rise during multiple OSA episodes. Further, findings from other related studies showed that systolic peaks tend to reach its maximum value within 5±1 s after breathing resumption [7, 68], which justifies the chosen window.

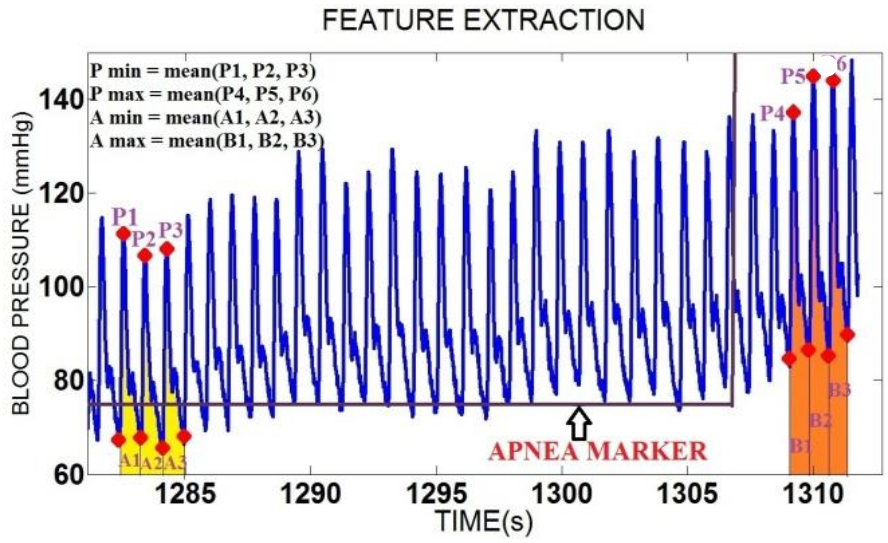

(a)

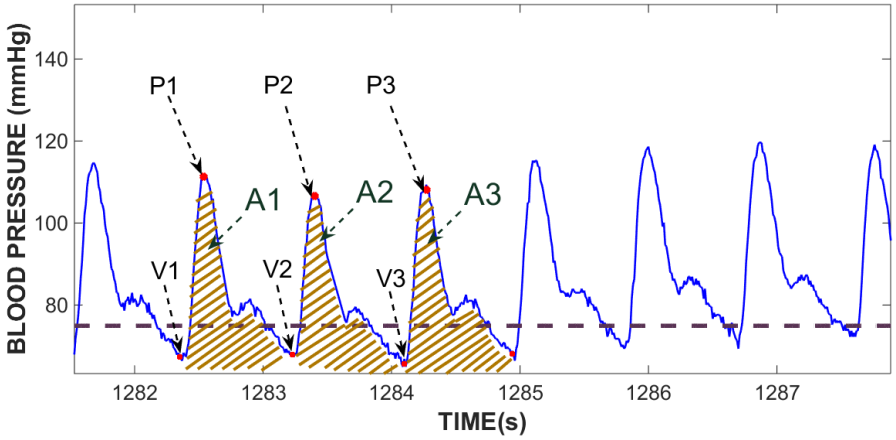

(b)

Figure 3-7 Percentage Rise in Amplitude and Area Calculations

Shaded region shows the pulses used for calculation of percentage rise in area and mean values.

The percentage change in peak and area were calculated as follows:

$$\%\, Sys = \frac{P_{max} - P_{min}}{P_{min}} x100 \qquad (2)$$

$$\%\, Area = \frac{A_{max} - A_{min}}{A_{min}} x100 \qquad (3)$$

Similar calculations were conducted to obtain percentage rise in diastolic and mean values. Time to peak (tp) was calculated as the time elapsed from the beginning of apnea marker till the occurrence of peak P5 (Figure 3-8).

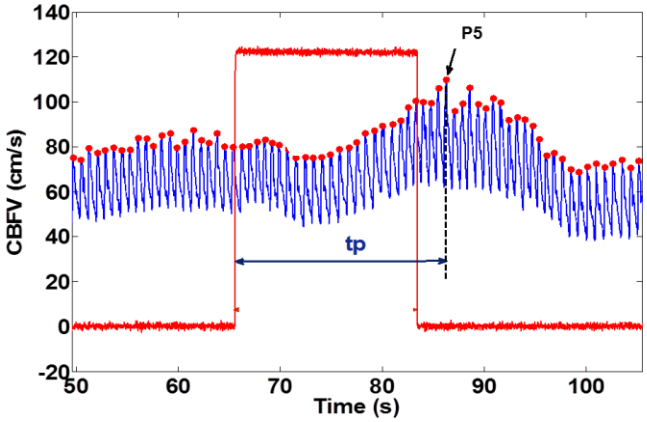

Figure 3-8 Calculation of Time to Peak (tp)

Sys_slope, dia_slope and mean_slope represents the rate of rise in their respective values due to physiological changes resulting from apnea. Sys_slope is estimated by fitting a linear line to the systolic values and evaluating the slope of that line and is shown in Figure 3-9. In example shown in Figure 3-9, a linear line with equation $y = m * x + c$ is fitted according to the systolic values and the m value gives slope which in the example shown is 0.65mmHg/s. The same procedure is used to find the slope of diastolic and mean values as well.

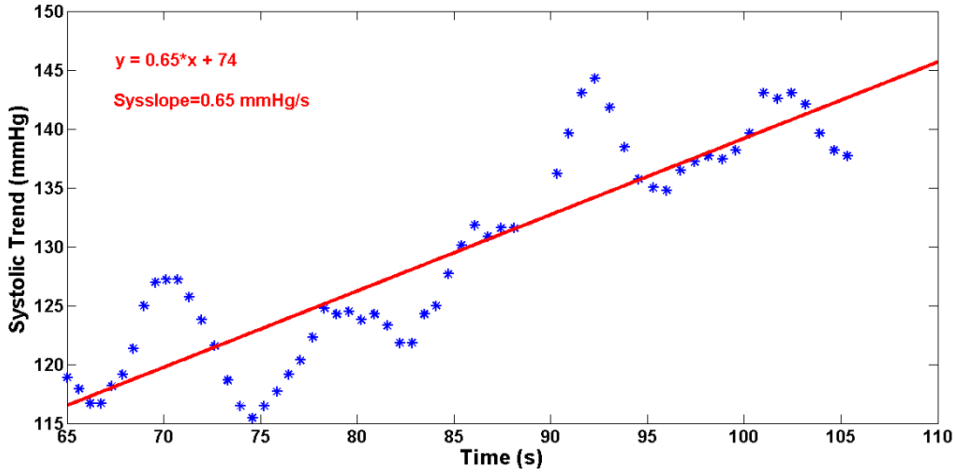

Figure 3-9 Slope of the Trends during an Apnea Episode

The * represents the systolic trend during an apnea episode. Solid red line represents the fitted linear line.

Brain Oxygenation Metrics: From the processed brain oxygenation data, HbO, HbR and HbT values were extracted. hbo_min was calculated as the apnea-induced drop in HbO compared to the HbO value at apnea initiation as seen in Figure 3-10. Further, the time elapsed from apnea initiation until the time when HbO dropped to lowest point was calculated as hbo_td.

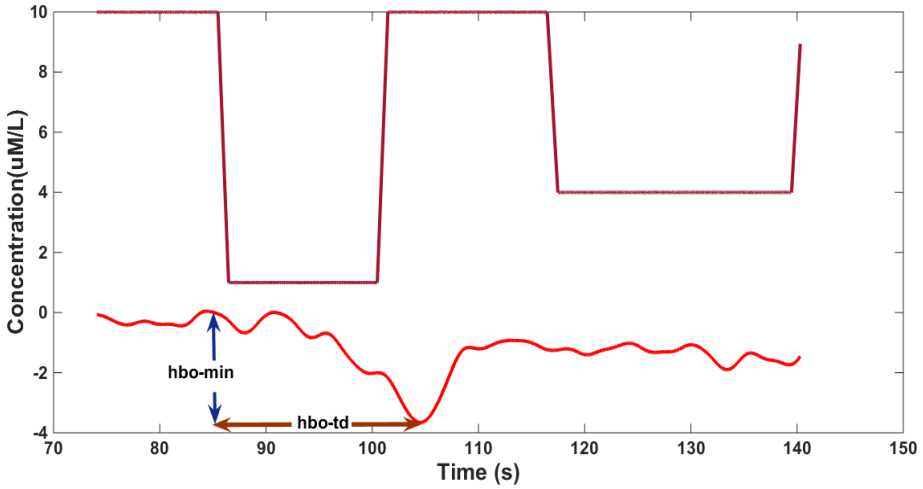

Figure 3-10 HbO Feature Extraction

From HbR data, hbr_max was calculated as the amount of rise in HbR compared to its value at apnea initiation as seen from Figure 3-11. The time HbR waveform reached its maximum value was indicated by hbr_tr.

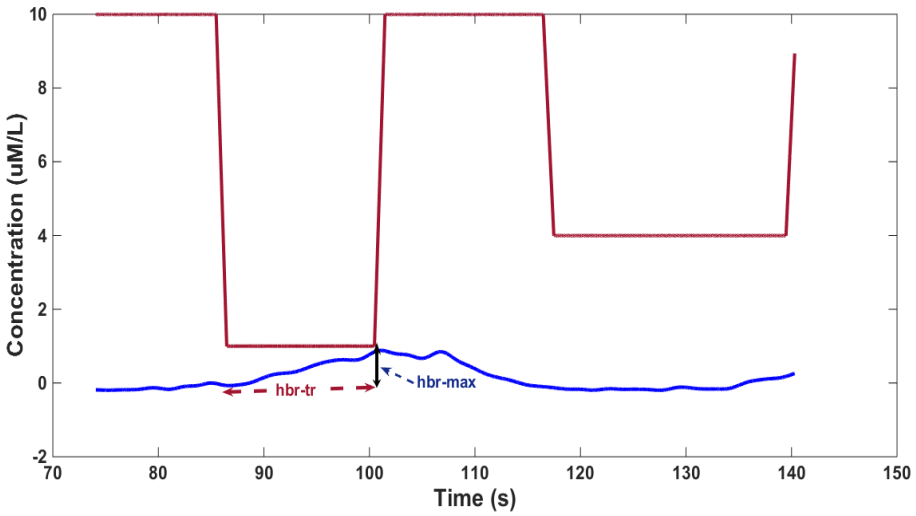

Figure 3-11 Features Extracted from HbR

HbO and HbR data were added together to get HbT which is an indicative of total blood volume. Similar to features derived from HbR waveform, maximum rise in HbT (hbt_max) and time to attain maximum HbT value (hbt_tr) were determined.

3.2 Quantitative Modelling of Cerebral Hemodynamics

The objective of this study is to attain insight into the interrelation between cerebral hemodynamics and systemic hemodynamics during apnea episodes. In order to achieve this goal we have used three different quantification methods: 1) Spearman's Correlation Coefficient, 2) Cross Correlation and 3) Autoregressive Moving Average model.

3.2.1 Spearman's Correlation Coefficient

Spearman's correlation coefficient is a non-parametric statistical method used to find the interdependence of variables. It is also less sensitive to the presence of outliers in the data [69]. Let the two variables whose interdependence to be obtained be labeled as x and y and each with *n* measurements. To obtain the correlation coefficient, the variables are first ranked. That is, if the measurements of x be denoted by *Xi* (i.e. X_1, X_2, . . ., *Xn*), then R*(Xi*) will represent the rank of *Xi*, where each rank is an integer, from 1 through *n*, indicating relative magnitude of X*i* with respect to either the maximum or minimum value of X*i*'s. That is, variables can be ranked either from high to low (e.g. rank 1 indicates the maximum value of x, rank 2 the second maximum, and so on, with rank *n* the lowest value of x) or from low to high. Similarly, the second variable Y will also be ranked based on the sequence of ranking in X. This test then utilizes the difference in ranks between the X and Y at the same position. In other words, Spearman rank correlation coefficient is obtained by subjecting the ranks, instead of the raw measurements, to the normal correlation calculations. Correlation coefficient is calculated using the following equation [70].

$$\rho = 1 - \frac{6\Sigma(di)^2}{n(n^2 - 1)}$$

where : di= Xi-Yi (difference between the ranks) and n= number of variables.

Perfect positive correlation (correlation coefficient=1.0) is obtained if the sequence of ranks were identical for both X and Y variables. A correlation coefficient of 0 indicates no correlation and -1 indicated strong negative correlation.

Spearman's correlation calculation also gives a p-value obtained from t-distribution [71]. The p-value does not provide an absolute measure of significance of correlation coefficients; however, it might be useful in deciding whether a correlation

exists at all. In other words, in Spearman's correlation, p-value is used to test the null hypothesis that the observed value of the Spearman rank correlation coefficient is obtained by completely random sampling of X and Y variables and does not represent the real correlation. If the p-value obtained is less than level of significance (in this study α=0.05), one can reject the idea that the observed correlation coefficient is due to random sampling; i.e. the correlation coefficient obtained indeed represent the degree of similarity between X and Y variable. However, if p-value obtained was greater than level of significance, it implies that the data do not give sufficient reason to conclude that the correlation is real and the observed correlation coefficient might be just due to chance.

3.2.2 Cross Correlation

Cross correlation is another method used to obtain the degree of similarity between two signals when the signals are shifted relative to each other. This method is primarily used to estimate small time delays between two finite length signals [72]. Cross correlation between two signals is obtained by first shifting one of the sequences and multiplying values in the shifted sequence by the values in the second (not shifted) sequence and finally summing all the product values for each shift. If there are two non-alternating-value signal sequences denoted by x(n) and y(n), then the cross correlation between x and y (r_{xy}) is given by the below equation:

$$r_{xy}(k) = \sum_{n=-\infty}^{\infty} x(n)y(n-k), \qquad k = 0, \pm 1, \pm 2, \ldots\ldots$$

where, k is the time shift or lag between x(n) and y(n). This means that the highest peak will occur in the cross-correlation signal when both x(n) and y(n) are properly aligned. The value of k at that point gives the time delay between x(n) and y(n). Using this information, it can be determined whether x(n) leads y(n) or x(n) lags behind

y(n). If time delay (i.e., k) is positive, then the signal x(n) lags behind y(n) by corresponding k samples. If time delay is negative, x (n) leads y(n).

3.2.3 System Identification: Dynamic Blood Pressure –Blood Flow Relationship

Correlation and cross correlation values give insight about the overall interdependence of two signals. However they do not describe the dynamics present within a system. System identification process can be used to model the dynamic response of a system and can be used to predict the physiological response for variations in system inputs [73]. One such mathematical model for linear systems is the autoregressive moving average model or the ARMA model. ARMA models can be used to predict behavior of a time series based on past values of output as well as present and past values of the input, using linear time invariant system. ARMA models are widely used for prediction of economic and industrial time series. They also have been applied to quantify the dynamics of biological systems [73].

3.2.3.1 ARMA Estimation Process

ARMA model is usually represented by shift operator notation of ARMA (p,q), where p is the autoregressive order and q the moving-average order. The difference equation of ARMA model for a system with one input and one output can be given as:

$$y(t) + a_1 y(t-1) + \ldots + a_{na} y(t-na) = b_1 x(t-nk) + \ldots + b_{nb} x(t-nb-nk+1) + e(t)$$

where, na and nb are the orders of the ARMA model, nk is the delay (number of input samples that has to occur before output is affected by the input); y(t) is the output at time t; y(t−1)…y(t−na) are the previous values of the output on which y(t) depends; x(t−nk)…x(t−nk−nb+1) are the previous and delayed inputs on which y(t) depends; and e(t) is the white noise. The parameter na also reflects the number of poles or the autoregressive (AR) parameters; whereas nb reflects the number of zeros.

Representation of physical system using ARMA model follows two major steps [73, 74]:

1) Identification of the model:

In this step appropriate model order (values of na, nb and nk) that are required to describe the system are determined. Several algorithms have been used to identify the best model order based on least mean squared error (MSE) criterion or using automated iterative procedure by fitting many different possible model structures and orders followed by using goodness-of fit statistic to select best model [73].

In this study, MSE has been used as a measure of goodness of fit. MSE gives an estimate of the error in prediction by ARMA model. MSE is calculated as the average of the square of errors between the actual CBFV measured from transcranial doppler machine ($CBFV_{measured}$) and the CBFV estimated by the ARMA model ($CBFV_{estimated}$) as shown below:

$$MSE = \frac{1}{n}\sum_{i=1}^{n}(CBFV_{estimated} - CBFV_{measured})^2 \; ; \qquad n = number\ of\ samples$$

Out of all the models considered for an OSA clip, model with the least MSE value was considered as the best fitted model for that clip.

Best fit model among a group of models for an OSA clip can also be selected via using Akaike information criterion (AIC). AIC criteria can be expressed as

$$AIC \; = \; -2(\log -likelihood) \; + \; 2k$$

where log-likelihood is the maximized natural logarithm of likelihood function for the model and k is the number of estimated parameters in the model [75]. AIC index takes into account both statistical goodness of fit and the number of parameters required to achieve this particular degree of fit. Further, it also imposes a penalty for increasing the number of parameters. Among a set of models, model with lowest values of the AIC

index is the preferred model (the model with the fewest parameters that still provides an adequate fit to the data).

2) Estimation of Model Parameters:

Once the model orders are determined, the next step is to estimate the ‘a’ and ‘b’ coefficients of the model. Estimation of model coefficients can be achieved using least squares estimation technique [74]. Final step is to verify the results to ensure that the residuals of the model are random, and that the estimated parameters are statistically significant. In most cases, the model estimation process depends on the principal of parsimony; i.e. the best model is often the simplest model possible with least number of parameters that can adequately describe the system.

Chapter 4

Results

The features extracted from CBFV, BP, HbO, HbR, SaO_2 and CO_2 were analyzed to obtain the effect of apnea on cerebral hemodynamics. Further, quantitative analysis was carried out to investigate the possible interactions between systemic and cerebral hemodynamics. This chapter will present the results obtained from different statistical and quantitative analysis used in this study.

4.1 Effect of OSA on Cerebral Hemodynamics

According to Hypothesis I, OSA induces significant variations in cerebral hemodynamics. Following subsections provide the results obtained in support of this hypothesis.

4.1.1 Overall Effect of OSA on Cerebral and Systemic Hemodynamics

Figure 4-1 shows a graphical illustration of apnea induced variations in CBFV, BP, SaO_2 and CO_2 signals.

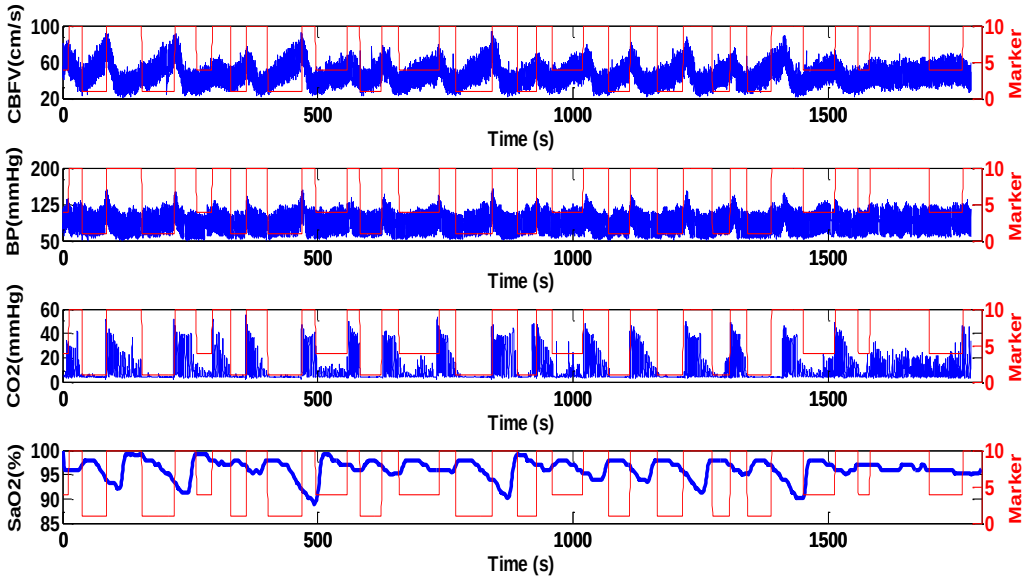

Figure 4-1 Variations in Physiological Signals during Apnea Episodes

Apnea and hypopnea episodes are marked by apnea marker signal indicated by red rectangle. OSA episodes are represented by marker amplitude of 1 (A.U), hypopnea as 4 (A.U), and as normal breathing as 10 (A.U). Detectable and fairly repeatable elevation in CBFV, during all OSA episodes, followed by recovery to baseline values during periods of normal breathing was observed. These variations occurred concomitantly with the changes in BP.

The changes observed in brain oxygenation i.e. HbO and HbR signals during apnea episodes are as shown in Figure 4-2. As seen from the figure, during OSA episodes the HbO concentration decreased reaching its lowest value at the apnea termination. There was a parallel rise in HbR concentration, with its maximum value occurring at apnea termination.

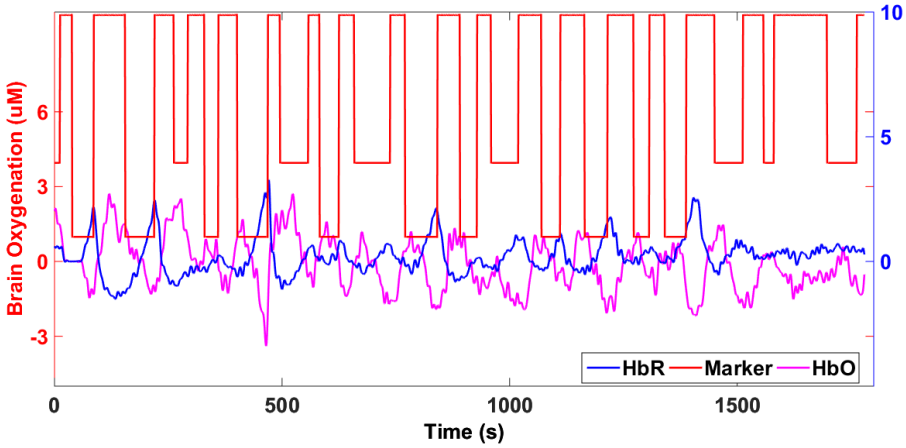

Figure 4-2 Effect of Apnea on Brain Oxygenation

4.1.2 Quantifying the Effect of OSA on Cerebral Hemodynamics

4.1.2.1 Selection of OSA Clips

OSA episodes were clipped from the overnight recordings of subjects as explained in 3.1.2.1. A subject can have multiple OSA episodes during the overnight

sleep study. Visual inspection of multiple synchronized sleep data files showed that OSA episodes can occur back to back resulting in less time for physiological signals to recover back to their baseline leading to a cumulative effect. Physiological variations due to these clusters of OSA episodes might be different from OSA episodes which have enough recovery periods between each other. Hence, to investigate the effect of single OSA episode on cerebral and systemic hemodynamics, only those OSA episodes which were separated by at least 15-20s of breathing period were considered for this analysis. Following this method a total of 178 OSA clips (N=178) were obtained from the all the 11 subjects which were used for all the further analysis. A drawback of this method was that a few severe OSA subjects had segments of OSA clusters with cumulative physiological effects and therefore were not included in this analysis. This leads to unequal representation of OSA clips from the subject population. Consequently, the results presented in this chapter might not be a representation of larger subject population. However, since each of the 178 selected OSA clips had sufficient time between each other, they can be considered independent of each other; hence the following results indicate a general representation of physiological mechanisms during single OSA episodes.

Further, the average values of cerebral and systemic hemodynamics signals given in this chapter and chapter 5 are expressed as Mean±SEM.

4.1.2.2 Cerebral Blood Flow Velocity

The percentage rise in systolic peak (%sys_cbfv), diastolic valley (%dia_cbfv), mean (%mean_cbfv) and area (%area_cbfv) of cerebral blood flow velocity was computed with respect to their respective values during the initiation of apnea (Section 3.1.2.2 Feature Extraction). The average values of the percentage rise across all the subjects are as shown in Figure 4-3.

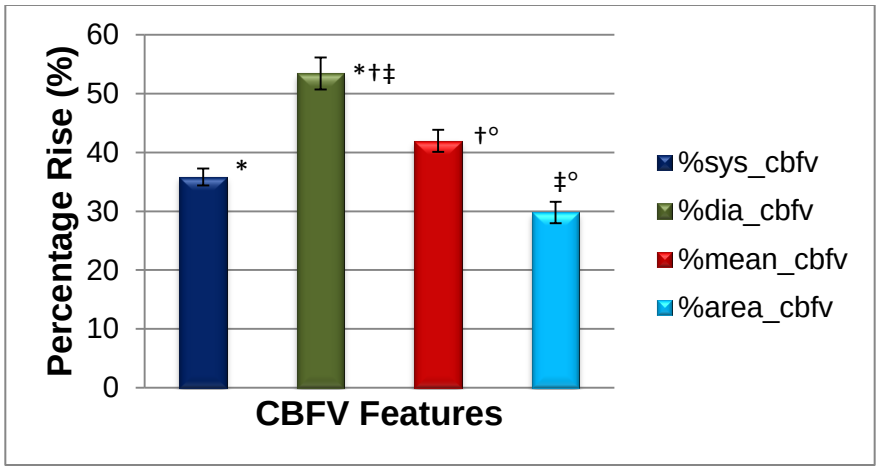

Figure 4-3 Percentage Rise in CBFV

Graph displays Mean ± Sem values for different CBFV features; N=178; % sys_cbfv refers to percentage rise in systolic peaks of CBFV; %dia_cbfv, percentage rise in diastolic valleys of CBFV; %mean_cbfv, percentage rise in mean CBFV; %area_cbfv, percentage rise in area of CBFV; *indicates that %sys_cbfv was significantly different from %dia_cbfv when ANOVA-post hoc analysis were conducted (α=0.05); †, ‡ indicates %dia_cbfv was significant different from %mean_cbfv and %area_cbfv respectively; ° denotes %mean_cbfv was different from %area_cbfv.

The average value of time required by CBFV to attain its maximum peak or tp_cbfv (see section 3.1.2.2 Feature Extraction) was found to be 29.19±0.98 s. The average values obtained for the rate of rise in systolic peaks, diastolic valleys and mean cerebral blood flow velocity are given in Figure 4-4.

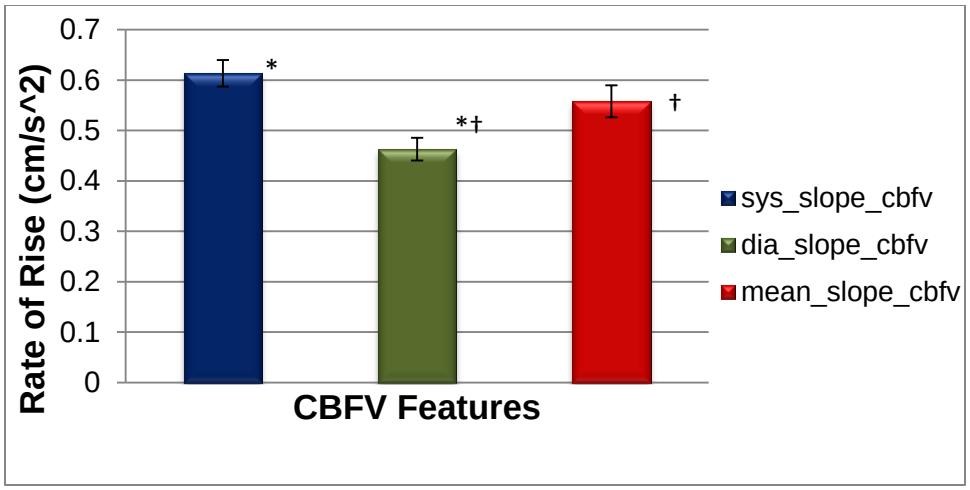

Figure 4-4 Rate of Rise in CBFV

Graph displays Mean ± Sem values for Rate of Rise in CBFV; N=178; sys_slope_cbfv refers to rate of rise in systolic peaks of CBFV; dia_slope_cbfv, rate of rise in diastolic valleys of CBFV; mean_slope_cbfv, rate of rise in mean CBFV; *indicates that sys_slope_cbfv was significantly different from dia_slope_cbfv when ANOVA-post hoc analysis were conducted (α=0.05); †, indicates dia_slope_cbfv was significant different from mean_slope_cbfv.

4.1.2.3 Brain Oxygenation

The fluctuations in brain oxygenation during OSA episodes were quantified. The average values for drop in oxyhemoglobin concentration (HbO_min), rise in deoxy hemoglobin (HbR_max) and rise in total hemoglobin (HbT_max) were calculated as explained earlier (section 3.1.2.2 Feature Extraction) and their mean values are given in Figure 4-5.

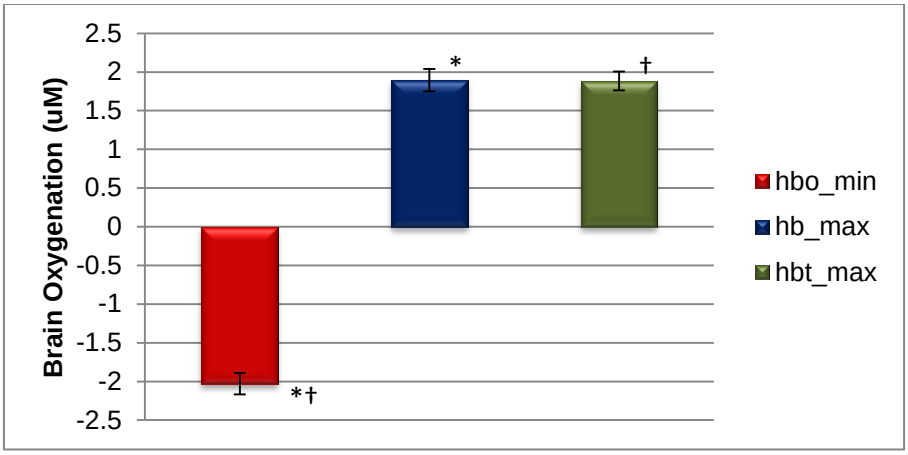

Figure 4-5 Mean Change in Brain Oxygenation during OSA

Graph displays Mean ± Sem values for Brain Oxygenation Data; N=178; hbo_min refers to drop in brain oxy-hemoglobin concentration; hbr_max, rise in deoxy-hemoglobin; hbt_max, rise in total hemoglobin; *,† indicates that hbo_min was significantly different from hbr_max and hbt_max when ANOVA-post hoc analysis were conducted (α=0.05);

From OSA beginning, the time required by HbO to reach its lowest value (HbO_td) as well as the time required by HbR (HbR_tr) and HbT (HbT_tr) to reach their maximum values were obtained (section 3.1.2.2 Feature Extraction). The average values were found to be 33.36±1.31s, 30.47±1.00s, and 34.00±1.25s for HbO_td, HbR_tr and HbT_tr respectively.

4.1.3 Quantifying the Effect of OSA on Systemic Hemodynamics

OSA induced changes in systemic signals such as blood pressure, arterial oxygen saturation and arterial carbon dioxide concentration were also quantified. From blood pressure signal, percentage rise in systolic peak (%sys_bp), diastolic valley (%dia_bp), mean (%mean_bp) and area (%area_bp) along with the rate of rise in systolic peaks (sys_slope_bp), diastolic valleys (dia_slope_bp) and mean blood pressure

(mean_slope_bp) were extracted (section 3.1.2.2 Feature Extraction). Further, time required by the BP signal to reach its maximum values (tp_bp) was also determined (section 3.1.2.2 Feature Extraction). From arterial oxygen saturation data, the drop in percentage SaO_2 (% SaO_2_drop) and time required to reach the lowest value (SaO_2_td) were extracted (section 3.1.2.2 Feature Extraction). Change in $ETCO_2$ ($\Delta ETCO_2$) was obtained from the CO_2 waveform (section 3.1.2.2 Feature Extraction). The Table 4-1 summarizes the average values of the features extracted from these signals along with the standard error.

Table 4-1 Effect of OSA on Systemic Hemodynamics

Systemic Signals	Features	Mean±SEM
BP	%sys_bp (%)	24.31±0.82
	%dia_bp (%)	29.26±1.07
	%mean_bp (%)	26.47±0.90
	%area_bp (%)	17.16±1.05
	Sys_slope_bp (mmHg/s)	0.88±0.05
	Dia_slope_bp (mmHg/s)	0.60±0.03
	Mean_slope_bp (mmHg/s)	0.81±0.04
	tp_bp (s)	33.27±0.98
SaO_2	% SaO_2_drop (%)	-6.45±0.29
	SaO_2_td (s)	44.08±1.27
CO_2	$\Delta ETCO_2$ (mmHg)	3.79±0.29

Table shows Mean ± Sem values for Systemic Hemodynamic signals; N=178;

4.1.4 Effect of OSA Duration on Cerebral and Systemic Hemodynamics

In order to obtain the relation between OSA duration and changes in cerebral and systemic hemodynamics, a correlation analysis was performed. Prior to correlation analysis, the normality of CBFV and brain oxygenation data was tested using

Kolmogorov-Smirnov normality test. The null hypothesis was that the features extracted from CBFV and HbO followed standard normal distribution. However, the data did not exhibit a Gaussian distribution ($p<5.60E-36$) for all the features extracted from CBFV and HbO. The p-values for the metrics are given in Appendix A. Hence non-parametric correlation analysis using Spearman's correlation analysis was performed. Table 4-2 and Table 4-3 show the correlation between OSA duration and cerebral hemodynamics.

Table 4-2 Effect of OSA Duration on CBFV

Features	Corr Coeff	P-value
%sys_cbfv (%)	0.58*	8.13E-17
%dia_cbfv (%)	0.48*	2.27E-11
%mean_cbfv (%)	0.27*	3.01E-04
%area_cbfv (%)	0.53*	5.19E-14
Sys_slope_cbfv (cm/s^2)	-0.25*	0.001
Dia_slope_cbfv (cm/s^2)	-0.13	0.09
Mean_slope_cbfv (cm/s^2)	-0.12	0.13
tp_cbfv (s)	0.93*	3.67E-78

N=178; * indicates significant correlation at α =0.05

Table 4-3 Effect of OSA Duration on Brain Oxygenation

Features	Corr Coeff	P-value
hbo_min	-0.089	0.24
hbr_max	0.35*	2.00E-06
hbt_max	0.27*	0.0004
hbo_td	0.76*	1.15E-33
hbr_tr	0.85*	1.26E-49
hbt_tr	0.77*	5.12E-35

N=178; * indicates significant correlation at α =0.05

For the systemic hemodynamics, a very strong and significant correlation ($r \geq 0.85$ and $p < 0.05$) was obtained only for tp_bp ($r = 0.95$; $p = 5.70E\text{-}87$) and SaO_2_td ($r = 0.85$; $p = 1.69E\text{-}49$). Weak significant correlations were obtained for all the rest of the features except for %area_bp. The correlation coefficients obtained for systemic hemodynamics are shown in Appendix B.

4.1.5 Effect of AHI on Cerebral and Systemic Hemodynamics

Association of apnea severity, measured as apnea –hypopnea index (AHI), with respect to the OSA induced variations in cerebral and systemic hemodynamics was also investigated. Since the cerebral hemodynamics did not exhibit a Gaussian distribution, Spearman's correlation analysis was performed. For this analysis, values of cerebral and systemic hemodynamics were averaged for each subject and compared with their respective AHI. None of the features showed a significant correlation with AHI ($p > 0.05$). The results are shown in Appendix C.

4.2 Quantitative Modelling of Relationship between Cerebral and Systemic Hemodynamics

4.2.1 Interactions between Systemic and Cerebral Hemodynamics

Spearman's correlation coefficient was used to investigate the relation between features extracted from systemic and cerebral data during OSA episodes. Only the moderate to very strong and significant correlation ($r \geq 0.5$ and $p < 0.05$) results are shown in Table 4-4 and Table 4-5. The complete results of correlation analysis are tabulated and given in Appendix D.

Table 4-4 Effect of Systemic Hemodynamics on CBFV

Systemic Features	CBFV Features	Corr Coeff	P-value
%dia_bp	%dia_cbfv	0.49	2.28E-12
%mean_bp	%mean_cbfv	0.49	1.75E-12
tp_bp	tp_cbfv	0.94	1.65E-79
SaO2_td	%sys_cbfv	0.59	1.16E-17
SaO2_td	%dia_cbfv	0.48	4.23E-11
SaO2_td	%mean_cbfv	0.54	1.38E-14
SaO2_td	tp_cbfv	0.84	4.49E-47

N=178; α =0.05

Table 4-5 Effect of Systemic Hemodynamics on Brain Oxygenation

Systemic Features	Features from Brain Oxygenation	Corr Coeff	P-value
%sys_bp	hbr_max	0.50	<0.00001
%dia_bp	hbr_max	0.46	4.94E-10
tp_bp	hbo_td	0.76	9.56E-34
sys_slope_bp	hbo_td	-0.46	3.26E-10
tp_bp	hbr_tr	0.84	5.28E-48
tp_bp	hbt_tr	0.73	1.99E-30
% SaO2_drop	hbr_max	0.57	5.45E-16
SaO2_td	hbo_td	0.71	5.04E-28
SaO2_td	hbr_tr	0.76	6.40E-34
SaO2_td	hbt_tr	0.70	7.98E-27

N=178; α =0.05

As seen from Table 4-4 and Table 4-5, time to peak/time to drop in all the systemic and cerebral signals were strongly correlated (r≥0.70). An illustrative plot of tp_bp *vs.* tp_cbfv is as shown in Figure 4-6.

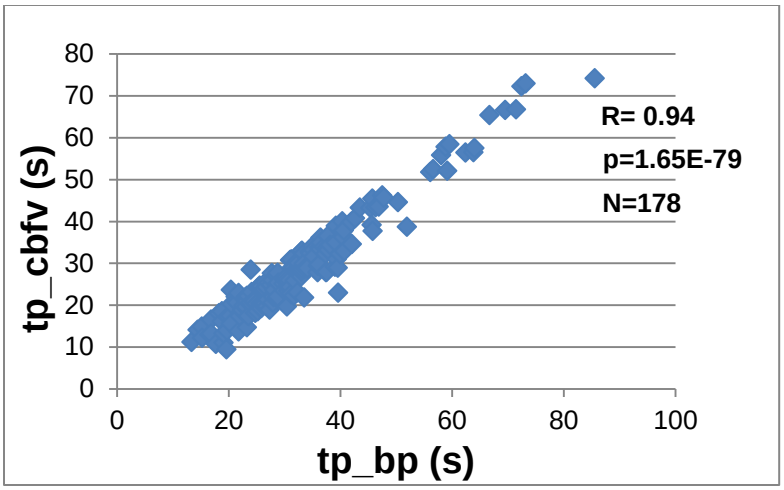

Figure 4-6 Time to peak in BP *vs*. Time to peak in CBFV

Further, all the features from CBFV were significantly correlated ($p<0.05$) with that of the BP features. The interrelation between mean blood pressure and mean cerebral blood flow velocity is as shown in Figure 4-7.

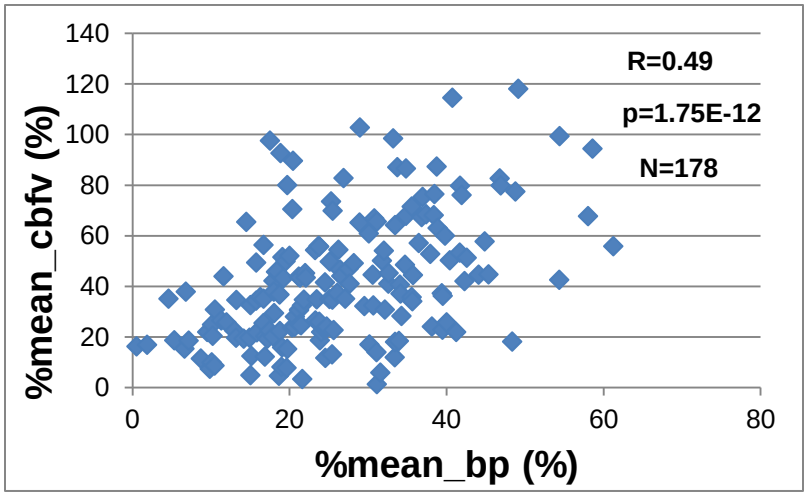

Figure 4-7 Mean Blood Pressure vs. Mean Cerebral Blood Flow Velocity

A weak significant correlation ($r<0.5$; $p<0.05$) was obtained between all CBFV features (except the slopes) and percentage drop in SaO_2 as well as with $\Delta ETCO_2$. As an

example, the association between $\Delta ETCO_2$ and percentage rise in systolic peaks of CBFV is as shown in Figure 4-8.

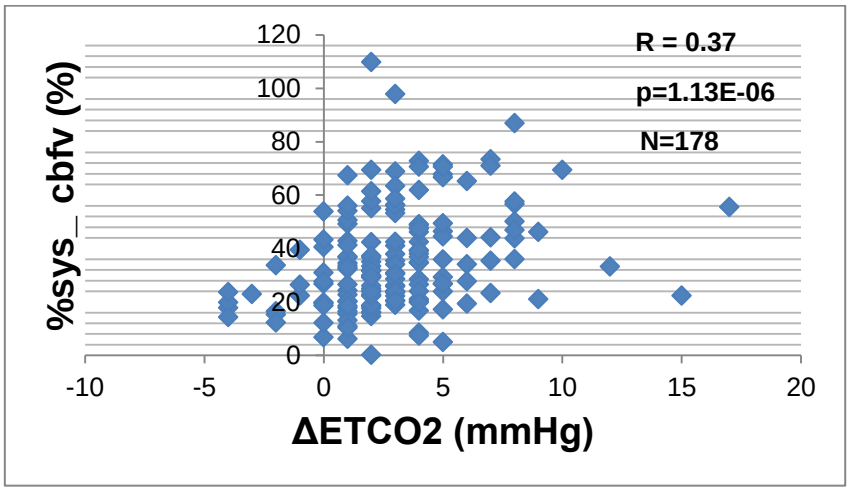

Figure 4-8 Relation between ETCO2 and CBFV Peaks

Statistically significant correlations were obtained between the percentage rise in systolic peaks, diastolic valleys and mean blood pressure with respect to the amount of drop in HbO as well as rise in HbR and HbT. An illustrative plot of the effect of percentage rise in systolic pressure to the HbO drop is shown in Figure 4-9. The time it took for HbO to reach its minimum value was significantly correlated with all the metrics of BP, except percentage rise in BP area. Similar results were obtained for the time to rise in HbR and HbT with respect to the BP features.

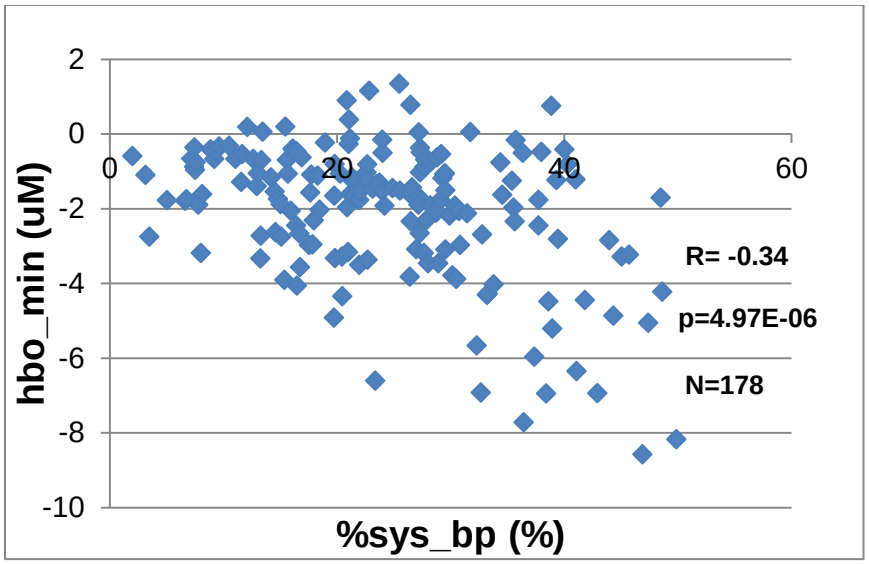

Figure 4-9 Effect of Percentage Rise in Systolic Pressure on HbO

$\Delta ETCO_2$ and percentage drop in SaO_2 did not have a statistically significant correlation with the drop in HbO concentration. However, $\%SaO_2$_drop was significantly associated with the rise in both HbR and HbT. The correlation between drop in arterial oxygenation and rise in cerebral deoxyhemoglobin concentration is as shown in Figure 4-10. $\Delta ETCO_2$ was significantly related to rise in HbT, but not in HbR. Furthermore, the time to rise in HbR and HbT as well as the time to drop in HbO were significantly associated with changes in $\Delta ETCO_2$, $\%SaO_2$_drop and SaO_2_td.

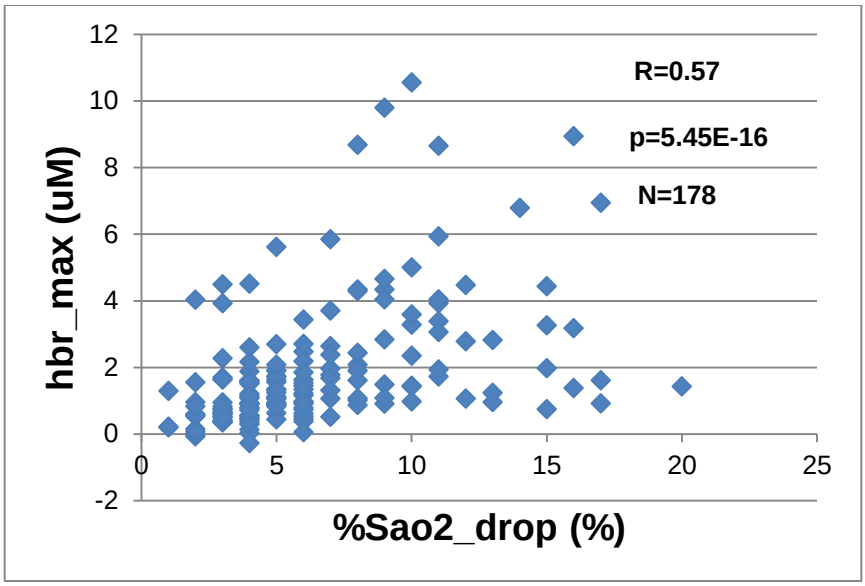

Figure 4-10 Correlation between Drop in Peripheral Oxygen Saturation and Cerebral HbR Concentration

4.2.2 Effect of CBFV on Brain Oxygenation

The diastolic velocity as well as the rate of rise in diastolic and mean cerebral blood flow velocity had a weak but significant correlation with the drop in HbO concentration. Rise in HbR and HbT were weakly associated with percentage rise in systolic, diastolic and mean blood flow velocity as well as the time to rise in CBFV. Percentage rise in CBFV area had a weak correlation with the HbT rise. The time it took for HbO to reach its minimum value was strongly correlated with CBFV_tp and weakly correlated with all the rest of the CBFV features except the percentage rise in area. The correlation between CBFV_tp and HbO_td is as shown in Figure 4-11.

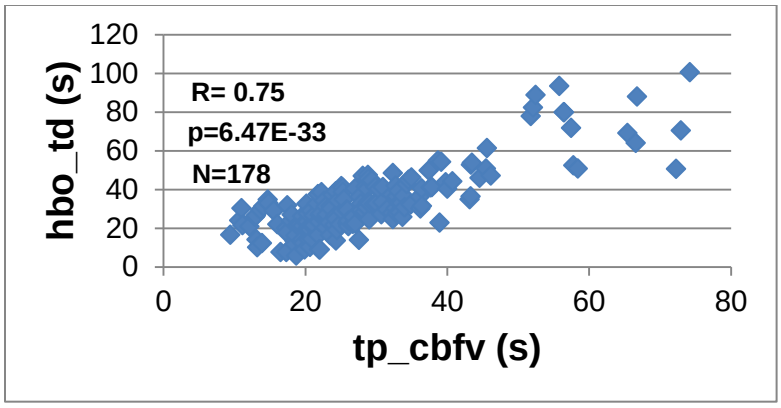

Figure 4-11 Effect of tp_cbfv on HbO_td

Time it took for HbR and HbT to reach its maximum values was correlated with the percentage rise in systolic, diastolic and mean velocities together with area and tp_cbfv. The hbr_tr was also correlated with the rate of rise in systolic velocity. The complete results of correlation analysis are tabulated and given in Appendix E.

4.2.3 Time Delay between Systemic and Cerebral Hemodynamics

4.2.3.1 Delay between Blood Pressure and Cerebral Blood Flow Velocity

Cross correlation analysis was performed to determine if there exist a time delay between BP and CBFV. Prior to cross correlation analysis the data were normalized by subtracting the respective mean from the signal and dividing by its standard deviation [76]. Normalization was done to make the amplitude of both BP and CBFV comparable to each other, since the process of cross correlation involves multiplication of signal amplitudes. Illustrative plot of normalized BP and CBFV data are shown in Figure 4-12 (a) and (b).

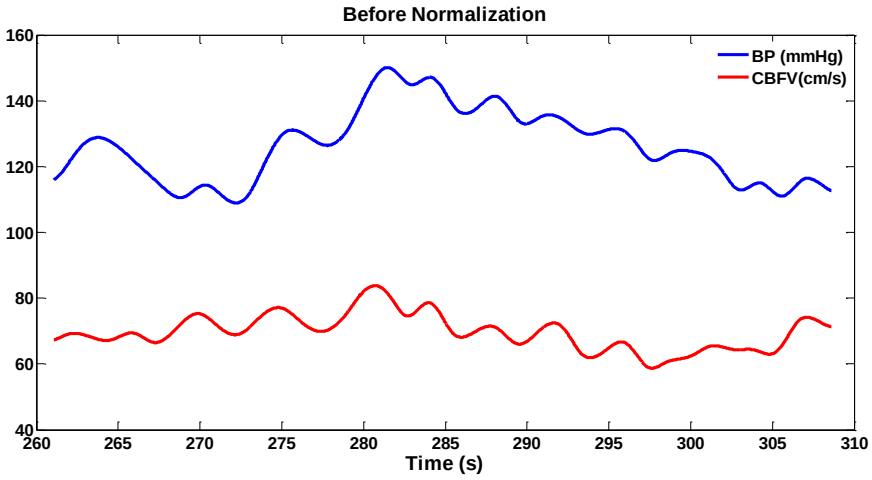

(a)

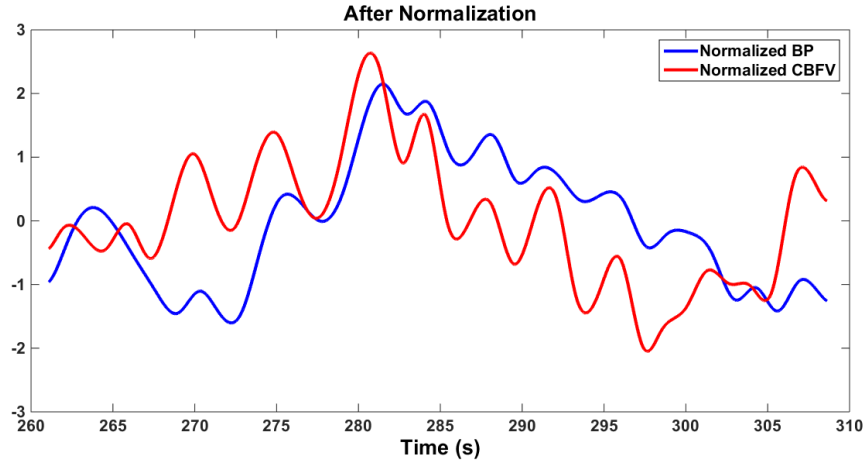

(b)

Figure 4-12 Illustrative Plot of BP and CBFV (a) before Normalization and (b) after Normalization

After normalizing the data, cross correlation analysis for CBFV and BP was done to determine if a time delay between these two signals exists. An example of cross correlation plot is as shown in Figure 4-13. As seen from the figure, it was observed that there is a positive lag between BP and CBFV indicating that the BP lags behind CBFV. The average delay between BP and CBFV systolic peaks was found to be 6.20±0.45s

(indicated by 'bp_cbfv_sys_delay' in Figure 4-14 Range of Delays between BP and CBFV) and for the diastolic valleys it was 3.98±0.27 (indicated by 'bp_cbfv_dia_delay' in Figure 4-14 Range of Delays between BP and CBFV). Box plot representation of the range of delays obtained between BP and CBFV are as shown in Figure 4-14.

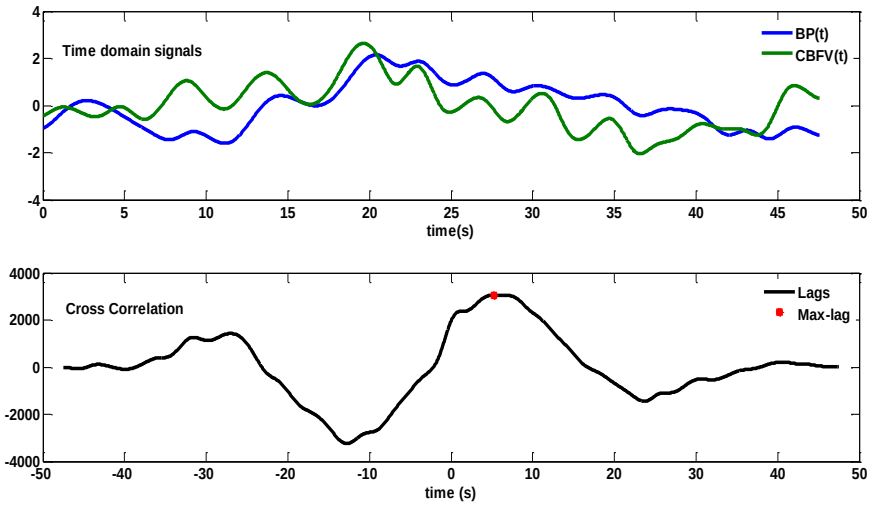

Figure 4-13 Illustrative Plot of Cross correlation between BP and CBFV

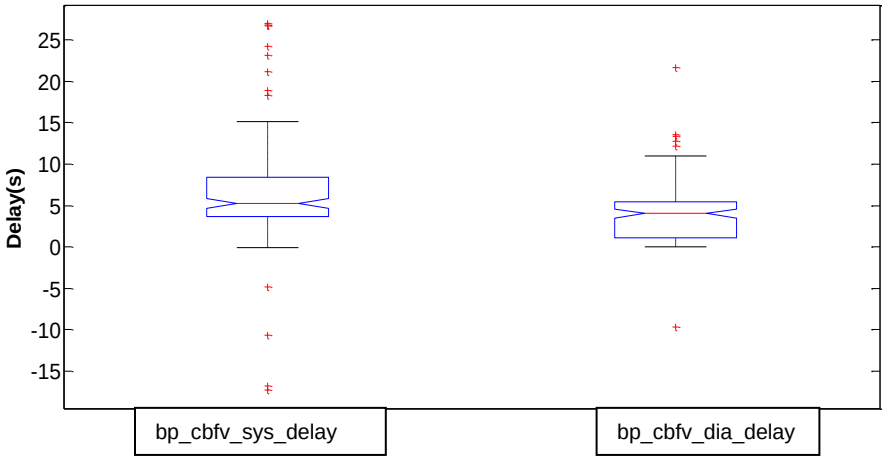

Figure 4-14 Range of Delays between BP and CBFV

Number of OSA episodes=178; Left most box plot shows the delay between systolic peaks of BP and CBFV. The right most box plot shows the delay between BP and CBFV diastolic valleys.

In Figure 4-14, the solid red line in the middle of each rectangle shows the median of the delays observed; vertical line that extends from the top of rectangle indicates the maximum delay and the bottom vertical line represents the minimum delays. Values above the maximum and below the minimum are considered to be outliers (indicated by red + sign in the figure).

4.2.3.2 Time Delay between Arterial Oxygen Saturation and Brain Oxygenation

Cross correlation analysis was also conducted between SaO_2 and HbO data as both of them showed a drop during OSA. Similar to the BP and CBFV signals, the peripheral and cerebral oxygenation signals were also normalized by removing the mean from the data and dividing by the respective standard deviation. A sample cross correlation plot between SaO_2 and HbO is as shown in Figure 4-15.

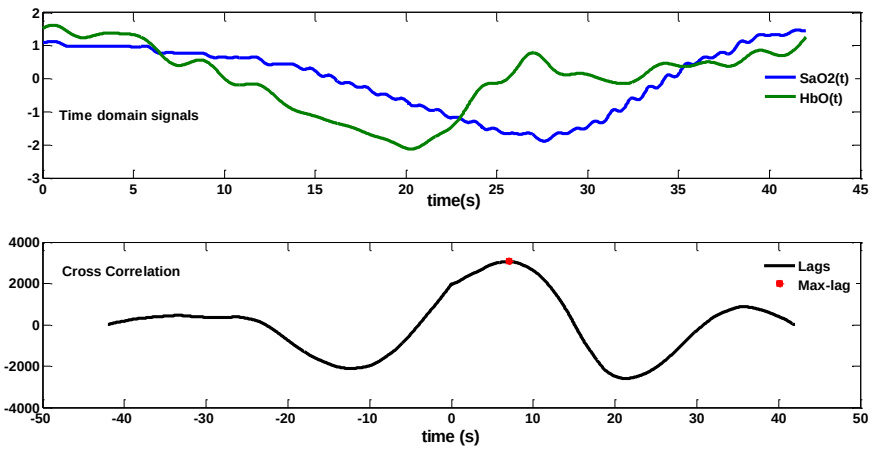

Figure 4-15 Illustrative Plot of Cross correlation between SaO_2 and HbO

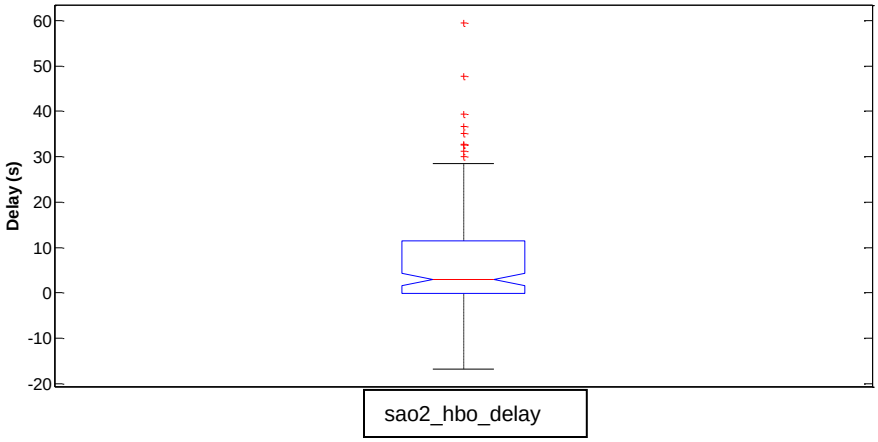

Figure 4-16 Range of Delay between SaO_2 and HbO

Number of OSA episodes=178.

The average delay between %SaO_2 drop and HbO was found to be 6.05±0.94 s. The range of delays obtained is as shown in Figure 4-16. Median value is indicated by the solid red line in the middle of the box plot; maximum and minimum values are represented by the top and bottom black vertical lines.

4.2.4 System Identification: Dynamic Blood Pressure –Blood Flow Relationship

ARMA model was used to identify the characteristics of dynamic cerebral autoregulation mechanism. For this ARMA model, arterial blood pressure was chosen as input and cerebral blood flow velocity as output. This process consisted of different steps and results from each of these are given in the below subsections.

4.2.4.1 FIR Filtering

For ARMA analysis, the interpolated systolic peaks of BP and CBFV during OSA episodes were used. The interpolated peaks were first down sampled to 10Hz and were filtered using an equiripple-zero phase finite impulse response (FIR) filter with cut off frequency at 0.1Hz. The frequency response of the FIR filter is as shown below in Figure 4-17. The BP and CBFV signals were filtered to remove 0.3Hz interference arising from

respiration pattern. Figure 4-18 shows both the unfiltered and filtered signals for both BP (top panel of Figure 4-18) and CBFV (bottom panel of Figure 4-18).

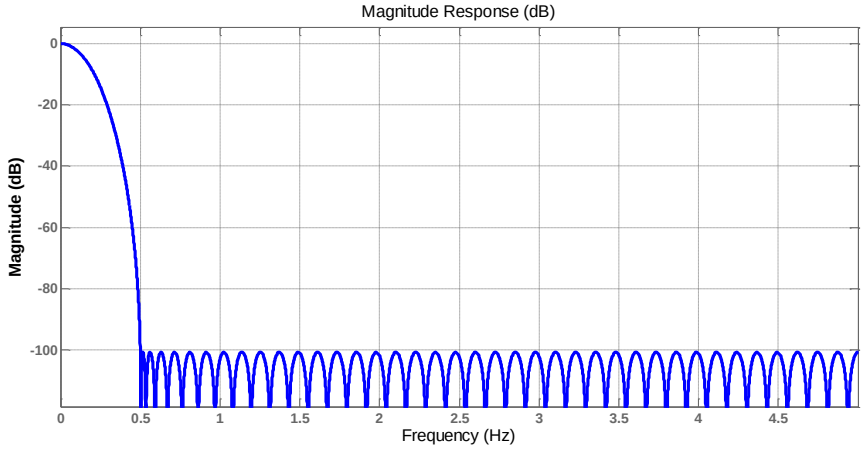

Figure 4-17 Frequency Response of FIR Filter

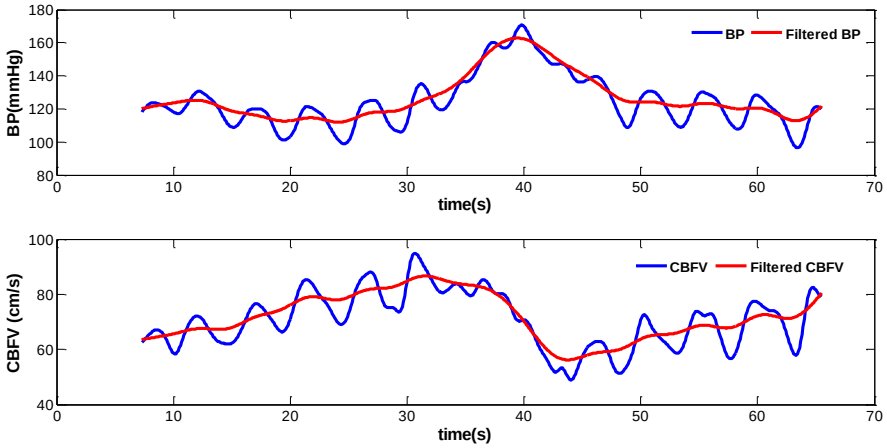

Figure 4-18 Filtering BP and CBFV Data

4.2.4.2 Identification of Patterns

Once the filtering of data is completed, the OSA clips were visually inspected to identify different patterns in BP and CBFV. OSA clips consist of data from the starting of OSA (indicated by apnea marker) until the SaO2 recovered from its lowest value. Hence

each of the OSA clips contains both OSA episode as well as 30-40 s after OSA termination. Based on the nature of BP and CBFV data during OSA episode as well as the during the post 30-40s, four different patterns were identified. They were named as 1) Unimodal 2) Bimodal 3) Drop_Preceding 4) Rise_Succeeding.

The unimodal pattern followed a single rise in systolic BP as well as in systolic CBFV due to the OSA. An example of unimodal pattern is as shown in Figure 4-19. As seen from the figure, both BP and CBFV began to rise gradually during the apnea, attaining the peak values within ±10s following apnea termination. The signal decreases following the OSA and stays constant near the baseline. In the figure, OSA is marked by rectangle marker signal. A total of 56 OSA clips selected from all the 11 subjects were grouped under this pattern.

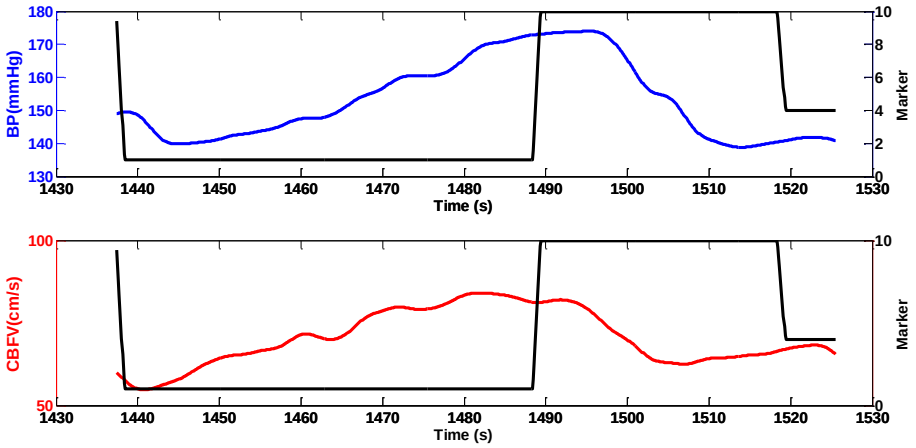

Figure 4-19 Illustrative Plot of Unimodal Pattern

In bimodal pattern, systolic BP and CBFV increased gradually during OSA followed by rapid decline at OSA termination. However, these hemodynamic signals did not stay stable near the baseline during the post 30-40s period. Instead there was another rise in either BP or CBFV or both giving rise to two or more rises within a

selected OSA clip. An example of bimodal pattern is as shown in Figure 4-20. A total of 51 OSA clips selected from all the 11 subjects were classified under bimodal pattern.

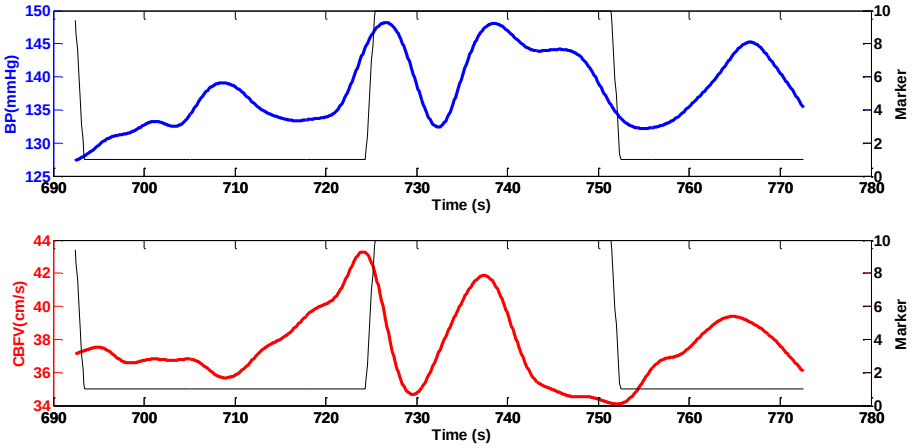

Figure 4-20 Illustrative Plot of Bimodal Pattern

Next pattern considered was 'Drop_Preceding', which had higher amplitude compared to the baseline values in either systolic BP or CBFV or both at the beginning of an OSA clip. Patterns were classified into drop_preceding, if its initial amplitude was atleast >50% when compared to the overall rise induced by the OSA. An example is given in Figure 4-21. In this figure, the systolic BP had initial amplitude of about 121 mmHg which is comparable to the maximum value attained due to OSA (~126mmHg) and is also greater than 50% of the total rise due to OSA. There were 36 OSA episodes from 11 subjects with drop_preceding pattern.

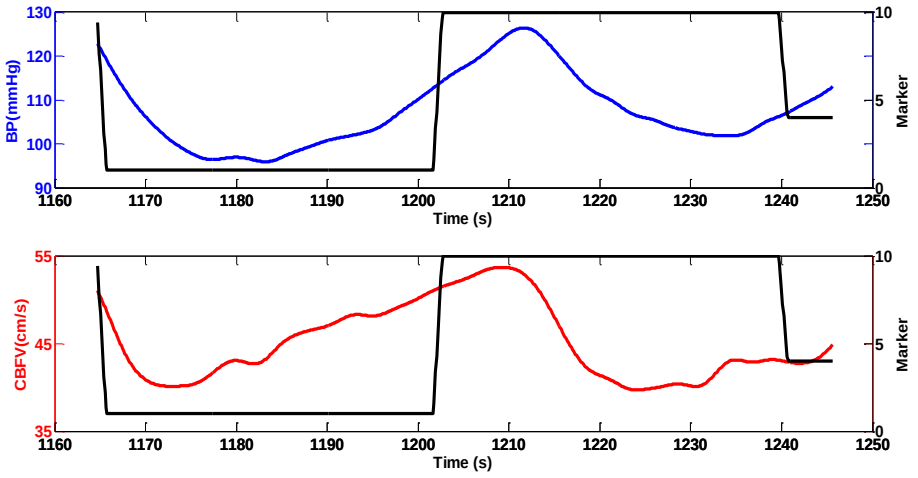

Figure 4-21 Illustrative Plot of Drop_Preceding Pattern

Last pattern considered was named as 'Rise_Succeeding', since these data sets had higher amplitude at the end of the OSA clips when compared to the baseline values. The higher amplitude can be present in either systolic BP or CBFV or both at the end of an OSA. Criteria required to include signals in this dataset was that the amplitude toward the end of OSA episode has to be atleast >50% when compared to the overall rise induced by the OSA. An example is given in Figure 4-22. In this figure, there was another OSA less than 10s after the first. Hence during the post 30-40s of first OSA clip, there was a rise in systolic CBFV (90 cm/s) which was comparable to the maximum value attained due to OSA (~89 cm/s). This amplitude was also greater than 50% of the total rise induced by OSA. Twenty six OSA episodes from 11 subjects were categorized into rise_succeeding pattern.

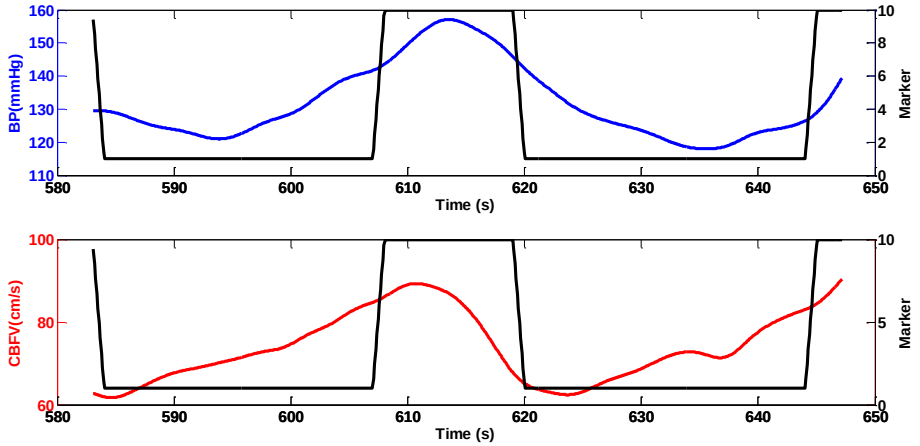

Figure 4-22 Illustrative Plot of Rise_Succeeding Pattern

4.2.4.3 Selection of Time Delay

As explained in section 3.2.3.1, for system identification, the model orders (na, nb) and delay (nk) has to be determined. As a pilot experimentation, the time delay between BP and CBFV was assumed to vary between 0 s to 15 s; i.e. ARMA models were estimated by varying the values of nk between 0 to 150 samples. For a large number of OSA clips, value of nk was found to be greater than 50 samples (5s) with a few ranging over 100 samples (10s). Further, as seen from cross correlation results in 4.2.3.1, the input to the model which is the BP data was lagging behind the CBFV. Hence, in order to attain a causal system (system where input does not lag behind the output), BP data was shifted to match with the CBFV data prior to system identification. This was achieved by shifting the BP waveform such that the highest peak in BP matches with that of CBFV data. An example plot is given in Figure 4-23.

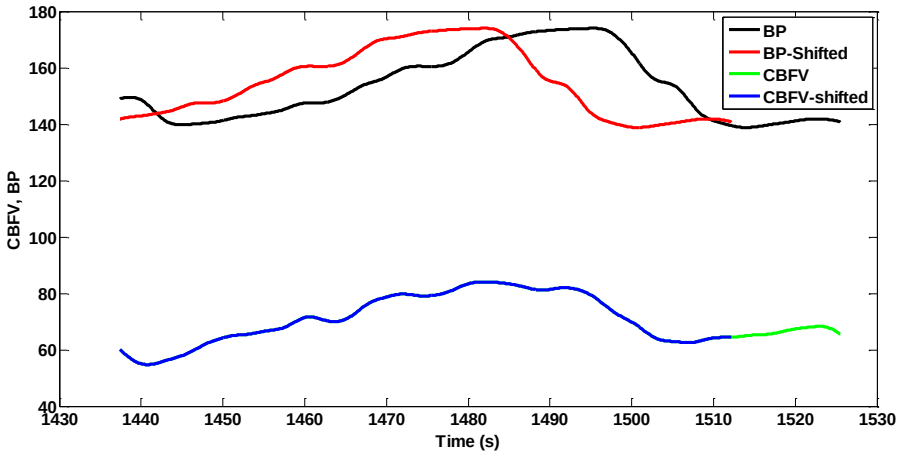

Figure 4-23 Illustrative Plot of Shifting BP Waveform

As seen from Figure 4-23, the BP is shifted to match with the TCD peak. In order to make both BP and CBFV of same length, the trailing edge of CBFV is also removed. The average values of shifts required in BP were 43±5, 71±9, 74±7 and 43±6 samples for unimodal, bimodal, drop_preceding and rise_succeeding patterns respectively. After shifting the BP data, AMRA models were estimated by varying the values of nk; nk values obtained were found to be lesser than before shifting. For comparison purpose, plots of nk vs shifts before and after BP shifting are given in Figure 4-24 to Figure 4-27.

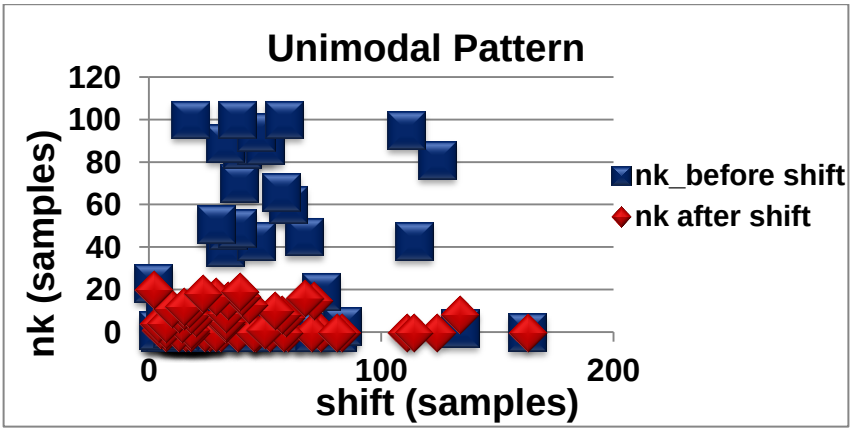

Figure 4-24 nk vs Sample Shift for Unimodal Pattern

Number of OSA episodes, N=56

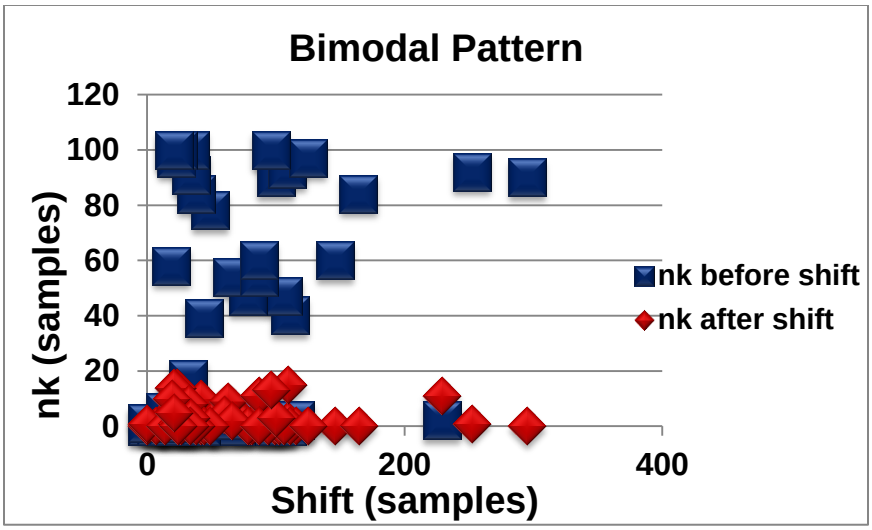

Figure 4-25 nk vs Sample Shift for Bimodal Pattern

Number of OSA episodes, N=51

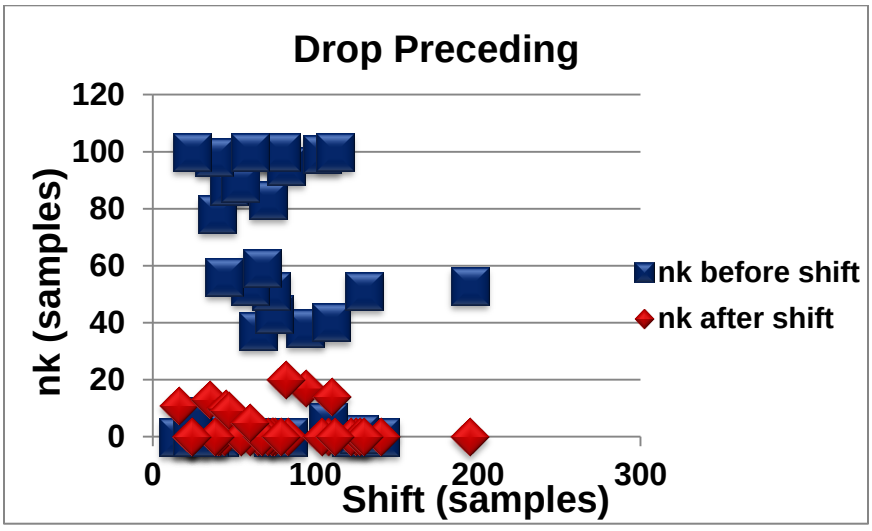

Figure 4-26 nk vs Sample Shift for Drop_Preceding Pattern

Number of OSA episodes, N=36

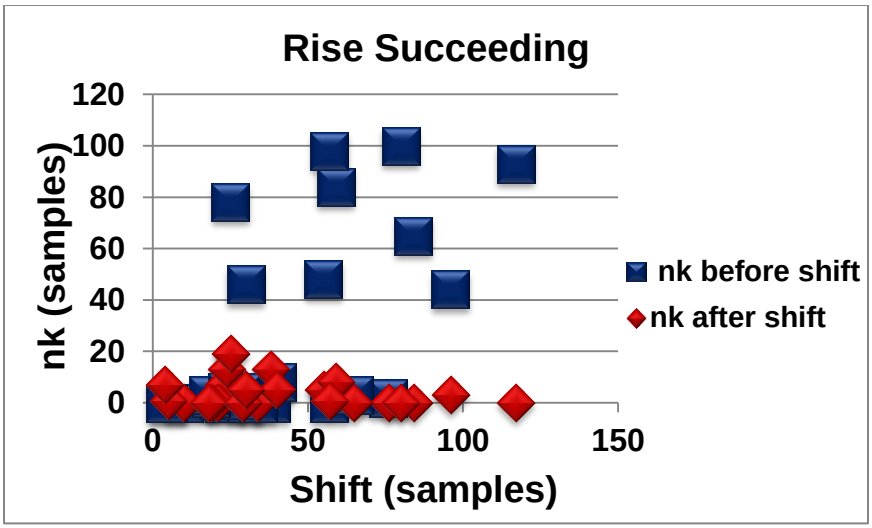

Figure 4-27 nk vs Sample Shift for Rise Succeeding Pattern

Number of OSA episodes, N=26

4.2.4.4 System Identification

OSA clips classified under each of the four patterns were fitted with ARMA models by varying na and nb (i.e. model order) from 1 to 5 and nk from 0 to 20. Hence for each OSA clip, 525 models (5x5x21) were fitted. Best fit model for each of the OSA clips were identified by using least MSE criterion. An example plot of model estimated CBFV vs. CBFV measured during the sleep study is shown in Figure 4-28.

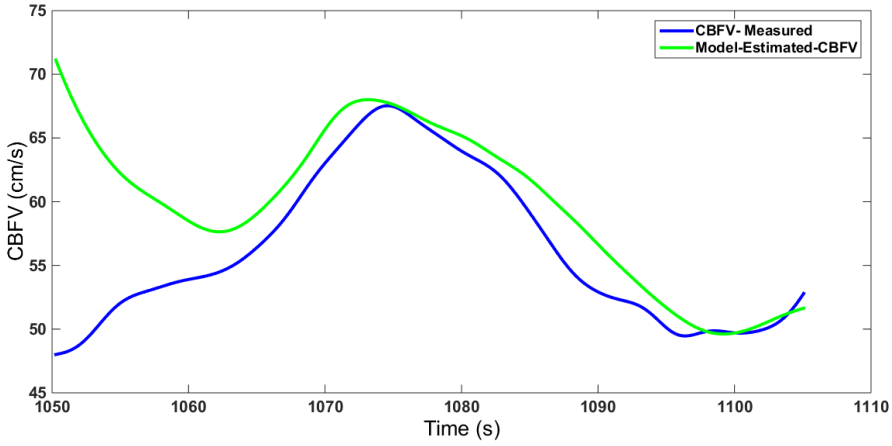

Figure 4-28 Illustrative Plot of Model Estimated CBFV vs. Measured CBFV.

Further, best fitted model orders for each of the 4 patterns were obtained by taking the mode of na, nb and nk for all the OSA clips under each pattern. Table 4-6 summarizes the result obtained.

Table 4-6 Best Estimated Model Order for Different Patterns

Pattern	Model Parameters			Avg BP shift (samples)
	na	nb	nk	
Unimodal	2	2	0	43±5
Bimodal	2	3	0	71±9
Drop-Preceding	2	2	0	74±7
Rise-Succeeding	1	2	0	43±6

Further, the pattern of MSE for different values of model order and delays are shown in following section.

1) Unimodal Pattern:

The MSE values were plotted by separating the models with different nk values such as nk=0, nk≤10 and nk>10. The plots are as shown in Figure 4-29 - Figure 4-31.

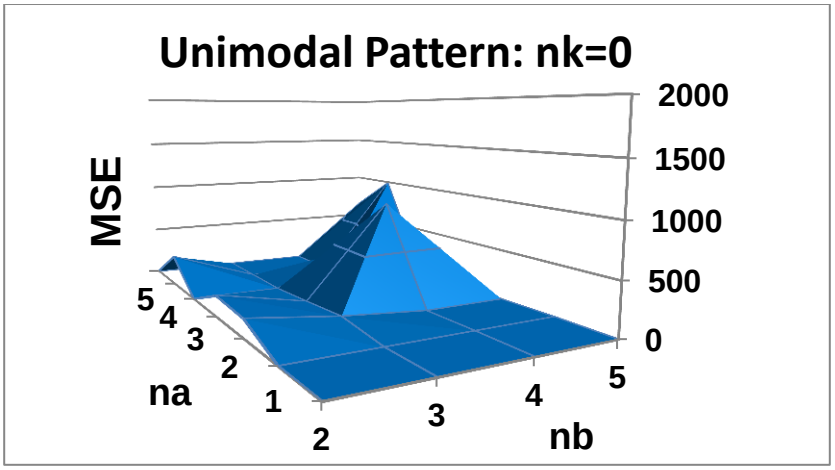

Figure 4-29 Range of MSE for Unimodal Pattern (nk=0)

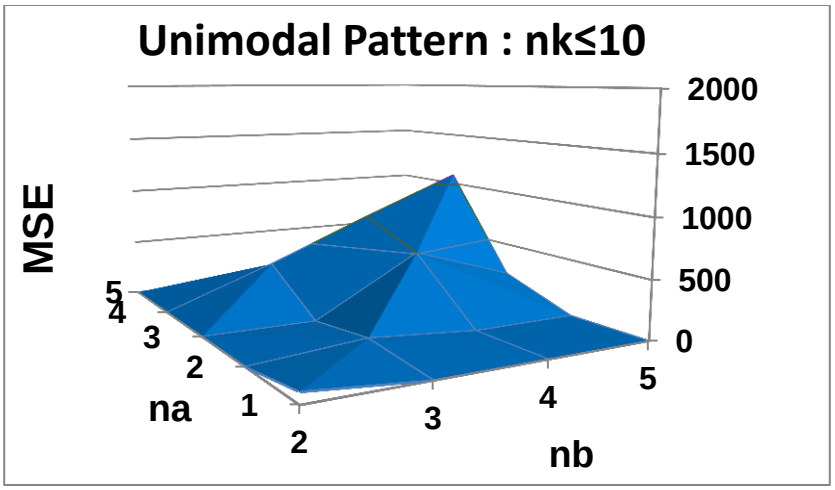

Figure 4-30 Range of MSE for Unimodal Pattern (nk≤10)

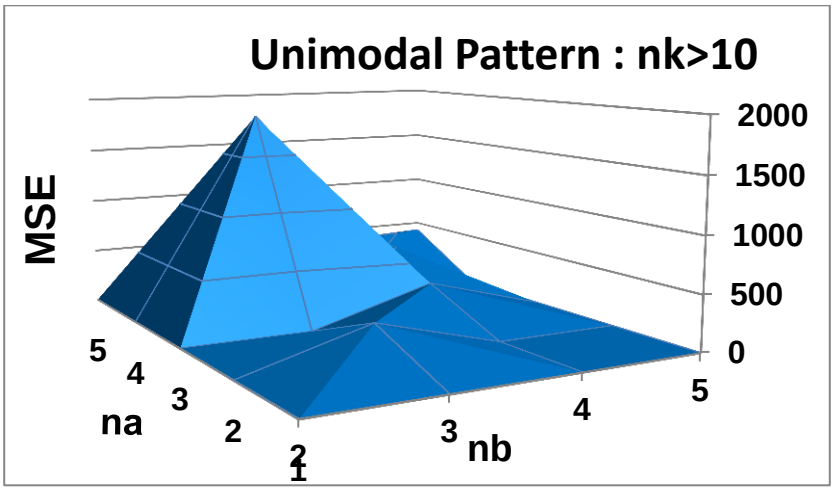

Figure 4-31 Range of MSE for Unimodal Pattern (nk>10)

Further, all the models irrespective of the order of nk was grouped together to get an overall MSE plot for Unimodal pattern as shown in Figure 4-32.

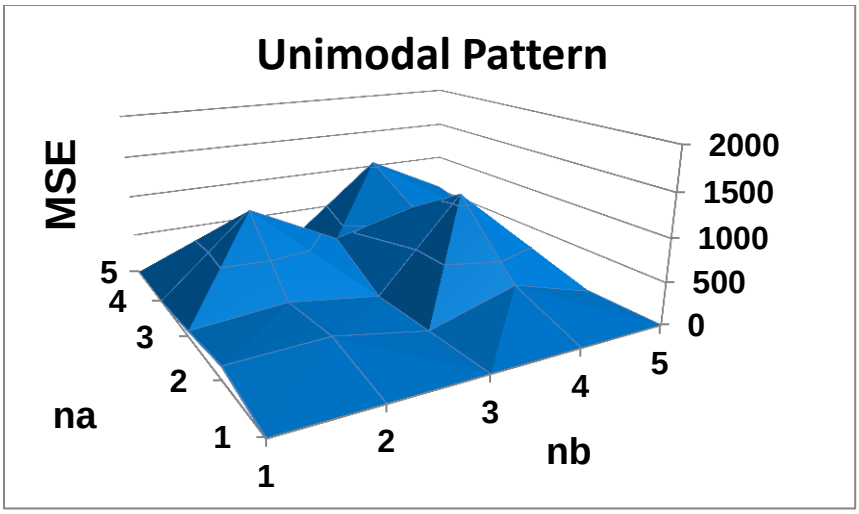

Figure 4-32 Overall MSE Range for Unimodal Pattern

Number of OSA episodes, N=56

2) Bimodal Pattern:

The MSE values were plotted for three different groups of models with different nk values (nk=0, nk≤10 and nk>10). The plots are as shown in Figure 4-33 - Figure 4-35 .

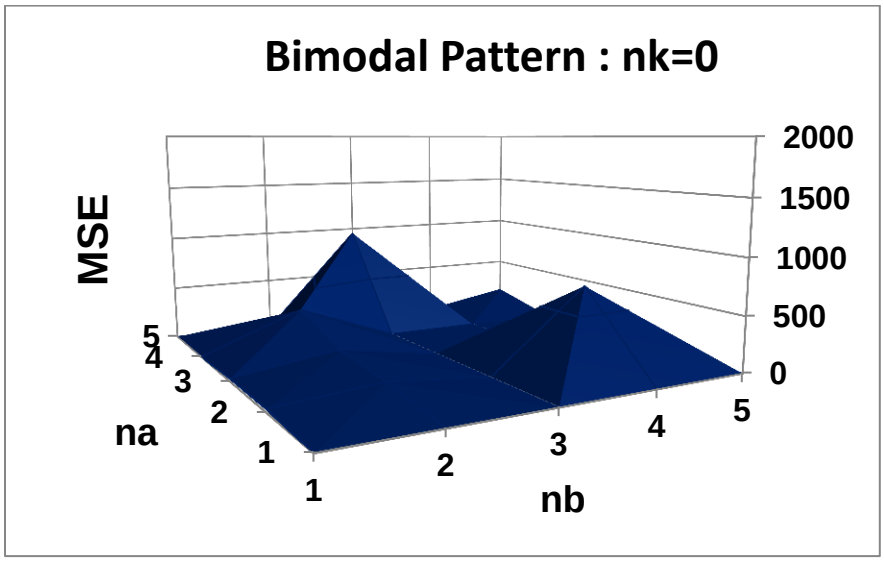

Figure 4-33 Range of MSE for Bimodal Pattern (nk=0)

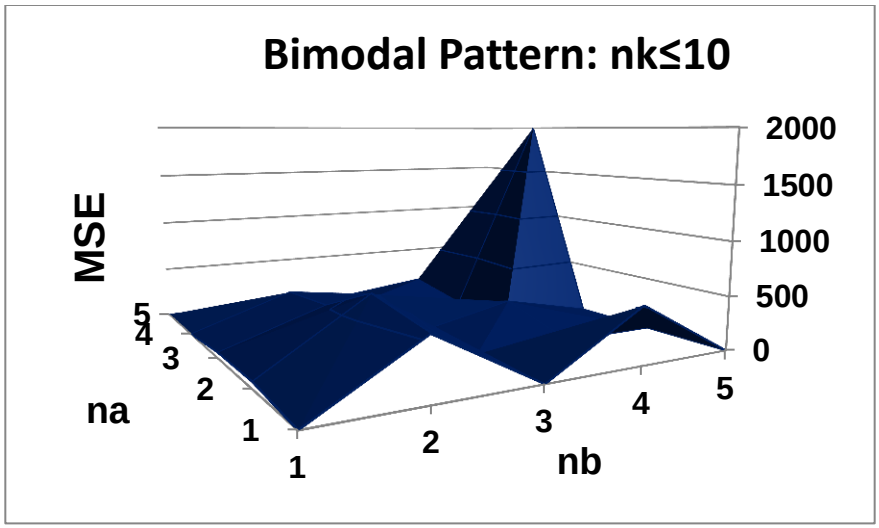

Figure 4-34 Range of MSE for Bimodal Pattern (nk≤10)

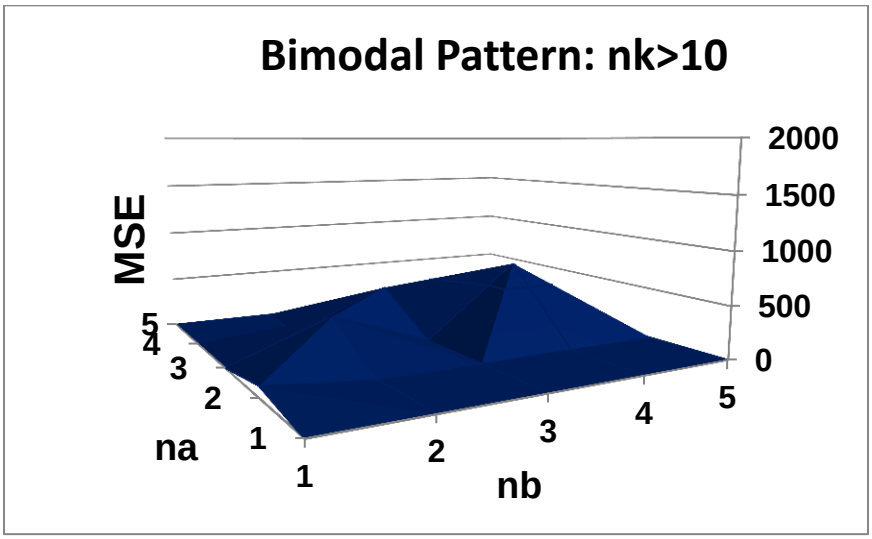

Figure 4-35 Range of MSE for Bimodal Pattern (nk>10)

The overall MSE plot irrespective of nk for Bimodal pattern is as shown in Figure 4-36.

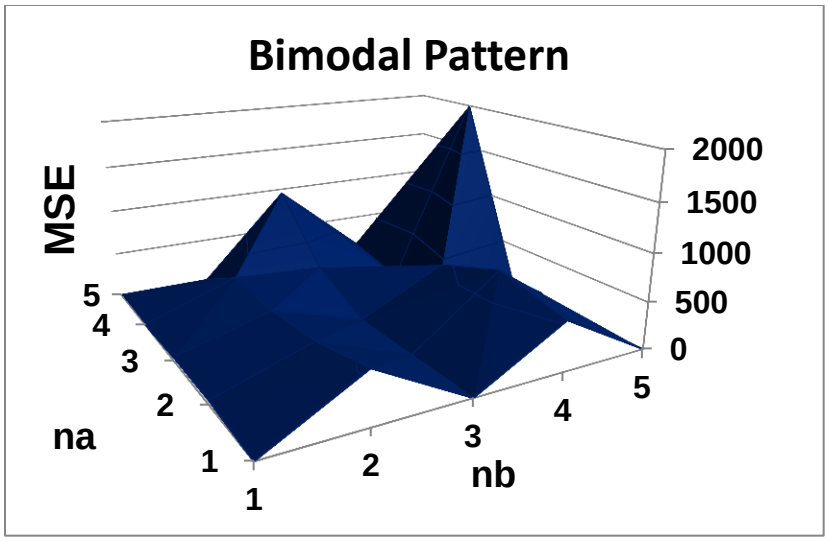

Figure 4-36 Overall MSE Range for Bimodal Pattern

Number of OSA episodes, N=51

3) Drop_Preceding Pattern:

The MSE for three different groups of models with nk=0, nk≤10 and nk>10 are shown in Figure 4-37- Figure 4-39.

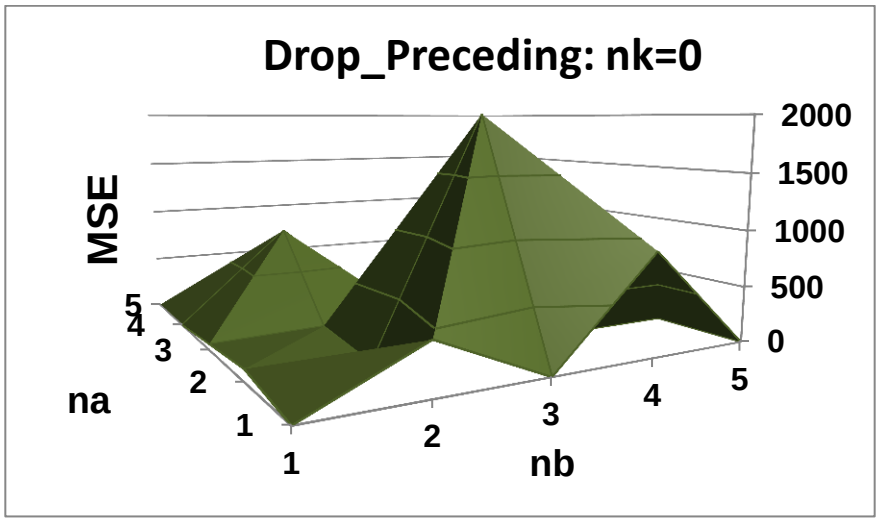

Figure 4-37 Range of MSE for Drop_Preceding Pattern (nk=0)

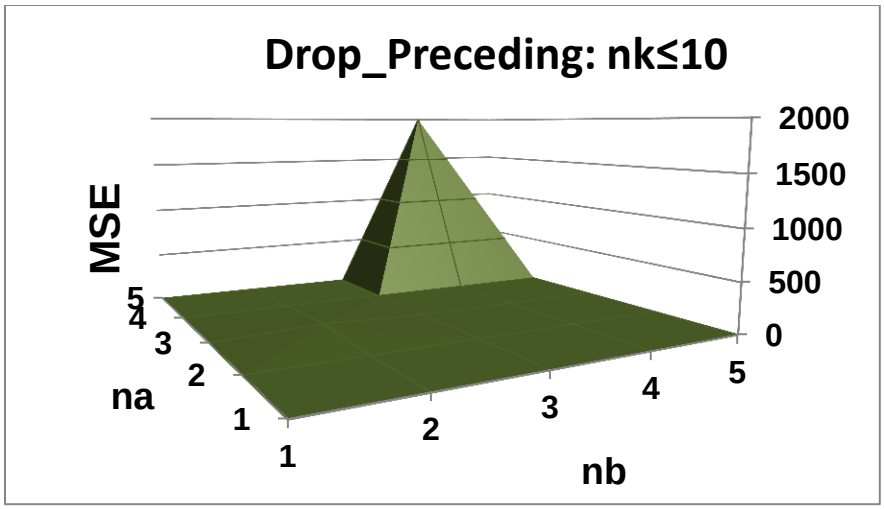

Figure 4-38 Range of MSE for Drop_Preceding Pattern (nk≤10)

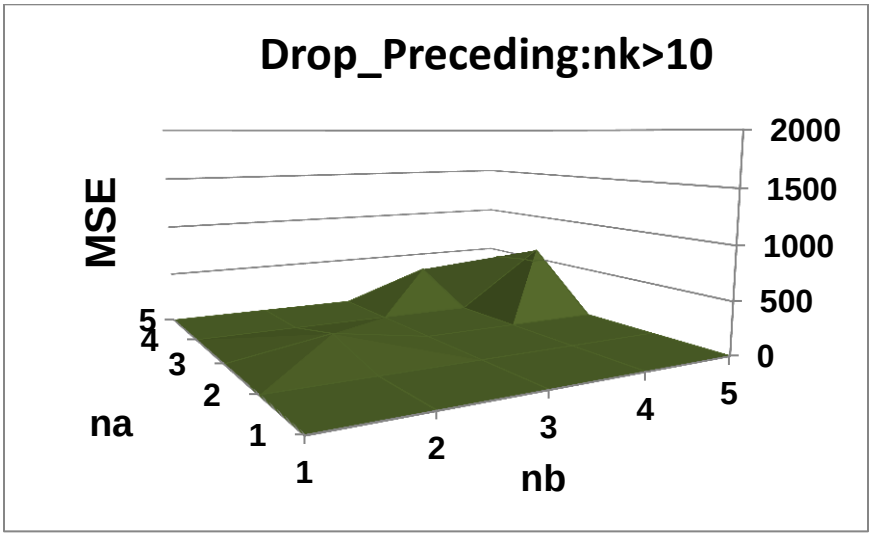

Figure 4-39 Range of MSE for Drop_Preceding Pattern (nk>10)

The overall MSE plot irrespective of nk was for Drop_Preceding pattern is as shown in Figure 4-40.

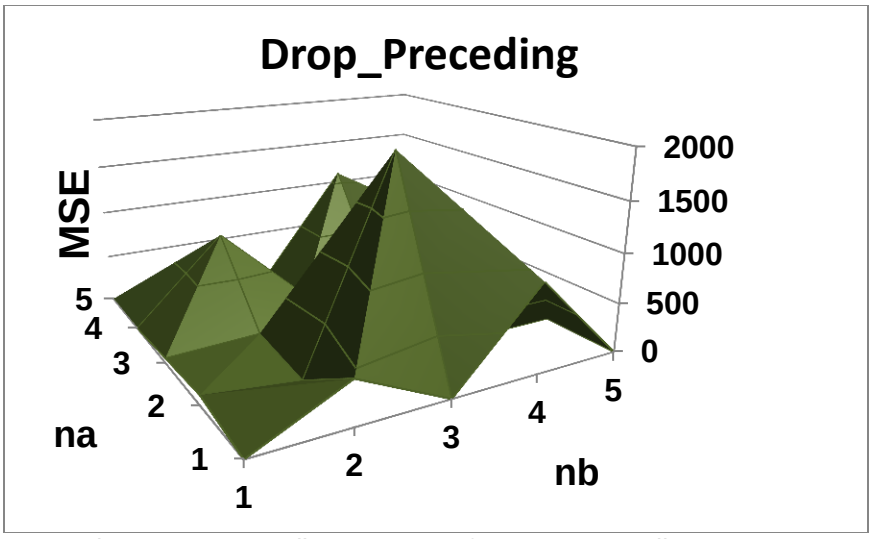

Figure 4-40 Overall MSE Range for Drop Preceding Pattern

Number of OSA episodes, N=36

4) Rise_Succeeding Pattern:

The MSE for three different groups of models with nk=0, nk≤10 and nk>10 as well as the overall MSE pattern for OSA clips with rise_succeeding pattern are shown in Figure 4-41- Figure 4-44.

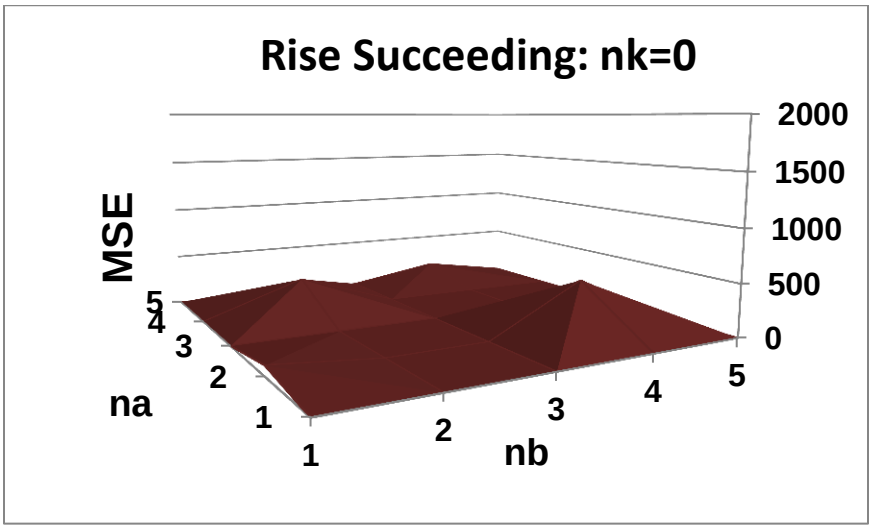

Figure 4-41 Range of MSE for Rise_Succeeding Pattern (nk=0)

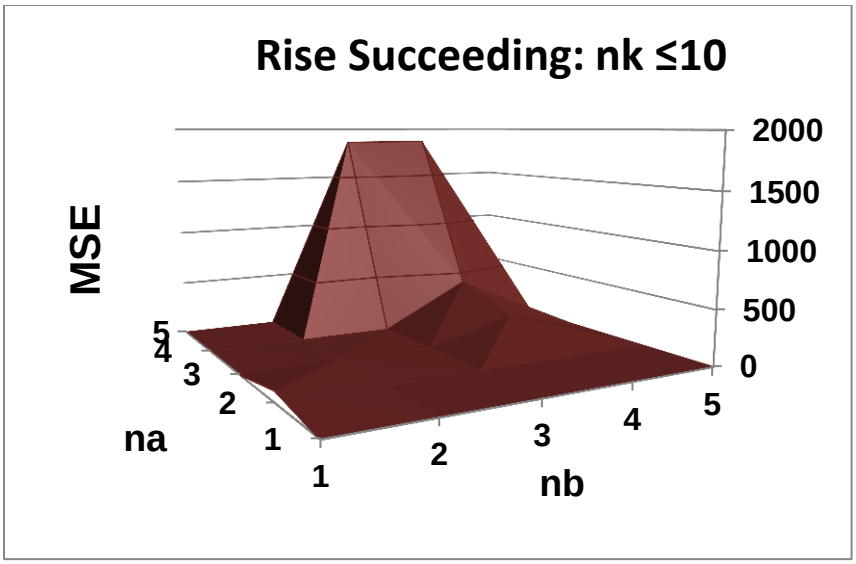

Figure 4-42 Range of MSE for Rise_Succeeding Pattern (nk≤10)

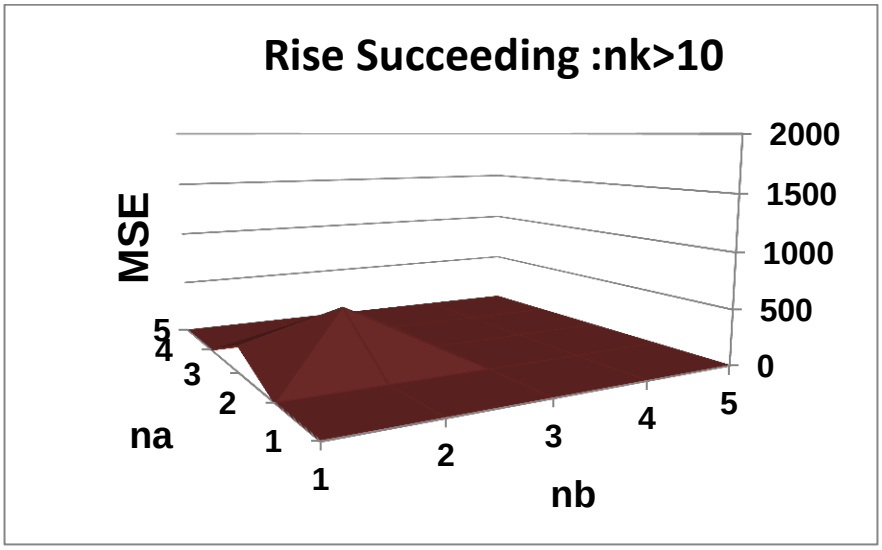

Figure 4-43 Range of MSE for Rise_Succeeding Pattern (nk>10)

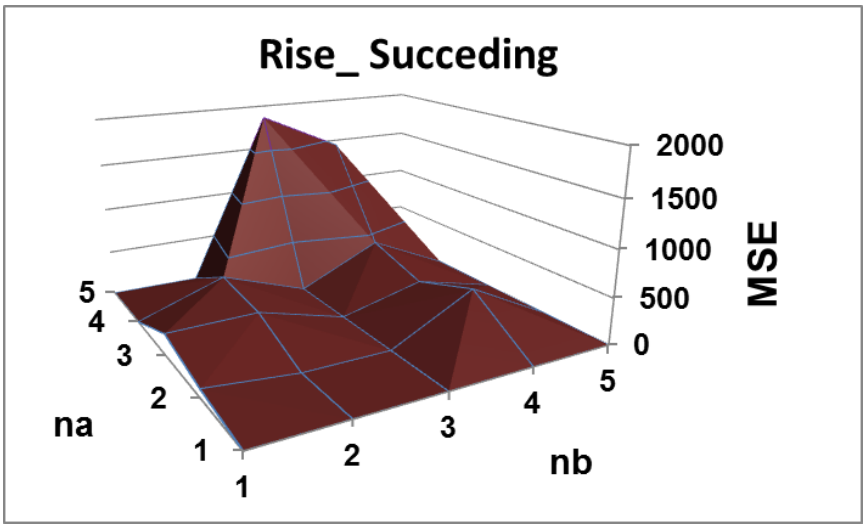

Figure 4-44 Overall MSE Range for Rise_Succeeding Pattern

Number of OSA episodes, N=26

4.2.4.5 System Coefficients

The model coefficients of the system (explained in 3.2.3.1) were determined by averaging the coefficients obtained for OSA clips with same values of na and nb. This was done for all the 4 patterns and results are summarized in Table 4-7 to Table 4-10.

Table 4-7 Averaged Model Coefficients for Unimodal Pattern

na, nb	a0	a1	a2	a3	a4	a5	b0	b1	b2	b3	b4
1,2	1	-0.99					0.40	-0.40			
1,3	1	-0.99					0.28	-0.29	0.01		
2,2	1	-1.99	0.99				0.01	-0.01			
2,3	1	-1.99	0.99				0.36	-0.72	0.36		
2,4	1	-1.99	0.99				1.94	-5.62	5.42	-1.74	
3,4	1	-2.99	2.99	0.99			0.49	-1.49	1.49	-0.50	
3,5	1	-2.99	2.99	0.99			0.48	-1.44	1.46	-0.50	0.01
4,2	1	-3.98	5.94	3.96	0.99		0.0001	-0.0001			
4,3	1	-3.98	5.95	3.95	0.99		0.004	-0.008	0.004		
4,4	1	-3.97	5.92	3.93	0.98		0.01	-0.02	0.02	-0.01	
4,5	1	-3.99	5.97	3.98	1.00		0.33	-1.34	2.02	-1.36	0.34
5,4	1	-4.95	9.81	9.73	4.83	0.96	0.01	-0.02	0.02	-0.01	
5,5	1	-4.96	9.86	9.81	4.89	0.98	0.01	-0.02	0.03	-0.02	0.003

Number of OSA episodes, N=56

Table 4-8 Averaged Model Coefficients for Bimodal Pattern

na, nb	**a0**	**a1**	**a2**	**a3**	**a4**	**a5**	**b0**	**b1**	b2	b3	b4
1,2	1	-1.00					0.33	-0.32			
1,3	1	-1.00					0.51	-0.76	0.25		
2,1	1	-2.00	1.00				0.00				
2,2	1	-1.99	1.00				0.00	0.00			
2,3	1	-1.99	0.99				0.30	-0.59	0.30		
2,4	1	-1.99	0.99				1.77	-5.22	5.11	-1.67	
3,4	1	-2.99	2.99	-0.99			0.50	-1.49	1.49	-0.50	
3,5	1	-2.99	2.97	-0.99			0.57	-1.84	2.07	-0.90	0.10
4,1	1	-3.99	5.98	-3.99	1.00		0.00				
4,2	1	-3.98	5.95	-3.97	0.99		0.00	0.00			
4,3	1	-3.96	5.89	-3.90	0.97		0.00	-0.01	0.00		
4,5	1	-3.98	5.95	-3.96	0.99		0.31	-1.22	1.82	-1.22	0.30
5,4		-4.97	9.89	-9.86	4.92	-0.99	0.00	0.00	0.00	0.00	

Number of OSA episodes, N=51

Table 4-9 Averaged Model Coefficients for Drop_Preceding Pattern

na, nb	**a0**	**a1**	**a2**	**a3**	**a4**	**a5**	**b0**	**b1**	**b2**	**b3**	**b4**
1,2	1	-0.99					0.49	-0.48			
1,3	1	-1.00					0.33	-0.25	-0.08		
2,1	1	-1.99	0.99				0.0002				
2,3	1	-2.00	1.00				0.27	-0.54	0.27		
2,4	1	-2.00	1.00				1.82	-5.31	5.17	-1.68	
3,2	1	-3.00	3.01	-1.00			0.001	-0.001			
4,1	1	-3.99	5.99	-4.00	1.00		0.000001				
4,5	1	-3.98	5.96	-3.97	0.99		0.10	-0.38	0.57	-0.38	0.10
5,4	1	-4.96	9.86	-9.81	4.89	-0.97	0.00	-0.01	0.01	0.00	

Number of OSA episodes, N=36

Table 4-10 Averaged Model Coefficients for Rise_Succeeding Pattern

na, nb	a0	a1	a2	a3	a4	b0	b1	b2	b3	b4
1,2	1	-1.00				0.44	-0.43			
1,3	1	-1.00				0.34	-0.13	-0.21		
2,3	1	-2.00	1.00			0.36	-0.73	0.36		
2,4	1	-2.00	1.00			0.35	-0.94	0.83	-0.24	
3,5	1	-3.01	3.02	-1.01		3.05	-11.97	17.59	-11.49	2.81
4,2	1	-3.98	5.94	-3.95	0.99	0.0001	-0.0001			
4,3	1	-3.97	5.92	-3.93	0.98	0.004	-0.01	0.004		
4,4	1	-3.97	5.90	-3.91	0.97	0.03	-0.09	0.09	-0.03	
4,5	1	-3.99	5.97	-3.98	1.00	0.26	-1.04	1.56	-1.04	0.26

Number of OSA episodes, N=26

Chapter 5

Discussion

The goals of this study were to investigate if OSA induced significant changes in cerebral hemodynamics as well as to find the interrelation between systemic and cerebral hemodynamics during OSA episodes. Using statistical and quantitative analysis, it was observed that many of the devised metrics of cerebral hemodynamics were responsive to OSA. This chapter deals with the interpretation and significance of the results observed in Chapter 4.

5.1. Effect of OSA on Cerebral Hemodynamics

5.1.1 Effect of OSA on Cerebral Blood Flow Velocity

Brain requires a consistent blood supply of about 50 to 54 ml of blood per 100 gm of tissue per minute irrespective of the fluctuations in arterial blood pressure. If the brain blood flow falls below the range of 8 to 10 ml per 100 gm of tissue per minute, brain tissue death occurs. On the other hand, excessive blood flow also results in brain tissue damage by compression resulting from increased intracranial pressure [29]. To avoid brain tissue death, the blood supply to brain is tightly regulated by the cerebral autoregulation mechanism. However, during all the OSA episodes (Figure 4-1), there was a progressive rise in CBFV (indicative of cerebral blood flow) followed by rapid decrease after termination of OSA. These changes in CBFV were concomitant with congruent changes in BP. In this study, the magnitude of systolic peaks and diastolic valleys of CBFV had an average rise of 35.82±1.42 % and 53.44±2.72% respectively, compared to its value at the beginning of an OSA episode (Figure 4-3). Moreover, mean CBFV had an average rise of 41.98±1.88 % and the rate of rise in systolic, diastolic and mean values of CBFV were found be to ≥ 0.5cm/s^2 (Figure 4-3, Figure 4-4). All these indicate that CBFV does not stay constant during OSA episodes. During an OSA episode, there is a

decrease in arterial O_2 and increase in CO_2 leading to a decrease in pH. In the OSA subjects considered for this study, there was an average drop of -6.45±0.29 % in SaO_2 concentration and an increase of 3.79±0.29mmHg in CO_2 concentration (Table 4-1). These changes in blood gas concentration can lead to vasoactive dilation resulting in rise in CBFV [7]. Furthermore, blood pressure can have a direct effect on CBFV if the cerebral autoregulation mechanism is not intact or if it does not get sufficient time to adapt. It has been shown that cerebral autoregulation mechanism is compromised in OSA subjects [7, 28, 42]. In this study an average rise of 26.47±0.90 % was observed in mean blood pressure with the rate of rise in mean BP as high as 0.81 mmHg/s (Table 4-1). Hence this rapid rise in BP as well as a possibly impaired cerebral autoregulation mechanism may contribute to the rise in CBFV. An increase in area under CBFV waveform was also observed in this study (Figure 4-3). This rise may be attributed to the increase in the amplitude or diastole to diastole interval (width of CBFV pulse). Reduction in heart rate can increase the temporal distance between successive diastolic valleys resulting in a rise in area and vice versa.

Another plausible reason for rise in CBFV during apnea can be attributed to the OSA induced increased sympathetic nerve activation. The cerebrovascular bed is abundantly innervated by sympathetic nerve fibers [77]. Nonetheless, the role of sympathetic nerve activity on regulation of cerebral blood flow is controversial [78]. However, it has been shown that cerebral blood flow regulation was altered during: (i) stimulation or denervation of nerves in the cerebrovascular bed with connections to cervical sympathetic chain, (ii) complete ganglionic blockade by trimethaphan (iii) using prazosin, an α-adrenoreceptor antagonist [78-81]. A recent study has also shown the frequency depend nature of sympathetic control of cerebral blood flow. It was shown that sympathetic blockade at higher frequencies (>0.05Hz) increased the gain relation

between BP and cerebral blood flow; but had little effect at slower frequencies [78]. Since it is established that OSA induces significant changes in sympathetic nerve activity [21, 22], it might contribute at least partially to the observed rise in CBFV.

5.1.2 Effect of OSA on Brain Oxygenation

Multiple hypoxia studies in healthy subjects as well as in animals have shown that cerebral autoregulatory mechanism can effectively prevent cerebral hypoxia thereby preventing ischemic damage [37, 43]. Hence, during an OSA episode, despite the reduction in arterial SaO_2, it is plausible to maintain a consistent supply of oxygen to the brain via increase in cerebral blood flow. However, the results of this study showed that during an OSA episode, oxyhemoglobin concentration or the HbO decreases while the amount of deoxy hemoglobin (HbR) in the brain increases (Figure 4-2). An average decrease of -2.03±0.14μM and an increase of 1.89±0.15μM has been observed in HbO and HbR concentrations respectively (Figure 4-5). This was followed by a rapid rise in HbO and reduction in HbR after the end of OSA episode. These cyclical cerebral desaturation and reoxygenation suggests that cerebral compensatory mechanisms fail to provide a consistent supply of oxygen leading to cerebral hypoxia during OSA episodes. This does not necessarily mean that blood flow to the brain was deficient (CBFV had a significant rise during OSA); but possibly the level of oxygen that was present in the blood had dropped. This might lead to ischemic damage and stroke. On the contrary, a few studies have shown that there is cerebral hyperoxygenation (increase in HbO and decrease in HbR) in response to voluntary breath holds and hypopnea. Hence, it is possible that cerebral autoregulation is capable of preventing cerebral hypoxia by increasing the oxygen delivery through increased cerebral blood flow during these maneuvers; however during complete airway obstruction, despite the rise in cerebral blood flow, cerebral hypoxia might occur [43, 44].

In summary, this study has observed significant changes in cerebral and systemic hemodynamics during OSA episodes and has quantified the degree of these variations. These findings are consistent with that of a recent study by Hou *et al*. using novel near-infrared diffuse correlation spectroscopy (DCS) flow-oximeter to investigate relative changes in cerebral blood flow and brain oxygenation [82]. Even though the subject population was small (OSA=9, healthy controls=4), the study by Hou *et al.* has observed relative changes (standard deviations) in cerebral hemodynamics during OSA episodes compared to normal breathing and these changes were found to be related to OSA severity. However, due to baseline shifts in the data obtained, absolute quantification of OSA induced changes in cerebral hemodynamics was not possible.

5.1.3 Effect of OSA Duration on Cerebral and Systemic Hemodynamics

An apnea is defined as cessation of breathing for a minimum of 10 seconds. However, the duration of these episodes can vary anywhere from 10 seconds to over a minute [83]. Currently, the measure of apnea severity is the number of total or partial breathing interruptions that a patient experiences per hour of sleep referred to as apnea-hypopnea index (AHI) [83, 84]. However, AHI does not indicate the total time of airway obstruction. Moreover, the longer the duration of apnea, the greater may be the activation of sympathetic nervous system leading to higher cardiovascular stress (change in heart rate and blood pressure) [84]. Hence it is important to explore whether OSA duration has a significant effect on the degree of fluctuations in systemic and cerebral responses.

The results obtained from this study showed that all features extracted from CBFV were significantly correlated with the OSA duration except the rate of rise in diastolic and mean velocity (Table 4-2). The rate of rise in systolic velocity was negatively correlated with the OSA duration. Since the slope or rate of rise is calculated by dividing the degree of rise in signal by the time required for the rise, a longer duration apnea will

lead to a lesser slope and vice versa. This might explain the observance of a negative slope for systolic velocity. Negative correlation between slope and OSA duration was obtained for diastolic and mean velocity; however, they were not statistically significant. Similarly, from the brain oxygenation data, it was observed that OSA duration had a significant effect on HbR and HbT, but not in HbO concentration (Table 4-3). In this study, drop in HbO was calculated with respect to the starting of an OSA episode and not with respect to the initial baseline data before initiation of OSA events. Hence, if a subject is experiencing severe OSA episodes back to back, the HbO concentration at the beginning of an OSA episode may not be a representative of actual baseline value. Further, in a few OSA episodes, during the initial stage there was a rise in HbO followed by the decrease. However, since the HbO drop was calculated with respect to the initial value at the onset of an OSA episode, the drop calculated might be less compared to the actual drop. For example: if the initial HbO value at beginning of OSA was 0μM, followed by an increase to 2μM and then a final drop to -0.5μM. In this case, the HbO drop calculated will be -0.5μM compared to the actual drop of -2.5μM. These might be the possible reasons why HbO did not show a significant correlation with the apnea duration.

One possible explanation for the observed relationship cerebral hemodynamics and apnea duration is that, for a longer duration apnea, the amount of CO2 accumulated in the body and the amount of oxygen desaturation will be higher compared to that of a shorter duration apnea. This is confirmed by the results obtained from correlation analysis between OSA duration and BP, arterial SaO2 and CO2 changes (Appendix B). Further, it has been reported that combined effects of hypoxia and hypercapnea can synergistically increase the sympathetic nerve activity [22]. Hence, for a longer duration apnea, the degree of sympathetic activation may be high which in turn can lead to elevated levels of blood pressure. These combined effects of peripheral hypoxia,

hypercapnea and elevated blood pressure may lead to a rise in the cerebral blood flow. Further, as the OSA duration increases, the amount of oxygen available will be lesser leading to an increase in deoxy hemoglobin in the brain leading to cerebral hypoxia [43].

5.1.4 Effect of AHI on Cerebral and Systemic Hemodynamics

AHI is widely accepted as the indicator of apnea severity [83, 84]. Hence in this study we investigated the effect of AHI on the average values of cerebral hemodynamic features. The results indicated that AHI did not have a significant effect on average values of features considered from cerebral or systemic hemodynamic data (Appendix C). Since majority of the cerebral and systemic features considered in this study showed a relation with OSA duration, but not with AHI, our results suggest that, it may be valuable to consider the duration of apneas along with the AHI to completely characterize the OSA severity. This is because AHI, though the most prevalent OSA severity index, just indicates the total number of apneas and hypopneas per night. It neither indicates the total duration of airway obstruction nor the severity of physiological changes induced by OSA. Hence a new index which incorporates OSA duration as well as changes in physiological responses in combination with the number of apneas and hypopneas might be a better predictor of severity of OSA. This is corroborated by findings from other researchers that, the AHI can be exact same number for a subject experiencing an apnea of 50s compared to another subject with OSA duration of 10s [83]. Hence, AHI can underestimate the severity of a subject's condition and might not be well correlated with the physiological responses.

5.2. Relationship between Systemic and Cerebral Hemodynamics during OSA

The second hypothesis considered in this study was to investigate the role of systemic hemodynamics in determining the changes in cerebral hemodynamics during OSA episodes.

5.2.1 Effect of Systemic Hemodynamics on CBFV Variations

As explained earlier in section 5.1.1, OSA induced changes in blood gases, pH and BP has a significant effect on the CBFV variations. The results from non-parametric correlation analysis showed that blood pressure variations during apnea were positively correlated with variations in corresponding CBFV features (Table 4-4, Appendix D). Further, the highest correlation was between the time to peak in BP and time to peak in CBFV (r=0.94). This indicates a parallel rise in CBFV concomitant with that of BP. Change in CO_2 and SaO_2 were significantly correlated with all the metrics except the rate of rise in cerebral blood flow velocity (Table 4-4, Appendix D). Moreover, time to peak in CBFV was significantly correlated with time to drop in SaO2 concentration. This might be due to the fact that, as the peripheral oxygen concentration decreases and CO2 concentration increases, the blood pH level decreases thereby resulting in vasodilation of cerebral arteries and arterioles. Interestingly, the rate of rise in CBFV was not correlated with the change in SaO2 or CO2 concentration. However, the slopes of systolic, diastolic and mean CBFV were significantly correlated with the corresponding slopes of BP ($r \geq 0.29$, $p \leq 0.0001$). Hence, it seems from the results that the rate of rise in CBFV during an OSA depends on BP variations to a greater extent than the variations in oxygen or CO2 concentrations. These findings are confirmed by the studies which have shown a parallel rise in CBFV in response to the OSA induced variations in BP, suggesting an impairment of cerebral autoregulation [7, 28].

5.2.2 Effect of Systemic Hemodynamics on Brain Oxygenation

None of the previous studies have investigated the effect of BP on brain oxygenation during OSA episodes. Results of this study indicated that OSA induced decrease in HbO was found to be negatively and significantly correlated ($r \geq -0.27$, $p \leq 4.27E-04$) with that of percentage rise in systolic, diastolic and mean BP (Table 4-5, Appendix D). In other words, the higher the percentage rise in systolic, diastolic and mean arterial pressure, the greater the reduction in HbO concentration. Further, the rate of rise in diastolic pressure was correlated with this HbO drop ($r=-0.17$, $p=0.03$). Blood pressure was positively correlated with the HbR and HbT data as well ($r \geq 0.36$, $p \leq 2.06E-06$). These parallel changes in brain oxygenation data with that of BP variations may be attributed to the fact that BP has a direct effect on the cerebral blood flow as well as cerebral perfusion [85, 86]. These in turn might affect the brain oxygenation during OSA. Changes in ETCO2 had significant effect only on HbT and not on HbR and HbO (Appendix D). This might be due to the fact that HbT is indicative of cerebral blood volume; and hypercapnea during OSA episodes can lead to vasodilation leading to rise in blood volume [7, 44]. The drop in peripheral oxygenation was significantly correlated to the rise in HbR and HbT ($r \geq 0.22$, $p \leq 0.003$) compared to the level of drop in HbO (Table 4-5, Appendix D). This suggests that the rise in HbR is concurrent with peripheral arterial desaturation. The time to drop/rise in brain oxygenation data was significantly correlated with the time to rise in BP as well as time to drop in SaO2. These results indicate that there is a concurrent change in oxygenation in the brain and rest of the body thereby supporting the hypothesis 2 considered in this study.

5.2.3 Effect of CBFV on Brain Oxygenation

The percentage rises in systolic, diastolic and mean velocities of cerebral blood flow were significantly correlated to changes in HbR and HbT ($r \geq 0.23$, $p \leq 0.002$)

(Appendix E). However, significant correlation coefficients were not obtained between HbO and CBFV features except for the diastolic velocity (r=-0.17, p=0.03). It has been suggested the rise in CBFV may not be sufficient to overcome the OSA induced drop in HbO [44]. Hence the rise in CBFV and drop in HbO may not be parallel and this might be the reason for not observing a significant relation between HbO and rise in CBFV.

5.2.4 Time Delay between CBFV and BP

Since the time to peak in BP and CBFV were highly correlated (r=0.94), a cross correlation analysis was performed to obtain the time delay between these two finite data sets. Even though, the time to peak was significantly correlated, an average delay of 6.20±0.45s was observed between BP and CBFV systolic peaks and 3.98±0.27s for diastolic valleys. Further, it was observed that the OSA induced peak in CBFV does not occur simultaneously with that of BP. CBFV signal tends to peak ahead of BP as indicated by positive lag in cross correlation results.

Since both BP and CBFV was measured using the same data acquisition device, sampled at same frequency (DAQ system in Figure 2-7), there will not be any time delay due to issues with synchronization. Also, based on the technical specification from Nexfin Operator's Manual, the inter-beat interval accuracy of BP monitor is pretty high (10ms). Hence the probability of instrumentation delays contributing to the observed time delay in cross correlation results is negligible.

However, there might be several other factors that might contribute to the observed delay. One such factor is the nature of OSA clips included in this study. Each OSA clip had at least 5 s before the OSA marker and 30-40 s after OSA marker depending on the recovery of SaO_2. If there were repetitive apneas (higher apnea

frequency) prior to or within this considered time interval, it is possible to have overlapping effects of previous and succeeding apneas within an OSA clip. This is also supported by the various patterns identified visually (see patterns in Figure 4-20- Figure 4-22) in this study. Since cross correlation involves multiplication of signal amplitudes, results might be influenced by the presence of different patterns in CBFV or BP. This is also supported by the fact that the highest delay (16 s) between BP and CBFV was observed for bimodal pattern. Furthermore, the changes in BP occur through sympathetic nerve activity and might take longer time to recover whereas changes in brain vasculature might be rapid. Hence mere amplitude multiplication by cross correlation may not be effective in finding the pure time delay in case of repetitive apneas separated by less than 30-40s.

Sleep stages have an effect on average rise in CBFV, but not in BP [42]. In this study, the effect of sleep stages on CBFV was not considered; and OSA episodes were selected irrespective of sleep stages. It is possible that sleep stages might influence the time to peak in CBFV vs BP and needs to be investigated in future studies.

Time delay between CBFV and BP has been observed in other studies as well [87, 88]. This phase shift is believed to arise due to the fast changes in arteriolar resistance by the cerebral autoregulatory mechanism in response to the oscillations in arterial blood pressure [87]. Further, a three-element Windkessel model consisting of two resistors and a capacitor has been used to explain the changes in dynamic blood flow in response to changes in arterial pressure [88, 89]. Detailed explanation of Windkessel model with the equations governing the dynamic cerebral blood flow change is given in Appendix F. As seen from equation (6) in Appendix F, the ratio of flow to pressure depends on vascular resistance. Hence, based on the equation, even if there is no

increase in BP, and if there is an initial decrease in peripheral and cerebral vascular resistance, CBFV can increase resulting in an initial rise in blood flow which may further lead to the rise in pressure. In case of OSA, it is known that accumulation of CO_2 results in vasodilation resulting in reduction of cerebral vascular resistance first, which might happen rapidly before the rise in BP due to sympathetic nerve activity. This might lead to a prominent increase in CBFV which may lead the rise in BP. Further, changes in the cerebrovascular resistance together with changes in vascular compliance can modulate the dynamic blood flow response to arterial blood pressure changes. Depending on the baseline vascular compliance, either vasoconstriction or vasodilation can induce time delay between CBFV and BP peaks [88].

In summary, combined effects of pattern of CBFV or BP within an OSA clip, sleep stages and changes in cerebrovascular resistance and vascular compliance might have led to a time delay of about 6s between CBFV peak and BP peak.

5.2.5 Time Delay between SaO_2 and HbO

The cross correlation analysis between arterial oxygen saturation and cerebral oxy hemoglobin saturation indicated a time delay of 6.05±0.94s (Mean±SEM). It has been suggested that the timing of maximum SaO2 desaturations occur around 20s after the completion of an OSA episode [7]. The reason for delay has been attributed to the delay in pulse oximeters. Average delay time for pulse oximetry, which can be ≥30s [7]. This instrumental delay might play a role in the observed cross correlation lag of SaO_2 compared to the HbO.

5.2.6 System Identification: Dynamic Blood Pressure and Cerebral Blood Flow Velocity Relationship

Dynamic autoregulation, ability of brain to rapidly stabilize the cerebral blood in response to the instantaneous fluctuations in arterial blood pressure has been of interest due to its clinical significance [90]. Frequency domain transfer function models has been widely used to quantify the transient rise in CBFV in response to abrupt changes in BP induced by interventions such as sudden deflation of thigh cuffs , Valsalva maneuvers, periodic squatting etc. [91]. Second order differential equation has been suggested to model the CBFV changes induced by pressure drop during sudden release of thigh cuff [92]. All these studies have been conducted in awake subjects performing an activity that induces rapid BP changes. OSA also induces rapid changes in BP as well as in CBFV. However, no such mathematical models have been proposed for the OSA study. Hence in this study, a linear autoregressive moving average model was used to attempt to quantify the CBFV changes during OSA events.

In previous studies, the changes in BP was induced by various interventions and hence degree of rise can be controlled; however OSA induced BP changes depends on a lot more factors such as frequency of apnea (presence of another breathing disruption ahead or succeeding the current apnea episode), apnea duration and changes in other physiological signals (SaO_2 and CO_2). Hence different patterns were observed and categorized for the OSA episodes and OSA clips in each of the four patterns were fitted with a set of models.

An ARMA model can describe the dynamics of system such as model orders (na, nb) and delay between input and output (nk). Cross correlation analysis showed an average delay of 6s between systolic CBFV and systolic BP. At 10 Hz sampling frequency, this delay corresponds to nk=60 samples. With model orders ranging from 1

to 5, and delay from 0 to 60 samples, the total number of models required for each OSA clip will be 1525 (5x5x61). Further a total of 169 OSA clips were used for system identification analysis (unimodal=56, bimodal=51, drop_preceding=36, rise_succeeding=26). Hence for this large range of delay (nk=0 to 60 samples), the total computation time and the number of models required will be enormous. Hence to reduce this computation time and number of models, delay between CBFV and BP were obtained prior to system identification. This was obtained by shifting the OSA induced peak in systolic BP to match that of the highest peak in systolic CBFV. Shifting in this manner does not alter the way ARMA model obtains the system dynamics. For example: assume that the BP and CBFV increased concurrently without any time delay; in this case nk will be equal to 0 samples; nevertheless there will be system dynamics present (whether the present value of CBFV depends on past values of CBFV or BP) which ARMA will be able to predict. Hence shifting the BP data just helps the model by accounting for the time delay present between BP and CBFV, since we already know the range of delay to be given to system or the range of nk values. The model can then determine the best model orders (na, nb) which governs the number of past inputs and outputs required to predict the present input.

AIC analysis explained in 3.2.3.1, often indicated a possible model order of above 5 and whereas least MSE criteria indicated a lower order model for the same OSA episodes. Hence the final selection of best fit model was performed via least MSE criteria. The distribution of MSE for various values of model orders and delays (Figure 4-29-Figure 4-44) indicated that MSE was lower when the model orders are less irrespective of different delays and patterns. Furthermore, second order system more frequently resulted in the best MSE for the ARMA models in all the four patterns considered (Table 4-6 Best Estimated Model Order for Different Patterns). Hence the

results indicate that a second order differential system might be able to predict the changes in CBFV in response to OSA induced BP variations. These results are similar to what has been suggested by previous studies using awake subjects [92].

Hence the results from this study support the hypotheses that 1) OSA induces significant variations in cerebral hemodynamics and 2) there exist a relation between OSA induced variations in systemic and cerebral hemodynamics.

5.3. Limitations of the Study

A few intrinsic limitations with the CBFV measurement using TCD as well as brain oxygenation measurement via fNIRS, for overnight sleep study can affect the data acquisition and analysis. First, in some subjects, it might be difficult to find a measurement window for CBFV as the Transcranial Doppler method depends on factors like the density of the skull bone. The same holds true for fNIRS measurement too. In fNIRS measurement, since the light has to reach the cortical layers of brain after travelling through the skin, skull and cerebrospinal fluid, increase in thickness of skull can adversely affect the data collected. Further, the skin pigment melanin can interfere with the quality of the reflected signal in fNIRS. Hence care has to be taken to avoid getting hair in between the optodes. Moreover, fNIRS measurements have to be used with caution in subjects with darker skin. Furthermore, CBFV and fNIRS are sensitive to motion artifacts and care has to be taken not to move the sensors during the test via making subject specific molds and strapping the sensors tightly using Velcro bands. However, due to subject movements during sleep, these signals may become distorted due to improper skin contact.

Another limitation of this study is that, due to the presence of baseline shift in raw brain oxygenation data obtained from fNIRS sensors over prolonged period (~8 hours) of data recording, change in brain oxygenation during an OSA episode was compared with

the corresponding values prior to the onset of that particular OSA episode. In order to attain reasonable comparisons between other signals and brain oxygenation, changes in all the systemic and cerebral signals were obtained with respect to their values preceding an OSA episode. These preceding values might represent hyperventilation period if enough time has not elapsed between two consecutive OSAs and might not reflect a true baseline. Considering the initial awake supine state of a subject before going to sleep as a baseline for systemic or cerebral hemodynamic signals would have improved the results of this study.

Furthermore, due to difficulty with simultaneous multi-modal recording of systemic and cerebral hemodynamic signals, the subject population in this study was small (n=11). Hence averaging the changes in hemodynamic signals for each subject would have resulted in less number of samples for correlation analysis (11 samples). However, since each of the selected OSA clips had sufficient time between each other, they can be considered independent of each other and will be legitimate to quantify the changes in each of these OSA episodes. Consequently, the results presented in this chapter might not be a representation of hemodynamic changes in larger subject population; nevertheless, the results indicate a general representation of physiological mechanisms during independent OSA episodes.

5.4. Conclusions and Future Directions

This study has simultaneously measured and quantified the changes in cerebral blood flow velocity and brain oxygenation data together with systemic hemodynamics during Obstructive sleep apnea disorder. The cerebral and systemic hemodynamics appears to be sensitive to apnea duration rather than commonly used apnea severity index of AHI. Most of the features derived from cerebral hemodynamics showed a significant correlation with their systemic counterparts. Further, a second order differential

system can be used to predict the blood pressure related dynamic changes in cerebral blood flow velocity during OSA.

There are a number of possible future investigations from this study:

1. The study indicates the necessity of developing an apnea severity index based on apnea duration as well as the physiological responses.

2. Inclusion of effects of SaO_2 and CO_2 on CBFV, to develop a multi- input single output model of dynamic cerebral autoregulation during OSA.

3. Development of a mathematical model for brain oxygenation changes during apnea.

4. A multi-regression model can be also be used to determine the combined contribution of BP, CO_2 and SaO_2 on CBFV and brain oxygenation rather than conducting individual correlation analysis. Strength of correlation can also be assessed by using a correlation matrix. However, regression analysis and correlation matrix depends only on point estimates as measures of association and not the entire waveform. Hence it might not be useful for completely predicting the underlying system dynamics between systemic and cerebral signals which can be accomplished by an ARMA model.

Appendix A

Kolmogorov-Smirnov Normality Test for CBFV and Brain Oxygenation Data

Table A-1 Normality Test Results for Cerebral Blood Flow Data

Features	p-value
%sys_cbfv (%)	1.45E-150
%dia_ cbfv (%)	4.99E-147
%mean_ cbfv (%)	2.02E-130
%area_ cbfv (%)	1.82E-150
sys_slope_ cbfv (cm/s^2)	1.43E-38
dia_slope_ cbfv (cm/s^2)	4.44E-36
mean_slope_ cbfv (cm/s^2)	5.60E-36
tp_ cbfv (s)	2.52E-152

Number of OSA episodes, N=178; α=0.05

Table A-2 Normality Test Results for Brain Oxygenation Data

Features	p-value
hbo_min	9.95E-47
hbr_max	2.33E-49
hbt_max	8.26E-51
hbo_td	2.52E-152
hbr_tr	2.52E-152
hbt_tr	2.52E-152

Number of OSA episodes, N=178; α=0.05

Appendix B

Effect of OSA Duration on Systemic Hemodynamics

Table B-1 Effect of OSA Duration on Systemic Hemodynamics

Systemic Signals	**Features**	**Corr. Coeff**	**p-value**
BP	%sys_bp (%)	0.29*	6.73E-05
	%dia_bp (%)	0.43*	5.04E-09
	%mean_bp (%)	0.39*	9.36E-08
	%area_bp (%)	-0.04	0.61
	Sys_slope_bp (mmHg/s)	-0.44*	1.92E-09
	Dia_slope_bp (mmHg/s)	-0.40*	4.89E-08
	Mean_slope_bp (mmHg/s)	-0.33*	8.86E-06
	tp_bp (s)	0.95**	5.70E-87
SaO_2	% SaO_2_drop (%)	0.44*	2.36E-09
	SaO_2_td (s)	0.85**	1.69E-49
CO_2	$\Delta ETCO_2$ (mmHg)	0.34*	1.01E-05

Number of OSA episodes, N=178; α=0.05

Appendix C

Effect of Apnea Severity on Cerebral and Systemic Hemodynamics

Table C-1 Effect of AHI on Cerebral Hemodynamics

Cerebral Signals	Features	Corr. Coeff	p-value
CBFV	%sys_cbfv (%)	-0.01	0.99
	%dia_cbfv (%)	0.29	0.39
	%mean_cbfv (%)	0.21	0.54
	%area_cbfv (%)	0.55	0.88
	Sys_slope_cbfv (cm/s^2)	0.36	0.27
	Dia_slope_cbfv (cm/s^2)	0.12	0.73
	Mean_slope_cbfv (cm/s^2)	0.14	0.69
	tp_cbfv (s)	-0.34	0.31
Brain Oxygenation	hbo_min	-0.24	0.49
	hbr_max	-0.34	0.31
	hbt_max	-0.32	0.34
	hbo_td	-0.34	0.31
	hbr_tr	-0.32	0.34
	hbt_tr	0.25	0.45

Number of OSA episodes, N=178; α=0.05

Table C-2 Effect of AHI on Systemic Hemodynamics

Systemic Signals	Features	Corr. Coeff	p-value
BP	%sys_bp (%)	0.01	0.99
	%dia_bp (%)	0.07	0.84
	%mean_bp (%)	0.06	0.86
	%area_bp (%)	0.48	0.14
	Sys_slope_bp (mmHg/s)	0.48	0.14
	Dia_slope_bp (mmHg/s)	0.35	0.29
	Mean_slope_bp (mmHg/s)	0.32	0.34
	tp_bp (s)	-0.05	0.88
SaO_2	% SaO_2_drop (%)	-0.35	0.30
	SaO_2_td (s)	0.02	0.97
CO_2	$\Delta ETCO_2$ (mmHg)	0.15	0.67

Number of OSA episodes, N=178; α=0.05

Appendix D

Influence of Systemic Hemodynamics on Variations in Cerebral Hemodynamics

Table D-1 Effect of Systemic Hemodynamics on Cerebral Blood Flow Velocity

Systemic Features		CBFV Features	Corr. Coeff	p-value
BP	%sys_bp	%sys_cbfv	0.33*	9.58E-06
	%dia_bp	%dia_cbfv	0.49**	2.28E-12
	%mean_bp	%mean_cbfv	0.49**	1.75E-12
	%area_bp	%area_cbfv	0.17*	0.02
	sys_slope_bp	sys_slope_cbfv	0.29*	0.0001
	dia_slope_bp	dia_slope_cbfv	0.41*	2.14E-08
	mean_slope_bp	mean_slope_cbfv	0.44*	3.39E-09
	tp_bp	tp_cbfv	0.94**	1.65E-79
$\Delta ETCO_2$	ΔETCO2	%sys_cbfv	0.37*	1.13E-06
	ΔETCO2	%dia_cbfv	0.29*	1.89E-04
	ΔETCO2	%mean_cbfv	0.31*	4.53E-05
	ΔETCO2	%area_cbfv	0.25*	1.41E-03
	ΔETCO2	sys_slope_cbfv	0.03	6.89E-01
	ΔETCO2	dia_slope_cbfv	0.07	3.66E-01
	ΔETCO2	mean_slope_cbfv	0.11	1.77E-01
	ΔETCO2	tp_cbfv	0.31*	4.55E-05
SaO_2	%SaO_2_Drop	%sys_cbfv	0.30*	5.23E-05
	%SaO_2_Drop	%dia_cbfv	0.31*	3.85E-05
	%SaO_2_Drop	%mean_cbfv	0.32*	2.38E-05
	%SaO_2_Drop	%area_cbfv	0.18*	0.019973
	%SaO_2_Drop	sys_slope_cbfv	-0.10	0.197771
	%SaO_2_Drop	dia_slope_cbfv	0.05	4.80E-01
	%SaO_2_Drop	mean_slope_cbfv	-0.09	2.50E-01
	%SaO_2_Drop	tp_cbfv	0.42*	7.71E-09
	SaO2_td	%sys_cbfv	0.59**	1.16E-17
	SaO2_td	%dia_cbfv	0.48**	4.23E-11

Table D-1—*Continued*

SaO_2	SaO2_td	%mean_cbfv	0.54**	1.38E-14
	SaO2_td	%area_cbfv	0.33*	1.12E-05
	SaO2_td	sys_slope_cbfv	-0.17*	0.027287
	SaO2_td	dia_slope_cbfv	-0.08	3.28E-01
	SaO2_td	mean_slope_cbfv	-0.05	4.77E-01
	SaO2_td	tp_cbfv	0.84**	4.49E-47

Number of OSA episodes, N=178; α=0.05

Table D-2 Effect of Systemic Hemodynamics on HbO

Systemic Features		**Brain Oxygenation**	**Corr. Coeff**	**p-value**
BP	%sys_bp	HbO_min	-0.34*	4.97E-06
		HbO_td	0.16*	3.80E-02
	%dia_bp	HbO_min	-0.28*	2.10E-04
		HbO_td	0.30*	5.67E-05
	%mean_bp	HbO_min	-0.27*	4.27E-04
		HbO_td	0.24*	1.41E-03
	%area_bp	HbO_min	-0.12	0.12408
		HbO_td	-0.08	0.276831
	sys_slope_bp	HbO_min	-0.15	0.05224
		HbO_td	-0.46**	3.26E-10
	dia_slope_bp	HbO_min	-0.17*	3.04E-02
		HbO_td	-0.38*	2.68E-07
	mean_slope_bp	HbO_min	-0.11	1.62E-01
		HbO_td	-0.34**	5.78E-06
	tp_bp	HbO_min	-0.03	6.72E-01
		HbO_td	0.76**	9.56E-34
$\Delta ETCO_2$	ΔETCO2	HbO_min	-0.06	4.10E-01
		HbO_td	0.30*	1.12E-04
SaO_2	$\%SaO_2$_Drop	HbO_min	-0.13	9.09E-02
		HbO_td	0.21*	6.23E-03
	SaO2_td	HbO_min	-0.04	6.43E-01
		HbO_td	0.71**	5.04E-28

Number of OSA episodes, N=178; α=0.05

Table D-3 Effect of Systemic Hemodynamics on HbR

Systemic Features		Brain Oxygenation	Corr. Coeff	p-value
BP	%sys_bp	HbR_max	0.50**	0.00E+00
		HbR_tr	0.18*	1.93E-02
	%dia_bp	HbR_max	0.46**	4.94E-10
		HbR_tr	0.32*	1.89E-05
	%mean_bp	HbR_max	0.38*	3.94E-07
		HbR_tr	0.31*	4.43E-05
	%area_bp	HbR_max	0.07	0.354423
		HbR_tr	-0.03	0.699299
	sys_slope_bp	HbR_max	-0.02	7.57E-01
		HbR_tr	-0.36*	1.33E-06
	dia_slope_bp	HbR_max	0.01	8.61E-01
		HbR_tr	-0.35*	3.40E-06
	mean_slope_bp	HbR_max	-0.15	4.96E-02
		HbR_tr	-0.21*	5.35E-03
	tp_bp	HbR_max	0.27*	3.95E-04
		HbR_tr	0.84**	5.28E-48
$\Delta ETCO_2$	ΔETCO2	HbR_max	0.14	0.07
		HbR_tr	0.30*	1.11E-04
SaO_2	$\%SaO_2$_Drop	HbR_max	0.57**	5.45E-16
		HbR_tr	0.21*	5.36E-03
	SaO2_td	HbR_max	0.27*	0.00039
		HbR_tr	0.76**	6.40E-34

Number of OSA episodes, N=178; α=0.05

Table D-4 Effect of Systemic Hemodynamics on HbT

Systemic Features		Brain Oxygenation	Corr. Coeff	p-value
BP	%sys_bp	HbT_max	0.37*	6.99E-07
		HbT_tr	0.26*	6.83E-04
	%dia_bp	HbT_max	0.38*	3.93E-07
		HbT_tr	0.34*	3.64E-06
	%mean_bp	HbT_max	0.36*	2.06E-06
		HbT_tr	0.33*	7.63E-06
	%area_bp	HbT_max	0.12	0.125859
		HbT_tr	-0.04	0.581674
	sys_slope_bp	HbT_max	-0.01	8.99E-01
		HbT_tr	-0.27*	3.25E-04
	dia_slope_bp	HbT_max	0.06	4.71E-01
		HbT_tr	-0.25*	8.42E-04
	mean_slope_bp	HbT_max	-0.01	8.48E-01
		HbT_tr	-0.22*	4.11E-03
	tp_bp	HbT_max	0.21*	6.48E-03
		HbT_tr	0.73**	1.99E-30
Δ $ETCO_2$	ΔETCO2	HbT_max	0.19*	1.50E-02
		HbT_tr	0.30*	8.76E-05
SaO_2	$\%SaO_2$_Drop	HbT_max	0.22*	3.39E-03
		HbT_tr	0.30*	7.86E-05
	SaO2_td	HbT_max	0.22*	3.66E-03
		HbT_tr	0.70**	7.98E-27

Number of OSA episodes, N=178; α=0.05

Appendix E

Effect of Cerebral Blood Flow Velocity on Brain Oxygenation

Table E-1 Effect of CBFV on HbO

CBFV Features	Brain Oxygenation	Corr. Coeff	p-value
%sys_CBFV	HbO_min	-0.07	3.40E-01
	HbO_td	0.37*	5.06E-07
%dia_CBFV	HbO_min	-0.17*	2.96E-02
	HbO_td	0.25*	1.05E-03
%mean_CBFV	HbO_min	-0.11	1.54E-01
	HbO_td	0.31*	3.92E-05
%area_CBFV	HbO_min	0.04	0.59101
	HbO_td	0.14	0.065541
sys_slope_CBFV	HbO_min	-0.12	0.10532
	HbO_td	-0.29*	1.31E-04
dia_slope_CBFV	HbO_min	-0.23*	2.74E-03
	HbO_td	-0.21*	4.90E-03
mean_slope_CBFV	HbO_min	-0.20*	7.92E-03
	HbO_td	-0.17*	2.39E-02
tp_CBFV	HbO_min	-0.03	6.72E-01
	HbO_td	0.75**	6.47E-33

Number of OSA episodes, N=178; α=0.05

Table E-2 Effect of CBFV on HbR

CBFV Features	Brain Oxygenation	Corr. Coeff	p-value
%sys_CBFV	HbR_max	0.24*	1.64E-03
	HbR_tr	0.50**	1.78E-12
%dia_CBFV	HbR_max	0.23*	2.28E-03
	HbR_tr	0.40*	8.04E-08
%mean_CBFV	HbR_max	0.24*	1.37E-03
	HbR_tr	0.44*	2.22E-09
%area_CBFV	HbR_max	0.06	0.40418
	HbR_tr	0.21*	0.004763
sys_slope_CBFV	HbR_max	-0.12	1.03E-01
	HbR_tr	-0.21*	5.84E-03
dia_slope_CBFV	HbR_max	0.07	3.82E-01
	HbR_tr	-0.15	5.12E-02
mean_slope_CBFV	HbR_max	-0.05	5.32E-01
	HbR_tr	-0.09	2.48E-01
tp_CBFV	HbR_max	0.31*	3.05E-05
	HbR_tr	0.83**	4.90E-45

Number of OSA episodes, N=178; α=0.05

Table E-3 Effect of CBFV on HbT

CBFV Features	Brain Oxygenation	Corr. Coeff	p-value
%sys_CBFV	HbT_max	0.35*	3.05E-06
	HbT_tr	0.44*	2.47E-09
%dia_CBFV	HbT_max	0.27*	4.08E-04
	HbT_tr	0.36*	1.31E-06
%mean_CBFV	HbT_max	0.34*	5.10E-06
	HbT_tr	0.40*	5.16E-08
%area_CBFV	HbT_max	0.22*	0.003523
	HbT_tr	0.18*	0.020337
sys_slope_CBFV	HbT_max	-0.02	8.21E-01
	HbT_tr	-0.15	5.45E-02
dia_slope_CBFV	HbT_max	0.07	3.75E-01
	HbT_tr	-0.05	4.78E-01
mean_slope_CBFV	HbT_max	0.04	5.65E-01
	HbT_tr	-0.05	4.85E-01
tp_CBFV	HbT_max	0.19*	1.22E-02
	HbT_tr	0.72**	1.22E-28

Number of OSA episodes, N=178; α=0.05

Appendix F

Three-Element Windkessel Model

Basis of Windkessel model as shown in Figure F-1 [88], is that the MCA can be considered as a conduit vessel; the arteries and arterioles branching off from MCA can be represented by resistance vessels (R_a) capable of dilating/constricting to regulate the blood flow in response to changes in perfusion pressure [88, 89]. Dynamic cerebral blood flow (Q_m) also depends on peripheral vascular resistance (R_p), and peripheral vascular compliance (C_p). Changes in cerebral perfusion pressure (P_m) can be approximated from changes in mean arterial blood pressure with the assumption that intracranial pressure (P_i) and cerebral venous pressure (P_v) is very small (~0). Additionally, the circuit also includes Q_i, Q_p and P_p which represents the intermediate flow and pressures.

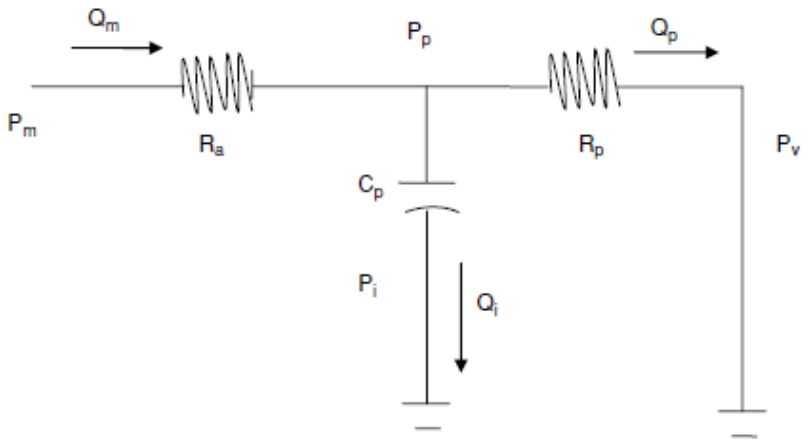

Figure F-1 Three Element Windkessel Model

Assuming the flow and pressure are related, the above Windkessel model can be expressed by a set of equations as given below in frequency and time domain (equations 1-5):

$$P_m - P_p = R_a\, Q_m \qquad (1)$$

$$P_p - P_v = R_p Q_p \qquad (2)$$

$$P_p - P_i = \frac{Q_m - Q_p}{iwC_p} \qquad (3)$$

Assuming (Pi) and (Pv) = 0, cerebrovascular impedance can be expressed as:

$$\frac{P_m}{Q_m} = \frac{R_p + R_a + iwC_pR_pR_a}{1 + iwC_pR_p} \qquad (4)$$

In time domain, the relation between flow and pressure can be expressed via differential equation as given below:

$$R_a\left[\frac{dQ_m}{dt} + \frac{(R_p + R_a)Q_m}{C_pR_pR_a}\right] = \frac{dP_m}{dt} + \frac{P_m}{C_pR_p} \qquad (5)$$

C_pR_p and $(C_pR_pR_a)/(R_p + R_a)$ represents the characteristic relaxation times in this model.

The ratio of flow to pressure can be expressed as [89] :

$$\frac{Q_m}{P_m} = \frac{1}{R_p + R_a} \qquad (6)$$

References

[1] T. Young, P. E. Peppard, and D. J. Gottlieb, "Epidemiology of obstructive sleep apnea: a population health perspective," *Am J Respir Crit Care Med,* vol. 165, pp. 1217-39, May 2002.

[2] T. Young, M. Palta, J. Dempsey, J. Skatrud, S. Weber, and S. Badr, "The occurrence of sleep-disordered breathing among middle-aged adults," *N Engl J Med,* vol. 328, pp. 1230-5, Apr 1993.

[3] A. Culebras, "Cerebrovascular disease and sleep," *Curr Neurol Neurosci Rep,* vol. 4, pp. 164-9, Mar 2004.

[4] J. A. Dempsey, S. C. Veasey, B. J. Morgan, and C. P. O'Donnell, "Pathophysiology of sleep apnea," *Physiol Rev,* vol. 90, pp. 47-112, Jan 2010.

[5] S. Javaheri and J. A. Dempsey, "Central sleep apnea," *Compr Physiol,* vol. 3, pp. 141-63, Jan 2013.

[6] V. K. Somers, D. P. White, R. Amin, W. T. Abraham, F. Costa, A. Culebras*, et al.*, "Sleep apnea and cardiovascular disease: an American Heart Association/american College Of Cardiology Foundation Scientific Statement from the American Heart Association Council for High Blood Pressure Research Professional Education Committee, Council on Clinical Cardiology, Stroke Council, and Council On Cardiovascular Nursing. In collaboration with the National Heart, Lung, and Blood Institute National Center on Sleep Disorders Research (National Institutes of Health)," *Circulation,* vol. 118, pp. 1080-111, Sep 2008.

[7] D. J. Durgan and R. M. Bryan, Jr., "Cerebrovascular consequences of obstructive sleep apnea," *J Am Heart Assoc,* vol. 1, p. e000091, Aug 2012.

[8] T. Young, L. Finn, P. E. Peppard, M. Szklo-Coxe, D. Austin, F. J. Nieto*, et al.*, "Sleep disordered breathing and mortality: eighteen-year follow-up of the Wisconsin sleep cohort," *Sleep,* vol. 31, pp. 1071-8, Aug 2008.

[9] T. Young, L. Evans, L. Finn, and M. Palta, "Estimation of the clinically diagnosed proportion of sleep apnea syndrome in middle-aged men and women," *Sleep,* vol. 20, pp. 705-6, Sep 1997.

[10] A. Romero-Corral, S. M. Caples, F. Lopez-Jimenez, and V. K. Somers, "Interactions Between Obesity and Obstructive Sleep Apnea: Implications for Treatment," *Chest,* vol. 137, pp. 711-719, Mar 2010.

[11] S. Ancoli-Israel, D. F. Kripke, M. R. Klauber, W. J. Mason, R. Fell, and O. Kaplan, "Sleep-disordered breathing in community-dwelling elderly," *Sleep,* vol. 14, pp. 486-95, Dec 1991.

[12] S. K. Roepke and S. Ancoli-Israel, "Sleep disorders in the elderly," *Indian J Med Res,* vol. 131, pp. 302-10, Feb 2010.

[13] P. Lavie, "Treatment of sleep apnea: unmet needs," *Chest,* vol. 116, pp. 1501-3, Dec 1999.

[14] M. R. Mannarino, F. Di Filippo, and M. Pirro, "Obstructive sleep apnea syndrome," *Eur J Intern Med,* vol. 23, pp. 586-93, Oct 2012.

[15] K. Kario, "Obstructive sleep apnea syndrome and hypertension: ambulatory blood pressure," *Hypertens Res,* vol. 32, pp. 428-32, Jun 2009.

[16] F. Torelli, N. Moscufo, G. Garreffa, F. Placidi, A. Romigi, S. Zannino*, et al.*, "Cognitive profile and brain morphological changes in obstructive sleep apnea," *Neuroimage,* vol. 54, pp. 787-93, Jan 2011.

[17] H. K. Yaggi, J. Concato, W. N. Kernan, J. H. Lichtman, L. M. Brass, and V. Mohsenin, "Obstructive sleep apnea as a risk factor for stroke and death," *N Engl J Med,* vol. 353, pp. 2034-41, Nov 2005.

[18] P. L. Smith, J. P. Kirkness, S. Patil, H. Schneider, and A. R. Schwartz, "Biomechanics of the upper airway during sleep," in *Sleep Apnea: Pathogenesis, Diagnosis and Treatment*, A. I. Pack, Ed., 2 ed Boca Raton, FL: CRC Press, 2011, pp. 27-52.

[19] K. Narkiewicz, F. H. S. Kuniyoshi, V. K. Somers, and B. G. Phillips, "Influence of Sleep and Sleep Apnea on Autonomic Control of the Cardiovascular System," in *Sleep Apnea : Implications in Cardiovascular and Cerebrovascular Disease*, T. D. Bradley and J. S. Floras, Eds., 2 ed Boca Raton, FL: CRC Press 2009, pp. 141-162

[20] T. D. Bradley and J. S. Floras, "Sleep apnea and heart failure: Part I: obstructive sleep apnea," *Circulation,* vol. 107, pp. 1671-8, Apr 2003.

[21] V. K. Somers, M. E. Dyken, M. P. Clary, and F. M. Abboud, "Sympathetic neural mechanisms in obstructive sleep apnea," *J Clin Invest,* vol. 96, pp. 1897-904, Oct 1995.

[22] V. K. Somers, A. L. Mark, and F. M. Abboud, "Sympathetic activation by hypoxia and hypercapnia--implications for sleep apnea," *Clin Exp Hypertens A,* vol. 10 Suppl 1, pp. 413-22, 1988.

[23] J. S. Floras, "Sleep apnea and cardiovascular risk," *J Cardiol,* vol. 63, pp. 3-8, Jan 2014.

[24] V. Mohsenin, "Obstructive sleep apnea and hypertension: a critical review," *Curr Hypertens Rep,* vol. 16, p. 482, Oct 2014.

[25] T. Kasai, J. S. Floras, and T. D. Bradley, "Sleep apnea and cardiovascular disease: a bidirectional relationship," *Circulation,* vol. 126, pp. 1495-510, Sep 2012.

[26] R. K. Malhotra and A. K. Desai, "Healthy brain aging: what has sleep got to do with it?," *Clin Geriatr Med,* vol. 26, pp. 45-56, Feb 2010.

[27] L. Xie, H. Kang, Q. Xu, M. J. Chen, Y. Liao, M. Thiyagarajan*, et al.*, "Sleep drives metabolite clearance from the adult brain," *Science,* vol. 342, pp. 373-7, Oct 2013.

[28] F. Urbano, F. Roux, J. Schindler, and V. Mohsenin, "Impaired cerebral autoregulation in obstructive sleep apnea," *J Appl Physiol,* vol. 105, pp. 1852-7, Dec 2008.

[29] G. Bhave, "A Study of the Physiological Effects of Sleep Apnea on Cerebral Blood Flow Velocity," M.S., Bioengineering Department, University of Texas at Arlington, Arlington, 2010.

[30] V. Mohsenin, "Sleep-related breathing disorders and risk of stroke," *Stroke,* vol. 32, pp. 1271-8, Jun 2001.

[31] N. Canessa, V. Castronovo, S. F. Cappa, M. S. Aloia, S. Marelli, A. Falini*, et al.*, "Obstructive sleep apnea: brain structural changes and neurocognitive function before and after treatment," *Am J Respir Crit Care Med,* vol. 183, pp. 1419-26, May 2011.

[32] P. M. Macey, L. A. Henderson, K. E. Macey, J. R. Alger, R. C. Frysinger, M. A. Woo*, et al.*, "Brain morphology associated with obstructive sleep apnea," *Am J Respir Crit Care Med,* vol. 166, pp. 1382-7, Nov 2002.

[33] A. Daurat, J. Foret, J. L. Bret-Dibat, C. Fureix, and M. Tiberge, "Spatial and temporal memories are affected by sleep fragmentation in obstructive sleep apnea syndrome," *J Clin Exp Neuropsychol,* vol. 30, pp. 91-101, Jan 2008.

[34] J. Greneche, J. Krieger, F. Bertrand, C. Erhardt, M. Maumy, and P. Tassi, "Short-term memory performances during sustained wakefulness in patients with obstructive sleep apnea-hypopnea syndrome," *Brain Cogn,* vol. 75, pp. 39-50, Feb 2011.

[35] T. Saunamaki, S. L. Himanen, O. Polo, and M. Jehkonen, "Executive dysfunction and learning effect after continuous positive airway pressure treatment in patients with obstructive sleep apnea syndrome," *Eur Neurol,* vol. 63, pp. 215-20, Mar 2010.

[36] E. Y. Joo, W. S. Tae, M. J. Lee, J. W. Kang, H. S. Park, J. Y. Lee*, et al.*, "Reduced brain gray matter concentration in patients with obstructive sleep apnea syndrome," *Sleep,* vol. 33, pp. 235-41, Feb 2010.

[37] A. M. Stowe, T. Altay, A. B. Freie, and J. M. Gidday, "Repetitive hypoxia extends endogenous neurovascular protection for stroke," *Ann Neurol,* vol. 69, pp. 975-85, Jun 2011.

[38] J. C. Felver-Gant, A. S. Bruce, M. Zimmerman, L. H. Sweet, R. P. Millman, and M. S. Aloia, "Working memory in obstructive sleep apnea: construct validity and treatment effects," *J Clin Sleep Med,* vol. 3, pp. 589-94, Oct 2007.

[39] L. Ferini-Strambi, C. Baietto, M. R. Di Gioia, P. Castaldi, C. Castronovo, M. Zucconi*, et al.*, "Cognitive dysfunction in patients with obstructive sleep apnea (OSA): partial reversibility after continuous positive airway pressure (CPAP)," *Brain Res Bull,* vol. 61, pp. 87-92, Jun 2003.

[40] R. Alex, G. Bhave, M. A. Al-Abed, A. Bashaboyina, S. Iyer, D. E. Watenpaugh*, et al.*, "An investigation of simultaneous variations in cerebral blood flow velocity and arterial blood pressure during sleep apnea," *Conf Proc IEEE Eng Med Biol Soc,* vol. 2012, pp. 5634-7, 2012.

[41] M. Siebler and A. Nachtmann, "Cerebral hemodynamics in obstructive sleep apnea," *Chest,* vol. 103, pp. 1118-9, Apr 1993.

[42] J. Klingelhofer, G. Hajak, D. Sander, M. Schulz-Varszegi, E. Ruther, and B. Conrad, "Assessment of intracranial hemodynamics in sleep apnea syndrome," *Stroke,* vol. 23, pp. 1427-33, Oct 1992.

[43] C. O. Olopade, E. Mensah, R. Gupta, D. Huo, D. L. Picchietti, E. Gratton*, et al.*, "Noninvasive Determination of Brain Tissue Oxygenation during Sleep in Obstructive Sleep Apnea: A Near-Infrared Spectroscopic Approach," *Sleep,* vol. 30, pp. 1747-1755, Dec 2007.

[44] F. Pizza, M. Biallas, M. Wolf, E. Werth, and C. L. Bassetti, "Nocturnal cerebral hemodynamics in snorers and in patients with obstructive sleep apnea: a near-infrared spectroscopy study," *Sleep,* vol. 33, pp. 205-10, Feb 2010.

[45] R. J. Davies, J. Crosby, K. Vardi-Visy, M. Clarke, and J. R. Stradling, "Non-invasive beat to beat arterial blood pressure during non-REM sleep in obstructive sleep apnoea and snoring," *Thorax,* vol. 49, pp. 335-9, Apr 1994.

[46] K. H. Wesseling, B. de Wit, G. M. A. van der Hoeven, J. van Goudoever, and J. J. Settels, "Physiocal, calibrating finger vascular physiology for Finapres," *Homeostasis,* vol. 36, pp. 67–82, 1995.

[47] B. P. Imholz, W. Wieling, G. A. van Montfrans, and K. H. Wesseling, "Fifteen years experience with finger arterial pressure monitoring: assessment of the technology," *Cardiovasc Res,* vol. 38, pp. 605-16, Jun 1998.

[48] K. H. Wesseling, "Finger arterial pressure measurement with Finapres," *Z Kardiol,* vol. 85 Suppl 3, pp. 38-44, 1996.

[49] D. W. Eeftinck Schattenkerk, J. J. van Lieshout, A. H. van den Meiracker, K. R. Wesseling, S. Blanc, W. Wieling*, et al.*, "Nexfin noninvasive continuous blood

pressure validated against Riva-Rocci/Korotkoff," *Am J Hypertens,* vol. 22, pp. 378-83, Apr 2009.
[50] J. R. Martina, B. E. Westerhof, J. Van Goudoever, N. De Jonge, J. J. Van Lieshout, J. R. Lahpor*, et al.*, "Noninvasive blood pressure measurement by the Nexfin monitor during reduced arterial pulsatility: a feasibility study," *ASAIO J,* vol. 56, pp. 221-7, May-Jun 2010.
[51] J. R. Martina, B. E. Westerhof, J. van Goudoever, E. M. de Beaumont, J. Truijen, Y. S. Kim*, et al.*, "Noninvasive continuous arterial blood pressure monitoring with Nexfin(R)," *Anesthesiology,* vol. 116, pp. 1092-103, May 2012.
[52] A. H. van Beek, J. A. Claassen, M. G. Rikkert, and R. W. Jansen, "Cerebral autoregulation: an overview of current concepts and methodology with special focus on the elderly," *J Cereb Blood Flow Metab,* vol. 28, pp. 1071-85, Jun 2008.
[53] G. Strangman, D. A. Boas, and J. P. Sutton, "Non-invasive neuroimaging using near-infrared light," *Biol Psychiatry,* vol. 52, pp. 679-93, Oct 2002.
[54] D. T. Delpy and M. Cope, "Quantification in tissue near-infrared spectroscopy," *Philos Trans R Soc Lond B Biol Sci,* vol. 352, pp. 649–659, Jun 1997.
[55] T. J. Huppert, S. G. Diamond, M. A. Franceschini, and D. A. Boas, "HomER: a review of time-series analysis methods for near-infrared spectroscopy of the brain," *Appl Opt,* vol. 48, pp. D280-98, Apr 2009.
[56] E. Okada, "Photon Migration in NIRS Brain Imaging," in *Application of Near Infrared Spectroscopy in Biomedicine*, T. Jue; and K. Masuda;, Eds., 1 ed: Springer US, 2013, pp. 37-58.
[57] C.-W. Sun and C.-C. Chuang, "Hemodynamics Study Based on Near-Infrared Optical Assessment," in *Hemodynamics - New Diagnostic and Therapeuric Approaches*, A. S. Artis, Ed., ed: InTech, 2012.
[58] F. Irani, S. M. Platek, S. Bunce, A. C. Ruocco, and D. Chute, "Functional near infrared spectroscopy (fNIRS): an emerging neuroimaging technology with important applications for the study of brain disorders," *Clin Neuropsychol,* vol. 21, pp. 9-37, Jan 2007.
[59] J. E. Sinex, "Pulse oximetry: principles and limitations," *Am J Emerg Med,* vol. 17, pp. 59-67, Jan 1999.
[60] P. D. Mannheimer, N. A. Asbaugh, and N. T. Staff, "Nellcor™ OxiMax Pulse Oximeter Accuracy," Covidien, Boulder, CO 2011.
[61] P. Hassett, M. Contreras, and J. G. Laffey, "Hypercapnia: Permissive, Therapeutic, or Not at All?," in *Intensive Care Medicine*, J.-L. Vincent, Ed., ed: Springer New York, 2008, pp. 269-281.
[62] K. R. Ward and D. M. Yealy, "End-tidal carbon dioxide monitoring in emergency medicine, Part 1: Basic principles," *Acad Emerg Med,* vol. 5, pp. 628-36, Jun 1998.
[63] C. W. Peters, G. H. Adkisson, M. S. Ozcan, and T. J. Gallagher, "Capnometry monitoring in high- and low-pressure environments," in *Capnography*, J. S. Gravenstein, M. B. Jaffe, N. Gravenstein, and D. A. Paulus, Eds., ed: Cambridge University Press, 2011, pp. 124-125.
[64] P. Respironics. (5/26/2015). *CAPNOGARD® Specifications*. Available: http://capnogard.respironics.com/Specifications.asp
[65] R. D. Boehmer, "Continuous, real-time, noninvasive monitor of blood pressure: Penaz methodology applied to the finger," *J Clin Monit,* vol. 3, pp. 282-7, Oct 1987.

[66] A. Rechtschaffen and A. Kales, *A Manual of Standardized Terminology, Techniques and Scoring System for Sleep Stages of Human Subjects*. Washington, DC: U.S. Government Printing Office, 1968.
[67] R. B. Berry, R. Budhiraja, D. J. Gottlieb, D. Gozal, C. Iber, V. K. Kapur*, et al.*, "Rules for scoring respiratory events in sleep: update of the 2007 AASM Manual for the Scoring of Sleep and Associated Events. Deliberations of the Sleep Apnea Definitions Task Force of the American Academy of Sleep Medicine," *J Clin Sleep Med,* vol. 8, pp. 597-619, Oct 2012.
[68] T. Przybylowski, M. F. Bangash, K. Reichmuth, B. J. Morgan, J. B. Skatrud, and J. A. Dempsey, "Mechanisms of the cerebrovascular response to apnoea in humans," *J Physiol,* vol. 548, pp. 323-32, Apr 2003.
[69] J. H. Zar, "Spearman Rank Correlation," in *Encyclopedia of Biostatistics* vol. 7, Peter Armitage and T. Colton, Eds., 2 ed. West Sussex, UK: Wiley, 2005, pp. 5095-5101.
[70] S. Siegel and N. J. Castellan Jr, *Nonparametric Statistics for the Behavioral Sciences*, 2 ed.: McGraw-Hill, 1988.
[71] J. D. Gibbons and S. Chakraborti, "Nonparametric Statistical Inference," in *International Encyclopedia of Statistical Science*, M. Lovric, Ed., ed: Springer Berlin Heidelberg, 2014, pp. 977-979.
[72] J. G. Proakis and D. K. Manolakis, *Digital Signal Processing*, 4 ed. Upper Saddle River, New Jersey: Pearson Prentice Hall, 2006.
[73] M. H. Perrott and R. J. Cohen, "An efficient approach to ARMA modeling of biological systems with multiple inputs and delays," *IEEE Trans Biomed Eng,* vol. 43, pp. 1-14, Jan 1996.
[74] L. Ljung, "System identification toolbox," ed. South Natick, MA, USA: The MathWorks Inc, 1988.
[75] K. P. Burnham and D. R. Anderson, *Model selection and multimodel inference: a practical information-theoretic approach*: Springer Science & Business Media, 2002.
[76] S. Araghinejad, *Data-Driven Modeling: Using MATLAB® in Water Resources and Environmental Engineering*, 1 ed.: Springer Netherlands, 2014.
[77] L. Edvinsson, P. Aubineau, C. Owman, R. Sercombe, and J. Seylaz, "Sympathetic innervation of cerebral arteries: prejunctional supersensitivity to norepinephrine after sympathectomy or cocaine treatment," *Stroke,* vol. 6, pp. 525-30, Sep-Oct 1975.
[78] J. W. Hamner, C. O. Tan, K. Lee, M. A. Cohen, and J. A. Taylor, "Sympathetic control of the cerebral vasculature in humans," *Stroke,* vol. 41, pp. 102-9, Jan 2010.
[79] G. I. McHedlishvili, "Vascular Mechanisms Pertaining to the Intrinsic Regulation of the Cerebral Circulation," *Circulation,* vol. 30, pp. 597-610, Oct 1964.
[80] R. Zhang, J. H. Zuckerman, K. Iwasaki, T. E. Wilson, C. G. Crandall, and B. D. Levine, "Autonomic neural control of dynamic cerebral autoregulation in humans," *Circulation,* vol. 106, pp. 1814-20, Oct 2002.
[81] S. Ogoh, R. M. Brothers, W. L. Eubank, and P. B. Raven, "Autonomic neural control of the cerebral vasculature: acute hypotension," *Stroke,* vol. 39, pp. 1979-87, Jul 2008.
[82] Y. Hou, Y. Shang, R. Cheng, Y. Zhao, Y. Qin, R. Kryscio*, et al.*, "Obstructive sleep apnea–hypopnea results in significant variations in cerebral hemodynamics detected by diffuse optical spectroscopies," *Physiological measurement,* vol. 35, p. 2135, Oct 2014.

[83] A. Otero, P. Félix, J. Presedo, and C. Zamarrón, "An Evaluation of Indexes as Support Tools in the Diagnosis of Sleep Apnea," *Annals of Biomedical Engineering,* vol. 40, pp. 1825-1834, Aug 2012.

[84] A. Muraja-Murro, J. Nurkkala, P. Tiihonen, T. Hukkanen, H. Tuomilehto, J. Kokkarinen*, et al.*, "Total duration of apnea and hypopnea events and average desaturation show significant variation in patients with a similar apnea-hypopnea index," *J Med Eng Technol,* vol. 36, pp. 393-8, Nov 2012.

[85] M. Reinhard, E. Wehrle-Wieland, D. Grabiak, M. Roth, B. Guschlbauer, J. Timmer*, et al.*, "Oscillatory cerebral hemodynamics—the macro- vs. microvascular level," *Journal of the Neurological Sciences,* vol. 250, pp. 103-109, 12/1/ 2006.

[86] L. Minati, I. U. Kress, E. Visani, N. Medford, and H. D. Critchley, "Intra- and extra-cranial effects of transient blood pressure changes on brain near-infrared spectroscopy (NIRS) measurements," *Journal of Neuroscience Methods,* vol. 197, pp. 283-288, Apr 2011.

[87] M. Reinhard, E. Wehrle-Wieland, D. Grabiak, M. Roth, B. Guschlbauer, J. Timmer*, et al.*, "Oscillatory cerebral hemodynamics--the macro- vs. microvascular level," *J Neurol Sci,* vol. 250, pp. 103-9, Dec 2006.

[88] R. Zhang, K. Behbehani, and B. D. Levine, "Dynamic pressure-flow relationship of the cerebral circulation during acute increase in arterial pressure," *J Physiol,* vol. 587, pp. 2567-77, Jun 2009.

[89] M. S. Olufsen, A. Nadim, and L. A. Lipsitz, "Dynamics of cerebral blood flow regulation explained using a lumped parameter model," *Am J Physiol Regul Integr Comp Physiol,* vol. 282, pp. R611-22, Feb 2002.

[90] A. S. Meel-van den Abeelen, A. H. van Beek, C. H. Slump, R. B. Panerai, and J. A. Claassen, "Transfer function analysis for the assessment of cerebral autoregulation using spontaneous oscillations in blood pressure and cerebral blood flow," *Med Eng Phys,* vol. 36, pp. 563-75, May 2014.

[91] R. B. Panerai, S. L. Dawson, and J. F. Potter, "Linear and nonlinear analysis of human dynamic cerebral autoregulation," *Am J Physiol,* vol. 277, pp. H1089-99, Sep 1999.

[92] F. P. Tiecks, A. M. Lam, R. Aaslid, and D. W. Newell, "Comparison of static and dynamic cerebral autoregulation measurements," *Stroke,* vol. 26, pp. 1014-9, Jun 1995.

Biographical Information

Raichel Mary Alex was born as the youngest daughter of Mr. and Mrs. Alexander in 1985. She was born and brought up in the southern state, Kerala, of the Indian subcontinent until her bachelor's studies. Being a master in the art of studies, she proved herself to be good in many cultural activities as well. Ms. Alex scored Rank 1 in University of Calicut, Kerala, India for her Bachelor's Degree in Biomedical Engineering, 2006. She joined the British Physical Laboratory Group Limited, as a Trainee Engineer in R & D division, where she worked on the basics of medical equipment design. Being highly motivated by her interest in medical equipment research, Ms. Alex enrolled for a Master's Degree in Bioengineering at the University of Texas at Arlington in August 2008. She has worked on the detection of sleep apnea and related biological parameters during her Master's degree from 2008 to 2010. She was always fascinated by the magic of medical electronics and hence seeks to study in medical instrumentation and research. To further strengthen her anticipated career in Biomedical engineering, she joined PhD program in bioengineering in August 2010. During her research, Ms. Alex has worked on acquiring clinical data and has developed quantitative models to explore changes in brain blood flow during apnea. Ms. Alex plans to develop her skills as an independent researcher by pursuing a post-doctoral training in bioengineering.